

Assembly of DNA-encapsulated lipid bilayers
and
their application to studies of GPCRs

DISSERTATION

zur Erlangung des akademischen Grades

Doctor rerum naturalium

(Dr. rer. nat.)

vorgelegt

**dem Bereich Mathematik und Naturwissenschaften
der Technischen Universität Dresden**

von

M.Pharm. Katarina Iric

geboren am 22.12.1990 in Belgrad, Serbien

Eingereicht am

Die Dissertation wurde in der Zeit von Januar 2016 bis Januar 2020 im
cfaed - Center for Advancing Electronics Dresden und am Helmholtz Zentrum
Dresden – Rossendorf angefertigt.

Dissertation eingereicht am:

Tag der Verteidigung:

- 1. Gutachter: Prof. Thorsten Stumpf**
- 2. Gutachter: Prof. Karim Fahmy**
- 3. Gutachter: Prof. Thorsten-Lars Schmidt**

Dedicated to my family and friends

Abstract

Lipid bilayers and lipid-associated proteins play crucial roles in biology. As *in vivo* studies and manipulation are inherently difficult, membrane-mimetic systems are useful for the investigation of lipidic phases, lipid–protein interactions, membrane protein function and membrane structure *in vitro*.

This dissertation describes a route to leverage the programmability of DNA nanotechnology to create DNA-encircled bilayers (DEBs), a novel nano-scaled membrane-mimetic system. DEBs are made of multiple copies of an alkylated oligonucleotide hybridized to a single-stranded minicircle, in which up to two alkyl chains per helical turn point to the inside of the toroidal DNA ring. When phospholipids are added, a bilayer is observed to self-assemble within the ring such that the alkyl chains of the oligonucleotides stabilize the hydrophobic rim of the bilayer to prevent formation of vesicles and support thermotropic lipid phase transitions. This straight-forward and robust route enables the rational design of DEBs so that their size, shape or functionalization can be adapted to the specific needs of biophysical investigations of lipidic phases and the properties of membrane proteins.

Next, we optimized the DEB system to provide proper anchoring of a large variety of lipids by creating an improved DNA scaffold. This scaffold, called DNA double-decker, consists of two interconnected DNA minicircles stacked on top of each other. In comparison to the DNA minicircle in DEB system, this scaffold is two times thicker and contains two times more hydrophobic strands, which should increase the stability of the lipid bilayer rim.

Finally, we explored the option of using DEBs in studies of GPCRs using CCR5 as a model protein. The CCR5 was labeled with DNA strands, purified and characterized. The strands on CCR5 are complementary to the protruding strands on the DNA minicircle in DEBs. This can allow reconstitution of GPCRs inside DEBs with controlled orientation of the receptor.

Publications

[A] **Iric, K.**, Subramanian, M., Oertel, J., Agarwal, N. P., Matthies, M., Periole, X., Sakmar, T. P., Huber, T., Fahmy, K. and Schmidt, T. L. (2018) DNA-encircled lipid bilayers. *Nanoscale*, 10, 18463–18467.

The results of paper [A] are discussed in detail in this dissertation.

Acknowledgements

This dissertation might have one author, but many of the results presented here have only been achieved with the support of several people. Some of them supported me professionally, some of them emotionally, but many of them both.

First, I want to thank my two supervisors, Prof. Thorsten-Lars Schmidt and Prof. Karim Fahmy for giving me the opportunity to work in their research groups. Their enthusiasm about this project, numerous discussions and support have been essential to me. They were motivating me to accomplish more and become a better scientist every single day. I learned so much from them and I am extremely grateful I had them as mentors. Dear Thorsten, thank you for helping me grow not only scientifically, but personally. Thank you for showing me how important the balance between work and free time is. I enjoyed equally both group meetings and group outings (dinners, hiking, camping) with you. Dear Karim, thank you for believing in me and having a vision about this project beyond the initially proposed one. Thank you for connecting me with Prof. Thomas P. Sakmar and Prof. Thomas Huber and giving me the opportunity to work with them for several months.

Furthermore, I would like to express gratitude to Prof. Thomas P. Sakmar for giving me the opportunity to do a research stay in his group. Although I was there for only nine months, I had unconditional support from him and other group members. I am thankful for many discussions and feedback that happened throughout the entire length of my PhD studies. I could not talk about my stay in the Prof. Sakmar lab without mentioning Prof. Thomas Huber. He was the first person to show me the great potential of this project. His enthusiasm about every single scientific area is contagious. I was learning more every single day during my stay because of him. He and his family, together with members from Prof. Sakmar lab, made my stay in New York unforgettable.

I would like to thank the members of my thesis advisory committee, Prof. Thorsten-Lars Schmidt, Prof. Karim Fahmy, Prof. Yixin Zhang and Prof. Michael Schlierf for the numerous and productive discussions.

Next, I would like to thank all members in the groups I was working in. I would like to thank everyone who was part of Prof. Schmidt group: Dr. Michael Matthies, Dr. Nayan Agarwal, Dr. Fatih Nadi Gür, Anne Schultze, Yavuz Uca, Eric Weiner, Foram Joshi, Shikhar Gupta, Bastian Joffroy, Ashwin Karthick, Dr. Diana Goncalves-Schmidt, Simon Ahrens, Olha Aftenieva, Kristin Joffroy and Chloe Jones. Thank you for creating an

amazing working environment. I was looking forward coming to the lab every day because of you. Coffee and lunch breaks, cooking sessions, dinners, cakes, Friday beer hours are one of my best memories in Dresden because of you. I especially want to thank Michael, Nayan, Fatih and Bastian, who were by my side every single day. Furthermore, I would like to thank members of Prof. Fahmy group: Dr. Jana Oertel, Madhumalar Subramanian, Lisa Nucke. My visits to HZDR were not as often as I expected, but you made me feel welcome every single time. Special thanks to Madhu, who was working closely with me on several parts of the project. Finally, I would like to thank all members of Prof. Sakmar lab: Mizuho Horioka, Dr. Alessandra Bonito-Oliva, Dr. Valen Graham, Manija Kazmi, Dr. Emily Lorenzen, Dr. Emilie Ceraudo, Jordan Mattheisen and Dr. Shahar Barbash. Special thanks to Mizuho, with whom I shared my research work in New York. I am so grateful I could work on that project with her.

I also sincerely express my gratitude to all the people who supported me throughout the last four years of my stay in Dresden, including all my friends, who strongly believed in me. Special thanks to Katarina, Petar, Nina, Milica, Biljana, Lora, Tijana and Jelena who were supporting me despite being far away. I would like to specially thank Adrian Romani Vazquez, who is the greatest support I could hope for. He keeps believing in me and pushing me forward every single day.

Finally, I would like to thank my parents and my brother Nemanja. They were supporting me my whole life and inspired me to pursue the career in science. I would not be here today if it was not for them.

Table of content

Abstract.....	v
Publications	vii
Acknowledgements.....	ix
Table of content	xiii
Chapter 1 Introduction	1
1.1 Lipid membranes	1
1.1.1 Cell membranes	1
1.1.2 Principles of membrane organization	3
1.2 Membrane proteins	7
1.2.1 Membrane proteins in biological membranes	7
1.2.2 G protein-coupled receptor family	8
1.2.3 Membrane protein solubilization strategies	11
1.2.4 Membrane protein reconstitution strategies	11
1.3 DNA nanotechnology	14
1.3.1 Structure and biological function of DNA	14
1.3.2 Structural DNA nanotechnology	18
1.3.3 Scaffolded DNA origami	20
1.3.4 DNA nanostructure interaction with lipid bilayers	22
Chapter 2 Motivation and objectives	26
Chapter 3 DNA-encircled lipid bilayers (DEBs).....	28
3.1 Introduction.....	28
3.2 Results and discussions.....	29
3.2.1 DEB design	29
3.2.2 DEB formation strategy	30
3.2.3 DEB analysis.....	33
3.2.4 Lipid phase transition in DEBs	35
3.2.5 Coarse-grained simulations of DEBs	36
3.3 Conclusions and outlook	38
3.4 Methods.....	38
3.4.1 Materials.....	38
3.4.2 Alkylation of short oligonucleotides	39
3.4.3 ss DNA MC design and preparation.....	40

3.4.4	dsDNA MC formation	41
3.4.5	DEB formation and purification	42
3.4.6	Expression and purification of MSP1D1	43
3.4.7	Assembly of MSP-based lipid nanodiscs	44
3.4.8	Fluorescence measurements of LAURDAN-labeled DEBs and vesicles	44
3.4.9	Coarse-grain molecular dynamics calculations	45
Chapter 4	Further improvements of DEBs	47
4.1	Introduction.....	47
4.2	Results and discussions.....	48
4.2.1	Strategy to design DNA double-deckers	48
4.2.2	Assembly strategy of functionalized DNA double-deckers.....	49
4.2.3	Optimization of double-decker staple alkylation	52
4.2.4	Double-decker characterization	55
4.2.5	Approaches for lipid bilayer assembly in double-deckers	57
4.3	Conclusion and outlook	58
4.4	Methods.....	59
4.4.1	Materials.....	59
4.4.2	Staple alkylation	60
4.4.3	Double-decker scaffold preparation	61
4.4.4	Double-decker preparation.....	61
Chapter 5	Applications of DNA-encircled lipid bilayers to study GPCRs	63
5.1	Introduction.....	63
5.2	Results and discussions.....	64
5.2.1	Strategy for DEB-CCR5 complex assembly.....	64
5.2.2	DNA labeling	66
5.2.3	CCR5 labeling and purification.....	68
5.2.4	Coarse-grained simulations of DEBs for CCR5 reconstitution	70
5.3	Conclusions and outlook	72
5.4	Methods.....	72
5.4.1	Materials.....	72
5.4.2	Labeling oligonucleotides for SNAp tag and CLIP tag	73
5.4.3	CCR5 preparation and labeling	74
5.4.4	NIR-immunoblotting	75
5.4.5	SMD-TIRF	76
	Bibliography.....	78
	Statement of academic honesty	89

Chapter 1 Introduction

1.1 Lipid membranes

1.1.1 Cell membranes

Cell membranes have an important role in both cell structure and cell function.¹ They enclose the cell and its compartments, maintaining their boundaries and the essential differences between them.² Furthermore, cell membranes participate in many cellular processes including protein synthesis, signal transduction and metabolite transport.³ The importance and complexity of the biological membranes was described in 1972 by Singer and Nicolson, who proposed the fluid mosaic model.⁴ This model describes the structure of the plasma membrane as a mosaic of components: membrane proteins have amphipathic structure and are embedded in a lipid bilayer that consists of two antiparallel lipid leaflets but assumes that the lipid bilayer has little to no effect on the proteins' behavior. Later on, other models were created in order to better explain the function and internal organization of the plasma membranes, focusing on structural diversity and asymmetric lipid distribution between the bilayers.⁵⁻⁸ While these models state that the lipids are essential for the membrane proteins to function properly, they agree with the fluid mosaic model in regards to the composition itself (Figure 1-1).

1.1 Lipid membranes

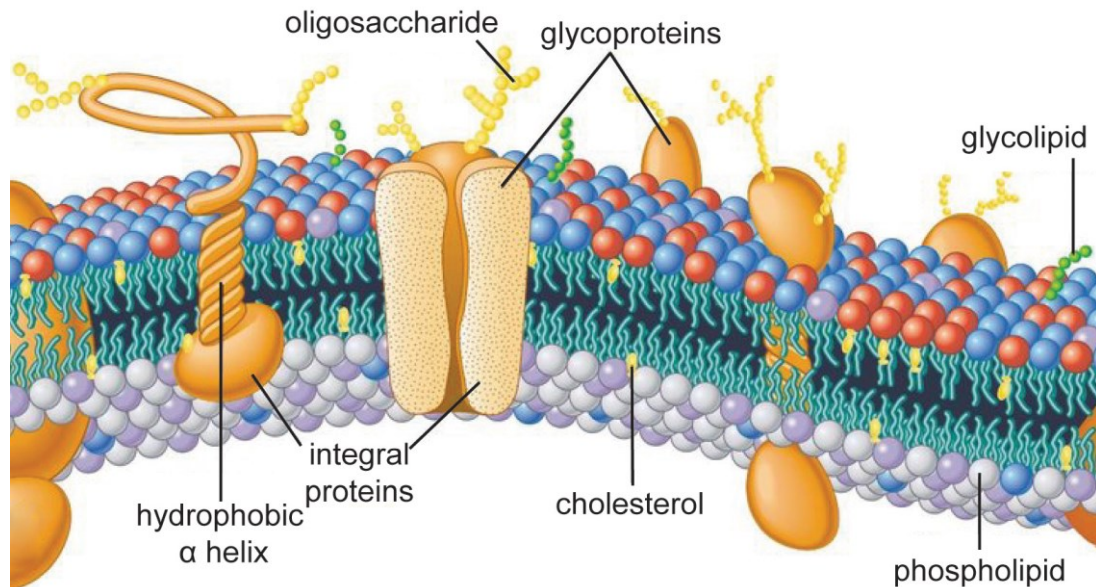


Figure 1-1. Current representation of the plasma membrane, showing the fluid mosaic organization proposed by Singer and Nicolson⁹ Adapted with permission from John Wiley & sons, Inc. [9], copyright (2010).

Although the composition of the cell membrane varies between different cells, they always contain three types of lipids: phospholipids, cholesterol and glycolipids.¹ The most common phospholipids are phosphoglycerides (phosphatidylethanolamine, phosphatidylserine, phosphatidylcholine) and sphingomyelin (Figure 1-2).¹⁰ Phosphoglycerides have a three-carbon glycerol backbone, whereas sphingomyelin is derived from sphingosine.¹¹ The difference in the lipid composition is present even within the same plasma membrane: namely, the zwitterionic phospholipids and glycolipids are present in the outer part of the membrane, whereas the negatively charged lipids (such as phosphatidylserine) are located primarily in the inner part of the cell membrane.^{12,13}

1.1 Lipid membranes

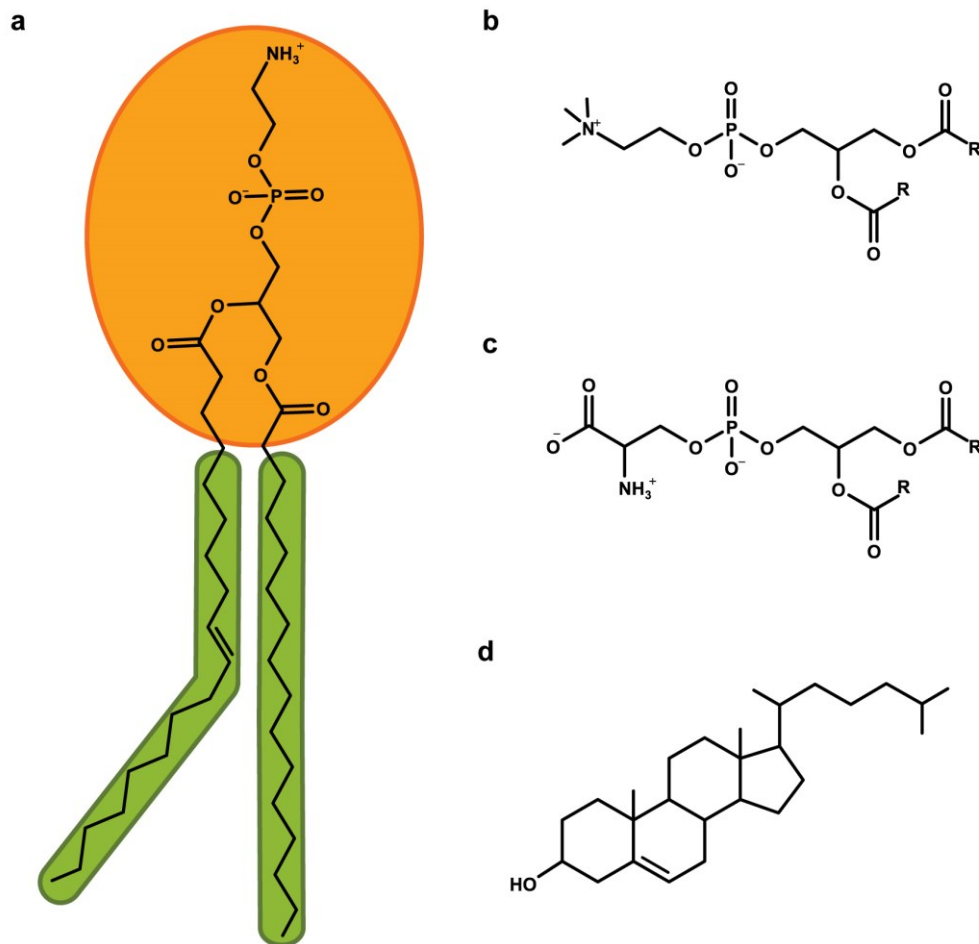


Figure 1-2. Common lipids in mammalian cell membranes. a) Schematic representation of a phospholipid (here, phosphatidylethanolamine) with hydrophilic head group (orange) and hydrophobic tails (green); the presence of double C-C bonds induces the kink in the tail. b) Phosphatidylcholine c) Phosphatidylserine d) Cholesterol.

1.1.2 Principles of membrane organization

The presence of hydrophobic groups in lipids causes them to spontaneously assemble into structures in which these groups will not be exposed to the water. This process is greatly affected by the shape of the lipid molecule, which can be characterized as a “shape factor” S :^{14,15}

$$S = \frac{V}{A_0 L_C}$$

1.1 Lipid membranes

Where V is the volume of the molecule, A_0 is the “optimal” area of the lipid headgroup considering its protonation state and dimensions, whereas L_C is the length of the straight acyl chain. Depending on S , lipids can form various structures: for $S < 1$ (inverted conical shape) they assemble micelles, for $S = 1$ (cylindrical shape) they form lamellar structures and for $S > 1$ (conical shape) they form inverted micelles (Figure 1-2). Since phospholipids are cylindrical, they form bilayers in aqueous environments. However, the planar phospholipid bilayer is not stable as its edges are still exposed to water. Therefore, it spontaneously closes and forms a spherical vesicle, called liposome.¹⁶

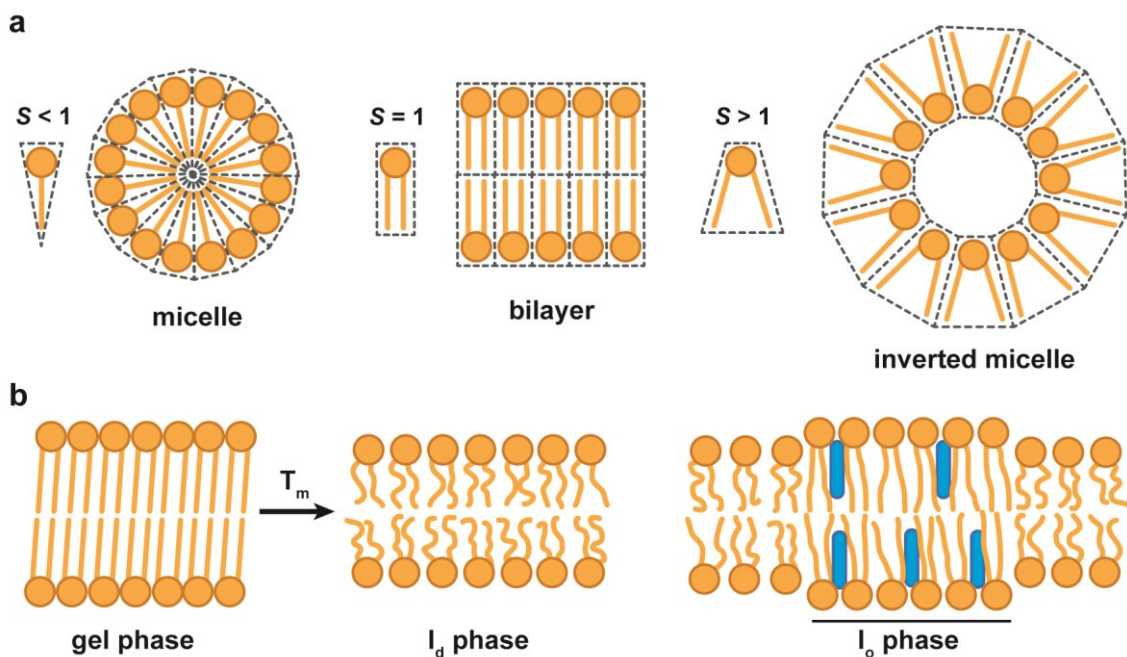


Figure 1-3. Principles of lipid organization. a) Schematic representation of lipids with different shape factor S and shape of their preferred assemblies: inverted cone shape lipids ($S < 1$) form micelles (left), cylindrical shape lipids ($S = 1$) form bilayers (middle), cone shape ($S > 1$) form inverted micelles (right). b) Schematic representation of different lipid bilayer phases: gel phase or ordered solid (left) at phase transition temperature (T_m) changes to liquid disordered (l_d , middle) phase. Right: liquid-ordered phase (l_o). Blue ovals represent cholesterol molecules.

The fluidity of the lipid membrane depends on the temperature and its composition. The temperature where a given lipid bilayer changes from a fluid (liquid disordered, l_d) phase to a gel (ordered solid) phase is called phase transition temperature (T_m).¹⁷ This depends on the structure of the lipids; namely, saturated lipids with longer hydrophobic tails will

1.1 Lipid membranes

have stronger hydrophobic interactions with each other, which leads to the formation of an ordered phase, increasing the phase transition temperature.¹⁸ Conversely, unsaturated or lipids with short chains will have lower phase transition temperature. The presence of cholesterol in the lipid bilayer greatly affects the fluidity of the membrane: it anchors between the hydrophobic tails and makes them more rigid, generating liquid-ordered (l_o) phase, which leads to increased order in the membrane without increased melting temperature.¹⁶

Lipids within a lipid bilayer are mobile: they can either rotate around their long axis, bend their flexible hydrocarbon chains, diffuse laterally within a monolayer, or migrate from one monolayer to other (flip-flop). Lateral diffusion of lipids in membranes is described by the modified Einstein relation:

$$\langle r^2(t) \rangle = 4Dt\alpha$$

Where $\langle r^2(t) \rangle$ is the mean square displacement (MSD), D is a constant called diffusion coefficient, t is time and α ($0 < \alpha < 1$) is the anomalous exponent. Diffusion coefficient D is the most important parameter of diffusion and can be determined experimentally by fluorescence correlation spectroscopy (FCS), fluorescence recovery after photobleaching (FRAP) and single particle tracking (SPT).¹⁹ While the lateral diffusion is fast, the flip-flop occurs less than once a month for any individual molecule. Cholesterol is an exception to this rule because it can flip-flop rapidly.¹⁴ Molecular dynamic simulations and experimental procedures mentioned above have shown that the lipids in the bilayers are disordered and confirmed that the lipid membrane is a two-dimensional liquid in which the lipids freely move laterally.^{20–22}

Lipid rafts

Lipid rafts are subdomains of the plasma membrane that contain high concentrations of cholesterol and sphingolipids.²³ They exist as distinct liquid-ordered regions of the membrane that are resistant to extraction with nonionic detergents and thicker than the surrounding membrane.²⁴ Lipid raft formation is driven and stabilized by lipid-lipid, lipid-protein and protein-protein interactions.²⁵ Although the size of individual rafts is small, they can constitute a large fraction of the plasma membrane's surface.¹⁸ While rafts have a distinctive protein and lipid composition, not all rafts are identical in terms of either the proteins or the lipids that they contain.

Solubilization of lipid membranes by detergents

As discussed in the previous section (1.1.1), biological membranes form supramolecular aggregates consisting of lipids and membrane proteins. In order to study membrane structure and function, it is usually necessary to dissociate the membrane into its components.²⁶ The most common membrane solubilization technique is using detergents. Detergents (also known as surfactants) are amphipathic molecules consisting of a hydrophilic head and a long hydrophobic tail.²⁷ Depending on their structure, detergents are classified as ionic, non-ionic or zwitterionic. Ionic detergents possess a net charge due to the presence of anionic or cationic head group.²⁸ They have either straight hydrophobic chains (e.g. sodium dodecyl sulfate – SDS) or rigid steroid groups (e.g. sodium cholate). On the other hand, non-ionic detergents have uncharged head groups containing such as glycosidic groups (octyl glucoside) or polyoxyethylene moieties (Triton™). Zwitterionic detergents (such as CHAPS (3-((3-cholamidopropyl) dimethylammonio)-1-propanesulfonate) have both positive and negative charge.

Due to their amphiphilic nature, detergents tend to form micelles. The minimal concentration needed for micelle assembly is called critical micelle concentration (CMC).²⁹ The average number of detergent molecules in a micelle is described as the aggregation number.³⁰ The CMC and aggregation number are highly dependent on the structure of the detergent: namely, ionic detergents with longer hydrophobic chains form bigger micelles and have lower CMC and aggregation number since fewer molecules are needed to form a micelle.³¹ The temperature at which a detergent solution near CMC separates into two phases is defined as the cloud point. The lower phase consists of aggregated micelles, whereas the upper phase is detergent-depleted. External factors, such as pH, temperature and ionic strength heavily influence the CMC, aggregation number and cloud point.³² Detergents are crucial for membrane protein solubilization and crystallization, which will be discussed in Section 1.2.3.

1.2 Membrane proteins

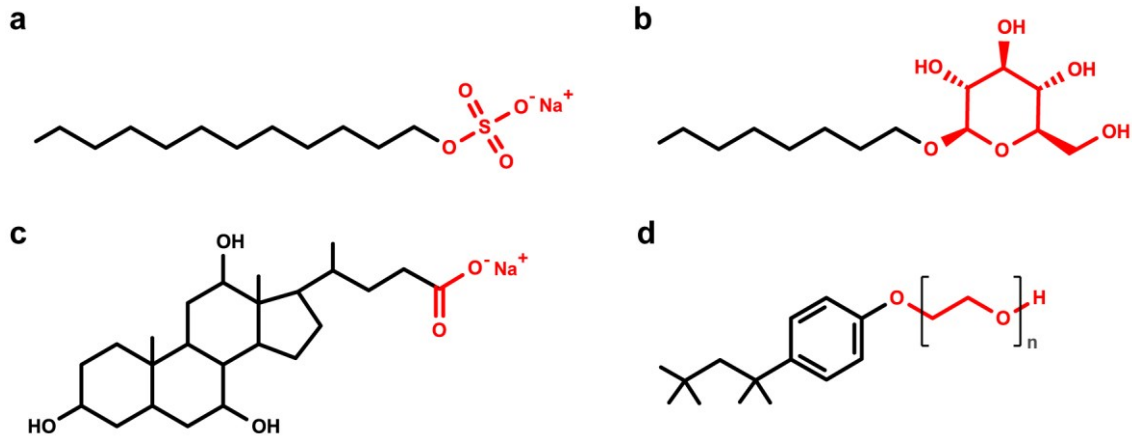


Figure 1-4. Common detergents used for solubilization of lipid membranes. a) SDS b) β -octyl glucoside c) Sodium cholate d) TritonTM. Hydrophilic heads are marked red.

1.2 Membrane proteins

1.2.1 Membrane proteins in biological membranes

As some models show, the lipid bilayer not only determines the shape and basic structure of the cell membrane but modifies the behavior of the proteins it contains.^{6,7} Despite this, the membrane proteins themselves are responsible for most membrane functions other than compartmentalization. They play the main role in the transport through the cell membrane and signal transduction, catalyze chemical reactions on the membrane, and participate in intercellular joining, cell-cell recognition and cell attachment.¹ Their crucial role is reflected in the fact that membrane proteins make up ~23% of the human proteome.³³ The importance of membrane proteins in, specifically, human health is even better stated in the fact that they represent about 60% of the targets for approved drugs and a 38% of all identified disease-related proteins.³⁴

Membrane proteins can be associated with the lipid bilayer in different ways (Figure 1-5). Integral membrane proteins are permanently attached to the membrane and can either span the entire membrane (transmembrane proteins) or be associated only to one side. All transmembrane proteins contain residues with hydrophobic side chains which interact with lipids and thus anchor the protein to the lipid bilayer.¹ In most cases, the hydrophobic domain of the protein spans the lipid bilayer in α -helical conformation once (e.g. LRR

1.2 Membrane proteins

receptor-like serine/threonine-protein kinase) or multiple times (eg. G-protein cell receptors - GPCRs)³⁵. Other transmembrane proteins, such as OmpA (Outer membrane protein A), span the membrane as a rolled-up β sheet, called β -barrel.³⁶ In comparison to the integral proteins, the peripheral proteins are temporarily attached to the surface of the lipid bilayer or to an integral protein.

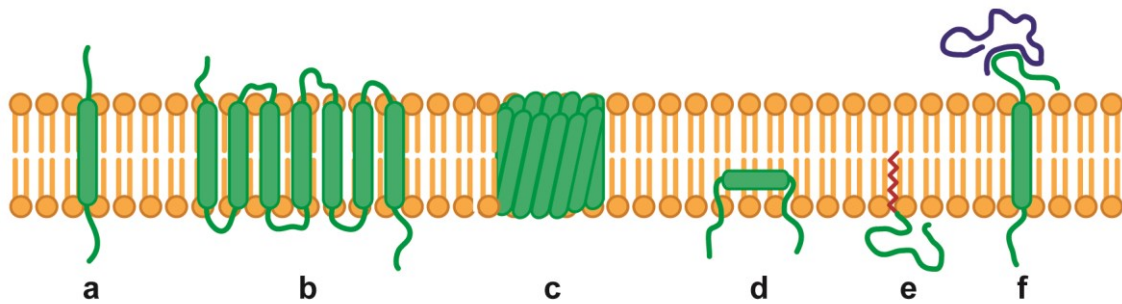


Figure 1-5. Different ways in which membrane proteins interact with lipid bilayer. a) membrane-spanning single α -helix b) multiple α -helices c) β -barrel d) Interaction by an amphipathic α -helix parallel to the membrane plane (in-plane membrane helix) e) Interaction by fatty acid chain hydrophobic loop (red) f) Interaction by a covalently bound membrane protein.

Irrespective of the type of the membrane protein, they all need certain conditions in the lipid bilayer in order to function properly. Whether the presence of certain lipids is important for the membrane protein function can be determined by various methods, including reconstitution in artificial membranes, X-ray crystallography and lipid array screening.³⁷ For example, the presence of cholesterol is crucial for the activity of the human β_2 -adrenergic receptor; phosphatidylserine increases the activity of D-lactate dehydrogenase and phosphatidylethanolamine binds to *Thermochromatium tepidum* photosynthetic reaction center.³⁸

One of the most important membrane protein families is the G protein-coupled receptor family, that will be further discussed in the following chapter.

1.2.2 G protein-coupled receptor family

G protein-coupled receptors (GPCRs), are transmembrane receptors with seven transmembrane spanning segments. These receptors are responsible for signal transduction:

1.2 Membrane proteins

they control key physiological functions, including neurotransmission, hormone and enzyme release from endocrine and exocrine glands, immune responses, cardiac- and smooth-muscle contraction and blood pressure regulation.³⁹ Their dysfunction contributes to some of the most prevalent human diseases, as reflected by the fact that GPCRs represent the target, directly or indirectly, of 34% of all current therapeutic agents.⁴⁰

The GPCR family has more than 800 receptors organized in 5 classes: rhodopsin (class A), secretin (class B), adhesion (originally class B), glutamate (class C), and frizzled/taste2. The physiologic function of a large fraction of GPCRs remains unknown; these receptors are known as orphan GPCRs.³⁵

GPCRs share common structural features: they all consist of the extracellular N-terminus, seven hydrophobic transmembrane (TM) helices connected with three intracellular and three extracellular loops, and an intracellular carboxyl terminus (Figure 1-6). GPCRs show the greatest homology within the TM segments, whereas the most variable structures are the carboxyl terminus, the intracellular loop between TM5 and TM6 and the N-terminus. The latter in particular shows the greatest diversity: namely, monoamine and peptide receptors have relatively short sequence (10-50 amino acids), whereas glycoprotein hormone receptors, adhesion and glutamate family receptors have 350-600 amino acids at their N-terminus.⁴¹

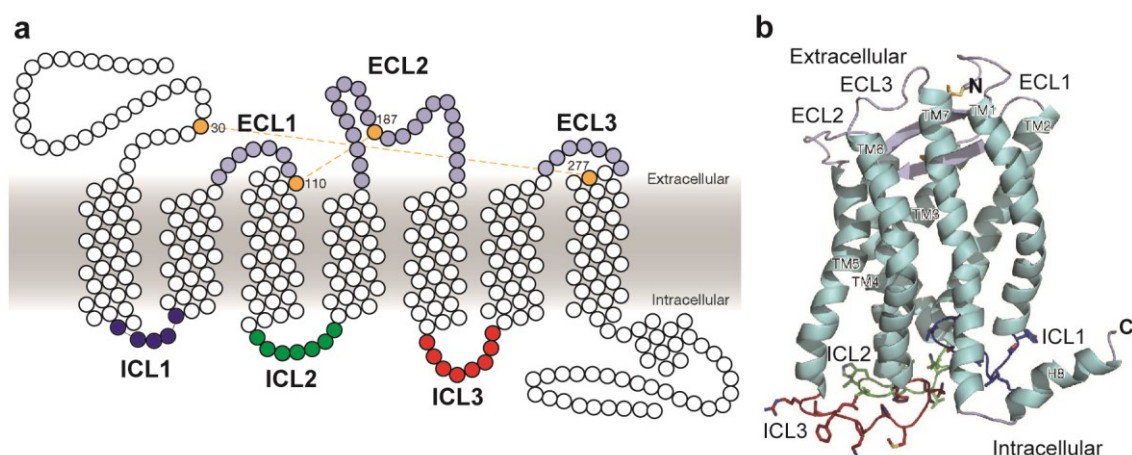


Figure 1-6. Structural features of GPCRs: structure determination of Interleukin 8 receptor, alpha (CXCR1). a) CXCR1 topology with two disulphide bonds (gold), extracellular loops (ECL1-ECL3) in grey and intracellular loops in blue (IC1), green (ICL2) and red (EC3) b) Backbone representation of CXCR1 showing helices in cyan (TM1–TM7 and

1.2 Membrane proteins

H8), and loops as described. Disulphide-bonded Cys pairs (Cys 30–Cys 277 and Cys 110–Cys 187) are shown as sticks.⁴² Adapted with permission from Springer Nature: Nature [42], copyright (2012).

Various ligands can bind to GPCRs, ranging from ions (H^+ and Ca^{2+}) to small organic molecules or peptides and proteins. They can bind either to the TM core (nucleosides, eicosanoids), to both the core and extracellular loops (small peptides), to extracellular loops and N-terminus (polypeptides < 90 amino acids) or exclusively to the N-terminal segment (glycoproteins > 30 kDa).³⁹ Ligand binding triggers the receptor activation, which consists of three steps: signal generation, TM signal transduction and signal transfer to cytoplasmic signal molecules. In the special case of photoreception by the visual photoreceptor rhodopsin, a covalently bound inverse agonist (11-cis retinal) turns into an agonist by photoisomerization (forming all-trans retinal at the transmembrane binding site). The classical signal transduction through GPCRs is dependent on receptor-mediated activation of heterotrimeric G proteins, which are composed of three subunits known as G_α , G_β and G_γ . These units dissociate and, depending on the GPCR-ligand complex, modulate the activity of different downstream effector proteins, inducing a cell response.⁴¹ The signaling pathways downstream of GPCRs are complex and their detailed description is reported elsewhere.^{35,41,43,44}

Chemokine receptors

Chemokine receptors are rhodopsin-like GPCRs found on the surface of certain cells that interact with a type of cytokine called a chemokine.⁴⁵ Chemokines are critical mediators of cell migration during routine immune surveillance, inflammation and development.⁴⁶ After interacting with their specific ligands, chemokine receptors trigger a flux in intracellular calcium ions known as calcium signaling.⁴⁷ This induces a response in the cell, including the onset of a process known as chemotaxis that traffics the cell to the location of an inflammation.

Chemokine receptors are divided into four classes, named according to the type of chemokine (CC, CXC, CX3C or XC, depending on the position of conserved cysteine residues involved in disulfide bond formation) with which they interact.⁴⁸ Since chemokines bind to the N-terminal of chemokine receptors, the main structural difference between the four classes of receptors comes from the spacing of cysteine residues near their N-termini.

1.2 Membrane proteins

Once a chemokine is tethered to a chemokine receptor, its unstructured N terminus enters the receptors' TM domains to induce a conformational change which is translated into an intracellular signal.⁴⁹

1.2.3 Membrane protein solubilization strategies

Due to their hydrophobic regions, membrane proteins are prone to aggregation and precipitation in solution.⁵⁰ Therefore, the solubilization of the membrane proteins is a prerequisite for *in vitro* functional or structural studies.

The most common membrane solubilization strategy is using detergents. Since detergents are amphiphilic molecules, their hydrophobic domains interact with hydrophobic domains of the membrane protein, while the hydrophilic domains are exposed to water, making the protein soluble in water (Figure 1-7 a).²⁶ However, this strategy does not provide the native environment for the membrane proteins due to the absence of membrane lipids, which are often crucial for the protein function.²⁸ Furthermore, some detergents (such as sodium-dodecyl-sulphate - SDS) can disrupt the bonds between the transmembrane domains of the protein, leading to its denaturation. This can be overcome by using mild detergents,⁵¹ followed by membrane protein reconstitution in the lipid bilayer.

Other strategies focus on substituting the detergents during the membrane protein solubilization. One of them, described in 1996 by Tribet and co-workers, uses molecules called Amphipols.⁵² These consist of hydrophilic polymers with several hydrophobic groups, which interact with hydrophobic domains of the protein and stabilize it in the solution. However, they are not used often and detergents are still the main way of solubilizing the membrane proteins.

1.2.4 Membrane protein reconstitution strategies

As mentioned in sections 1.2.1 and 1.2.3, in order to ensure that the isolated membrane protein of interest is both functional and in a native state, it needs to be reconstituted in a system that mimics its native environment as good as possible. Since the function of a membrane protein depends on the lipids present in the cell membrane,⁵³ the reconstitution strategies described below contain an abundance of lipids in comparison to the detergent-solubilized micelle of the protein.

1.2 Membrane proteins

Bicelles

Bicelles are disk-shaped lipid bilayers usually containing detergents and several types of lipids. Long-chain phospholipids form the planar region, whereas the short-chain lipids or detergents form flanking rims that stabilize the system (Figure 1-7 b).⁵⁴ The size of the bicelles can be controlled by adjusting the molar ratio of long chain to short-chain component. Due to their magnetic alignability, they are frequently used for solution and solid-state nuclear magnetic resonance (NMR) studies.^{55,56} Applications of bicelles outside of NMR spectroscopy include the crystallization of membrane proteins from bicelle formulations, their use as delivery vehicles for membrane proteins to oocyte membranes,⁵⁷ and as templates for the synthesis of platinum nanowheels.⁵⁸ Nevertheless, the size and exact composition of the bicelles cannot be fully controlled since other proteins might reconstitute in the bicelle together with the target membrane protein, which makes the studies inherently challenging.

Liposomes

As mentioned in Section 1.1.2, when phospholipids are dispersed in water, they self-assemble to form spherical vesicles of phospholipid bilayers with an aqueous core, called liposomes.¹ Liposomes can have one (unilamellar) or more (multilamellar) lipid bilayers.⁵⁹ Unilamellar liposomes have been widely used for membrane protein studies, especially ion channels and fusion proteins (Figure 1-7 c).^{60,61} Furthermore, they are used as a model system for investigating phospholipid dynamics, cell invaginations, endo- and exocytosis and location of the membrane proteins in the cell membrane (lipid rafts).^{5,60,62–64} However, both the orientation and number of the membrane proteins inserted into the bilayer cannot be controlled, making this system inadequate for single-molecule studies. Furthermore, the liposome samples are unstable for extended periods of time, precipitate and tend to segregate into phase-separated domains.

Nanodiscs

Nanodiscs consist of a phospholipid bilayer encircled by polymers, peptides or proteins. Most commonly, nanodiscs are encircled by the 2 amphipathic α -helical membrane scaffold proteins (MSPs), derived from Apolipoprotein-A1 (Figure 1-7 d).^{65,66} The length of MSPs determines the diameter of the nanodiscs, which is usually less than 17 nm. Depending on the length of MSP, nanodiscs can have diameters up to 17 nm.⁶⁷ Lately, covalently circularized nanodiscs have been assembled with polypeptides circularized

1.2 Membrane proteins

by sortase A. These nanodiscs have diameters of 8, 11, 15 and 50 nm.⁶⁸ Nanodiscs with incorporated membrane proteins can be assembled from a detergent solubilized mixture of all components by gradual removal of detergent via adsorption on hydrophobic beads or by dialysis.⁶⁹ Nanodiscs are used for structural studies of membrane proteins including single molecule investigations,⁷⁰ X-ray crystallography,⁷¹ cryo electron microscopy⁷² and analytical⁷³ and functional studies of membrane proteins. However, since the chemical modifications of MSP are challenging, the reconstituted protein cannot easily be chemically attached to a MSP and therefore will have a large number of possible orientations. Furthermore, the size distribution of assembled nanodiscs is heterogeneous. However, it is attractive for many applications to form a complex with a molecule that will be capable of attaching to the membrane protein and locking it into the desired orientation. Compared to MSPs, double-stranded deoxyribonucleic acid (DNA) is more suitable for chemical modifications. Furthermore, DNA can be self-assembled and form rigid structures that are compatible with other biomolecules. The properties of DNA and DNA structures will be discussed in the following section (1.3).

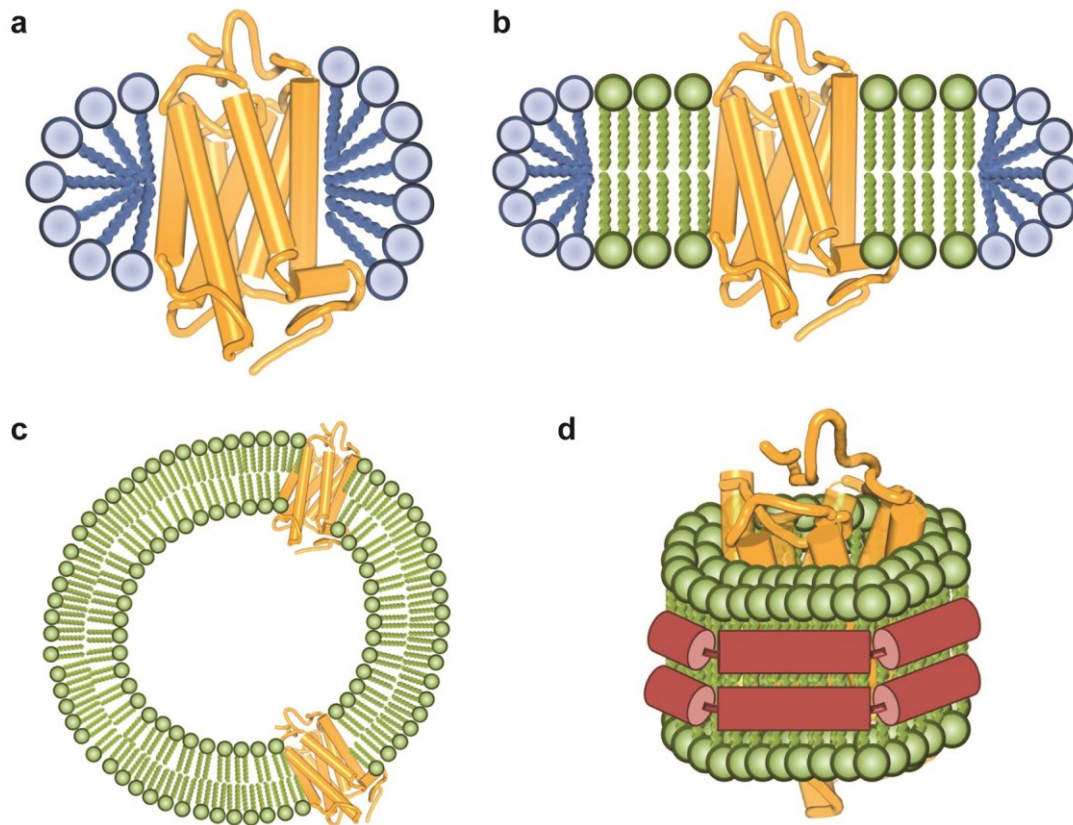


Figure 1-7. Membrane protein solubilization and reconstitution strategies. Membrane proteins (yellow) can be solubilized using detergents (blue) by forming a detergent-solubilized micelle of the protein (a). In presence of lipids (green), membrane proteins can be reconstituted into bicelles (b), liposomes (c) and nanodiscs (d)⁷⁴. Adapted from ref. [74] (CC BY 4.0).

1.3 DNA nanotechnology

1.3.1 Structure and biological function of DNA

All living cells store their hereditary information in the form of double-stranded polymer chains, called deoxyribonucleic acid (DNA). In prokaryotic cells, DNA is stored in the nucleoid, whereas in eukaryotic cells it is stored in chromosomes. Histones are proteins responsible for packing DNA inside into chromatin fibers in chromosomes, which replicate during cell division, providing the same genetic material to both daughter cells. The

1.3 DNA nanotechnology

transfer of genetic information is carried away from DNA to proteins via RNA. The process where information from a small segment of DNA gets translated to messenger-ribonucleic acid (mRNA) is called transcription. Later on, the mature mRNA gets transcribed into a protein. The flow of the genetic information through replication, transcription and translation is known as the central dogma of molecular biology.

The structure of DNA helix as described by Watson and Crick consists of two long polynucleotide antiparallel chains composed of four different nucleotides (Figure 1-8). Each nucleotide is composed of a β -D-deoxyribofuranose linked by phosphodiester bonds to a phosphate and nucleobase at 3' and 5' position, respectively.⁷⁵ DNA consists of 4 nucleobases: adenine (A), guanine (G), cytosine (C) and thymine (T). In the DNA helix, nucleobases and sugars are roughly perpendicular to each other, while the nucleobases are perpendicular to the central axis. The backbone of the DNA strand is 10 Å away from the central axis and consists of phosphate and β -D-deoxyribofuranose molecules, whereas the nucleobases, due to their hydrophobicity in comparison to other parts of the DNA, are located on the inside. Nucleobases form hydrogen bonds with each other: namely, A pairs with T whereas C pairs with G. This complementary base pairing, together with π - π stacking among the nucleobases, stabilizes the DNA helix.⁷⁶ Each turn of the DNA helix consists of 10.4 base pairs and (bp) the center-to-center distance between adjacent nucleotide pairs is 0.335 nm. The coiling of the two strands around each other creates two grooves in the DNA helix: major groove and minor groove.

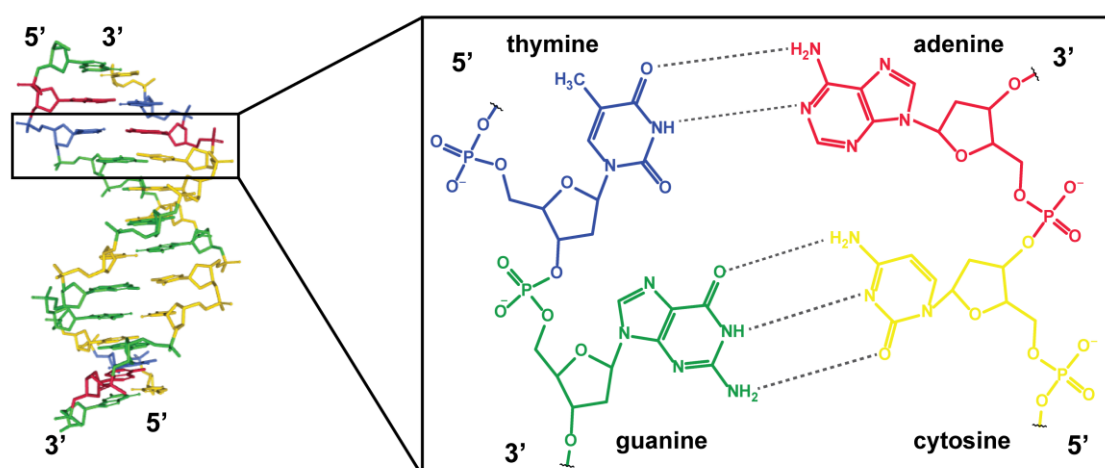


Figure 1-8. Structure of DNA. Left: Crystal structure of DNA dodecamer at high resolution (adapted from PDB: 2HKB). Right: Watson-Crick base pairing.

Conformations of DNA

The DNA helix changes its conformation due to external factors such as the hydration level, concentration of metal ions and polyamines, and internal factors such as the nucleotide sequence or the chemical modification of nucleobases. Changes in these factors can then lead to changes in the handedness of the DNA helix, length of the helical turn, numbers of the bases per turn and difference in major and minor grooves.⁷⁷ The most common conformations of DNA double helix include B-DNA, A-DNA and Z-DNA. B-DNA is the most common conformation of the DNA helix that occurs at high hydration levels present in cells. As described by Watson-Crick, B-DNA is right-handed and has a wide major groove, providing an easy access to DNA-binding proteins.⁷⁵ In comparison to B-DNA, A-DNA conformation is favored under dehydrating conditions. The A-DNA helix is wider, more rigid than B-DNA, right-handed and has about 11 bp per turn.⁷⁸ A-form helix is common for DNA-RNA hybrids, double-stranded RNA triplex-DNA and protein-DNA. On the other hand, Z-DNA is a left-handed form which occurs in DNA sequences containing methylated bases or alternating purine-pyrimidine tracts. In cells, Z-DNA plays a role as a transcription enhancer.⁷⁹ The Z-DNA helix has 12 bp per turn and it is narrower than B-DNA and A-DNA.^{80,81}

A-tracts

As mentioned above, the DNA sequence can greatly affect the conformation of the helix. One example are 'A-tracts', which consist of 4-6 adenine base pairs repeated with the helical periodicity.⁸² They produce an overall helix axis bend from 11-28° by decreasing the minor groove width from the 5' to the 3' direction along the A-strand. This is a result of propeller twist in the A-T pairs, which increases negative inclination of the adenine bases at the 3' side of the run of adenine bases.⁸³ Macroscopically, the A-tract-containing DNA migrates slower on the gel when compared with the same length DNA.⁸⁴ The curvature of the A-tracts can be explained by two models: the first one, called the wedge model, proposes that the curvature of the A-tract DNA occurs due to cumulative changes in dinucleotide steps, while retaining a normal B-DNA conformation; namely, the curvature is produced by uniform roll angles at ApA steps.⁸⁵ Another version of the wedge model proposes that all B-DNA sequences can be characterized by roll between base pairs and that ApA steps exhibit little or no roll with the curvature taking place outside the A-tract.^{83,86} The second model, however, proposes that the A-tract has an anomalous structure which yields base-pairs with negative inclination relative to the overall helix

1.3 DNA nanotechnology

axis.⁸⁷ Due to its anomalous structure, when A-tract is in the contact with the B-DNA, the bend at the junction is predicted. This model is based on fiber diffraction measurements of poly(dA)·poly(dT) and proposed by Crothers.⁸⁸ The presence of the A-tracts is of crucial importance when it comes to assembly of small circular DNA structures, which will be discussed in the following section.

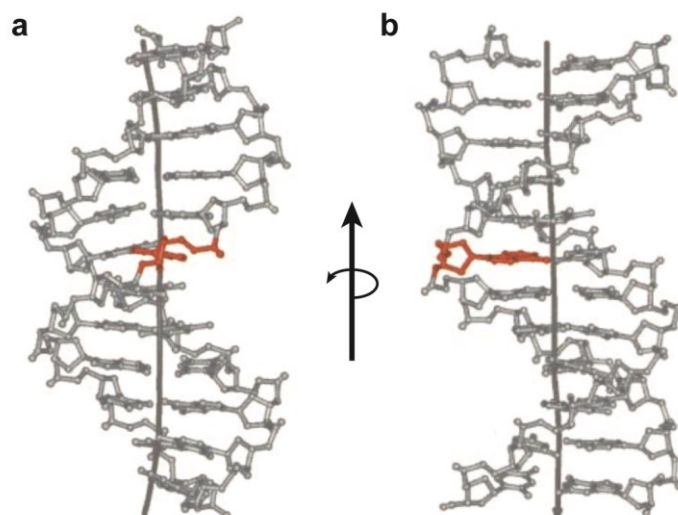


Figure 1-9. Structure of an A-tract DNA bend. The third adenosine nucleotide of the A-tract at position 6 in each helix is shown in red for orientation a) the deoxyribose of adenosine 6 is viewed in line with the best helical axis as computed by CURVES 5.3. b) 270° rotation of the A-tract about the z-axis.⁸³ Adapted with permission from Elsevier: Journal of Molecular Biology [81], copyright (2001).

Sticky ended cohesion of DNA double helix – DNA minicircles

The intrinsic bending of A-tracts has been widely employed, including the assembly of structural elements such as double-stranded DNA minicircles (dsDNA MCs).^{89–94} They have been assembled for the first time in 1986 by hybridizing two 21-base strand precursors (Figure 1-9 a).⁸⁹ These precursors had two A-tracts and were partially complementary, forming dsDNA with sticky ends as the main building unit for the DNA minicircle assembly. Due to the sticky-end cohesion, dsDNA MCs in various sizes (105 bp – 168 bp) were assembled. The presence of A-tracts in the design is crucial since they induce bending of the helical axis and therefore drastically reduce the ring strain. Furthermore, their presence is necessary for defining the directionality of the functional groups attached to the MCs. Thus, DNA MCs with gaps for versatile functionalization

1.3 DNA nanotechnology

have been assembled, which can be hybridized with any desired functionalized oligonucleotide to yield DNA MCs with specific properties.⁹² Moreover, DNA catenane⁹¹ and DNA rotaxane⁹⁰ have been assembled by interlocking dsDNA MCs, which have a great potential as components for molecular machines and motors. In 2015 it has been demonstrated that catenanes can be used to show switchable cyclic catalytic properties.⁹⁵ dsDNA MCs can be used as a building unit for higher-ordered structures: namely, when dsDNA MCs are labeled with polyamide struts, they can form multimeric structures in a controlled manner.^{93,94}

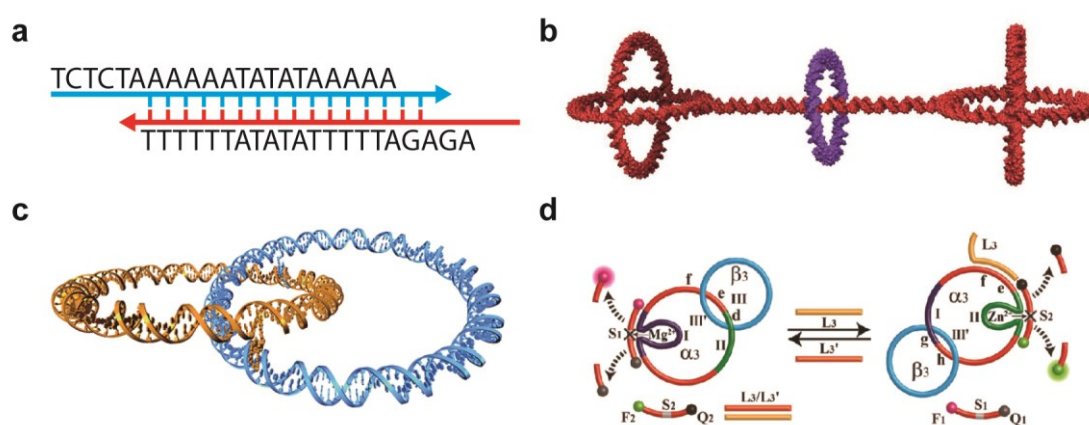


Figure 1-10: DNA minicircles applications. a) A-tract containing 21 nt precursor for circularized DNA assembly⁸⁹ b) double-stranded DNA rotaxane⁹⁰ Adapted with permission from Springer Nature: Nature Nanotechnology [90], copyright (2010). c) double-stranded DNA catenane⁹¹ Adapted with permission from ref. [91], copyright (2011), American Chemical Society. d) Switchable, cyclic, reconfiguration of a two-ring catenane system between the Mg²⁺-dependent DNAzyme, state A, and the Zn²⁺-dependent DNAzyme, state B, using L3 and L3' strands as reconfiguration promoters. The Mg²⁺-dependent DNAzyme cleaves substrate S1 leading to the fluorescence of F1, while the Zn²⁺-dependent DNAzyme cleaves substrate S2, leading to fluorescence of F2.⁹⁵ Adapted with permission from ref. [95], copyright (2015), American Chemical Society.

1.3.2 Structural DNA nanotechnology

Structural DNA nanotechnology aims at synthesizing and building sequences of nucleic acid complexes with nanoparticles and nanomaterials. It is based on two main effects: DNA hybridization induced by Watson-Crick base-pairing and stably branched DNA. The concept of DNA nanotechnology was established by crystallographer Nadrian Seeman

1.3 DNA nanotechnology

in early 1980s. He envisioned that a branched DNA can be used to create 3D lattices for orienting large molecules (such as proteins), which would simplify their crystallographic studies.⁹⁶ He was inspired by the Holliday junction, a naturally occurring branched DNA structure that is a key intermediate in genetic recombination. Holliday junctions consist of four DNA strands arranged into four double-helical arms. Since a naturally occurring Holliday junction contains sequences with homologous symmetry, it can isomerase (branch migration).⁹⁷ In order to overcome that, Seeman created a first asymmetric Holliday junction (4-arm junction) with single-stranded sticky ends, that self-assembled into a quadrilateral shape (Figure 1-11 a).⁹⁸ Consequently, the structure can be extended to form an infinite 2D lattice. Later on, asymmetric 3-arm, 5-arm and 6-arm junctions were created, followed by a synthetic cube made of DNA and DNA-truncated octahedron.^{99,100}

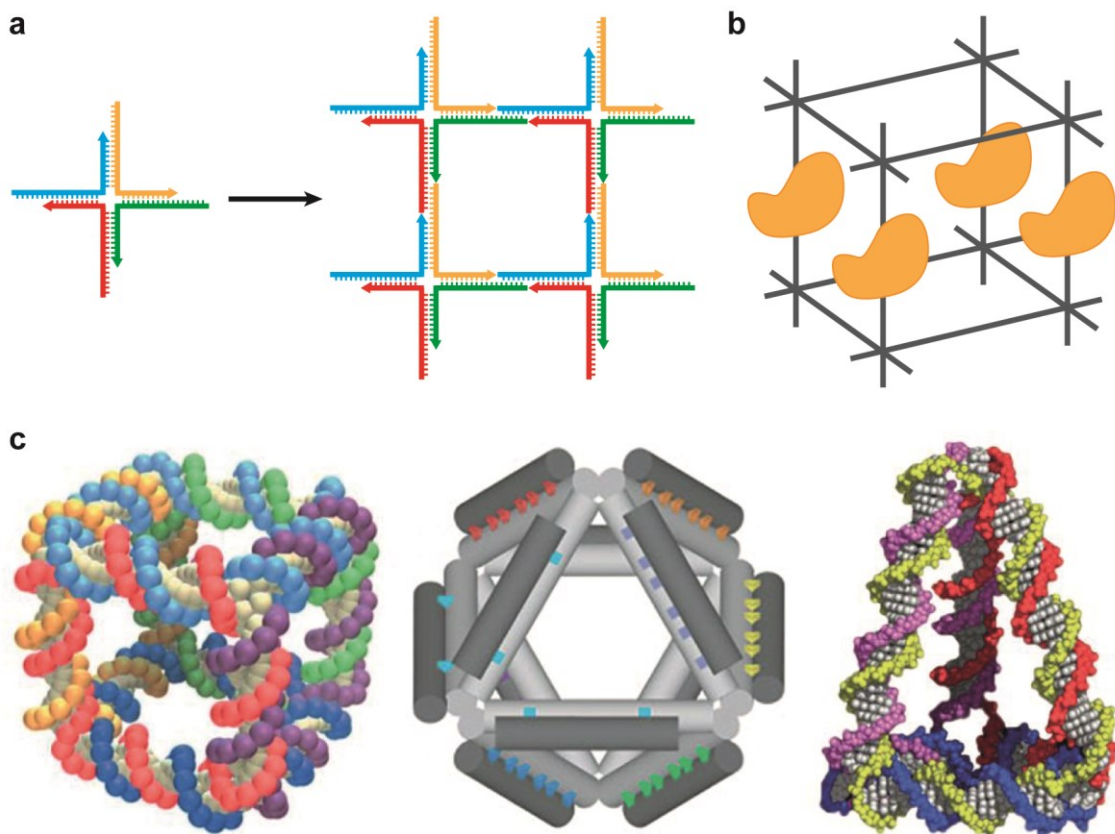


Figure 1-11. Foundations of DNA nanotechnology a) Immobile branched DNA (Holliday junction) with self-complementary sticky ends (left) can form a quadrilateral (right). The sticky ends outside of the quadrilateral are available so that the structure can be extended to form a 2D lattice. b) branched DNA with self-complementary sticky ends can

1.3 DNA nanotechnology

be used to form a crystalline array to which biomolecules can be attached. The artistic representations in panels a) and b) were inspired from the ref. [98] c) 3D DNA structures assembled from immobile junctions: DNA cube constructed from connected three-arm junctions⁹⁹ (left), DNA octahedron constructed from a long DNA strand and five connecting strands¹⁰⁰ (middle) and tetrahedron constructed from four DNA single strands.¹⁰¹ Panel c (left) is adapted with permission from ref. [99], copyright (2003), American Chemical Society. Panel c (middle) is adapted with permission from Springer Nature: Nature [100], copyright (2004). Panel c (right) is adapted with permission from The American Association for the Advancement of Science: Science [101], copyright 2004.

1.3.3 Scaffolded DNA origami

The first assembled structures based on immobile junctions and crossovers proved that DNA can be used as a building material for nanometer-size structures. However, the assembly of relatively complex structures was still challenging because it required multiple reaction steps and purifications, which resulted in low yields. Therefore, in 2006 Paul Rothemund published a method where the DNA structures are based on a long single stranded DNA ‘scaffold’ strand that folds into a designed pattern. This was achieved by the addition of many short single-stranded DNA strands, called ‘staple strands’, that bring together the parts of the scaffold strand to give the designed shape.¹⁰² This method creates DNA structures that approximate the outline of any desired shape, such as squares, discs and stars. Furthermore, it creates an addressable surface with area of $\sim 60 \times 90 \text{ nm}^2$ and enables the assembly of structures with arbitrarily shaped holes. DNA origami has been widely employed for building various 2D and 3D structures.^{103–105} These structures were used for embedding nanomechanical,¹⁰⁶ plasmonic¹⁰⁷ and drug delivery^{103,108} devices, as an aid to NMR structure determination^{109,110} and support for nanomechanical assembly line.¹⁰⁹ One of the interesting applications of DNA origami structures is for interaction with biological systems, which will be discussed in the next chapter.

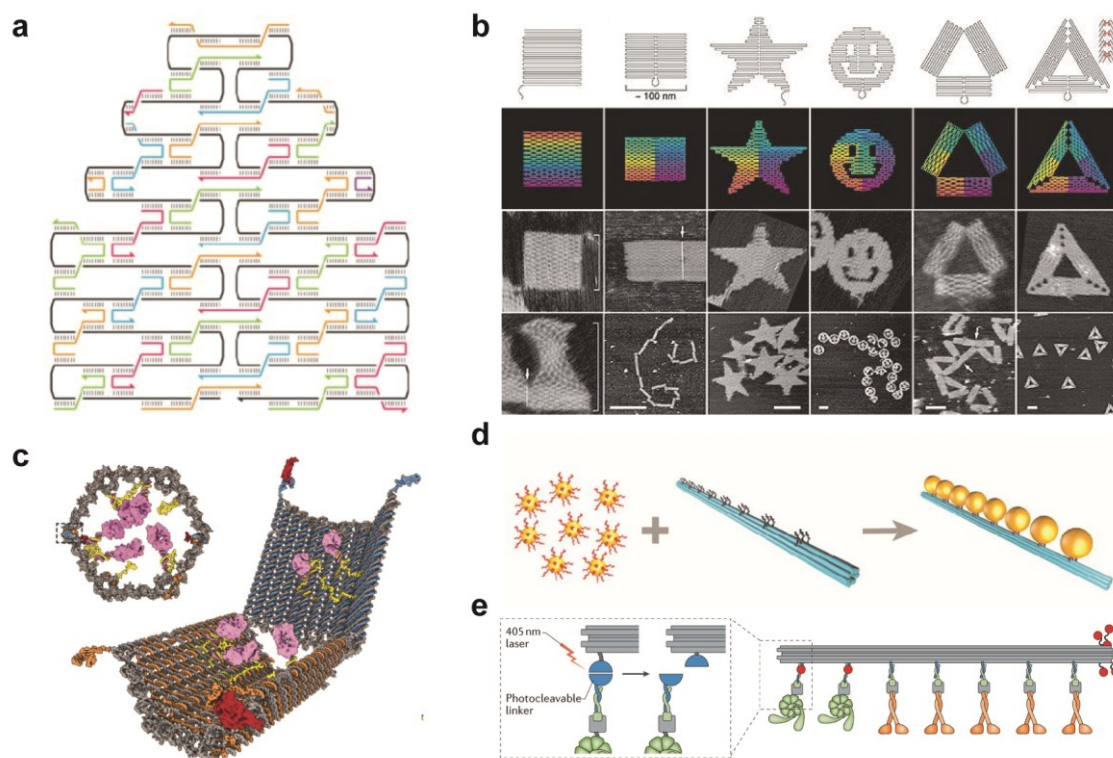


Figure 1-12. Scaffolded DNA origami principle and applications. a) Scaffolded DNA origami technique is based on folding a long, single-stranded DNA (black) with many short staples (orange, green, blue and red) into desired, programmable shapes¹⁰² b) first DNA origami assemblies proving that the method can be used to form arbitrary shapes. Scale bars: 100 nm. Panels a and b are adapted with permission from Springer Nature: Nature [102], copyright (2006). c) aptamer-gated DNA nanorobot for targeted drug delivery loaded with a protein payload (pink) in closed (left) and open (right) state. Aptamer locks consist of a DNA aptamer (blue) and a partially complementary strand (orange).¹¹¹ Adapted with permission from The American Association for the Advancement of Science: Science [111], copyright 2012. d) DNA origami as a platform for self-assembled plasmonic waveguide precursors: gold nanoparticles are arranged on a 6-helix bundle DNA origami in a programmable manner by mixing the DNA-functionalized gold nanoparticles with 6-helix bundles containing complementary strands.¹⁰⁷ Adapted with permission from ref. 107, copyright (2016), American Chemical Society. e) DNA origami-directed protein assembly: DNA origami is used to attach two motors of opposite polarity, dynein (green) and kinesin (orange), slowing or stalling its motion as a result of this ‘tug of war’. When dynein is photochemically cleaved (inset), motility is restored.¹¹² Adapted

with permission from The American Association for the Advancement of Science: Science [112], copyright 2012.

1.3.4 DNA nanostructure interaction with lipid bilayers

As mentioned above, DNA nanostructures can advance the understanding of biological processes: namely, they have been used as novel diagnostic tools,¹¹³ synthetic compartments of cells,¹¹⁴ modified-release systems for current drugs¹¹⁵ and targeted delivery of small molecules,¹¹⁶ peptides, proteins¹¹⁷ and mRNA.¹¹⁸ Since most of the structures mentioned above need to interact with lipid membranes in the cells, they need to be assembled in such a way that they interact with lipids, which usually does not occur in nature. In order to conjugate a charged molecule such as DNA with amphiphilic molecules such as lipids, two strategies have been developed: electrostatic interactions and hydrophobic functionalization of DNA.¹¹⁹

Electrostatic interactions

Due to its negatively charged backbone, DNA can electrostatically interact with positively charged lipids, such as DOTAP (1,2-dioleoyl-3-trimethylammonium-propane) and DOTMA (1,2-di-O-octadecenyl-3-trimethylammonium propane) in low salt concentrations.^{119–121} The presence of divalent cations (such as Mg^{2+} and Ca^{2+}) enables the electrostatic interaction between DNA and zwitterionic lipids, where divalent cations insert between phosphates of the neighboring lipids and neutralize them, resulting in a net positive charge. These interactions have been utilized to direct self-assembly of DNA origami structures into 2D lattices on supported lipid bilayer.¹²²

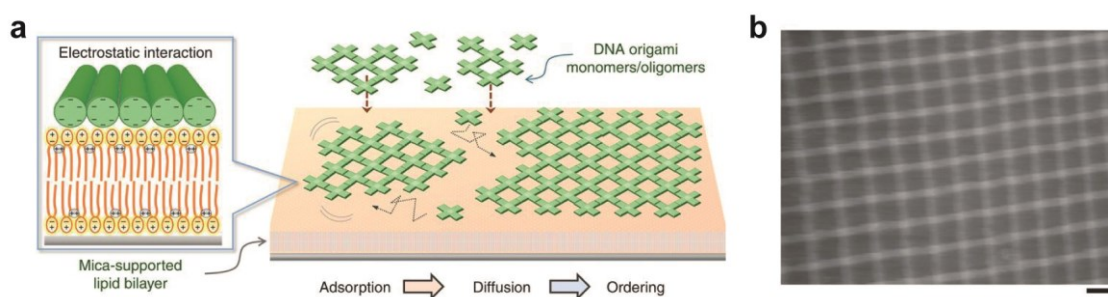


Figure 1-13. Utilizing electrostatic interactions between DNA and lipids: in the presence of divalent cations, mica-supported lipid bilayers can serve as a platform for self-assembly of DNA origami nanostructures.¹²² a) schematic representation of the assembly,

1.3 DNA nanotechnology

where DNA origami monomers (green) can stack together on the mica-supported lipid bilayer (orange), forming large 2D DNA origami structures b) AFM image of the lattice made from the DNA origami monomers. Scale bar: 100 nm. Adapted from ref. [122] (CC BY 4.0).

Hydrophobic functionalization

The most common way of assembly of DNA-lipid conjugates is by introducing hydrophobic groups to DNA. DNA can be hydrophobically functionalized either during the solid-phase synthesis and after the synthesis.

Modifications during the solid-phase synthesis include introducing porphyrin,¹²³ α -tocopherol,¹²⁴ poly(propylene oxide)¹²⁵ and lipids, particularly cholesterol to DNA.^{126–129} Due to its commercial availability, cholesteryl-labeled DNA has been used the most. The binding properties of cholesteryl-modified DNA structures depend on the linker on which cholesterol is attached: namely, the cholesterol itself tends to go to L_o phase, whereas cholesterol linked to tetraethylene glycol (TEG) partitions to liquid disordered phase (L_α).^{119,130} Cholesteryl-modified DNA structures have been used for the controllable assembly of DNA nanostructures on lipid membranes. This way, membrane sculpting can be monitored or membranes can serve as a support for DNA assembly.¹³¹ Cholesterol and porphyrin are used for anchoring the DNA nanopore into the lipid bilayer, which has a great potential for nanopore sequencing.^{128,132,133}

After the solid-phase synthesis and cleavage from the solid phase, DNA can be hydrophobically functionalized by reacting with thiol-, phosphorothioate-, amino- and azido-modified DNA. Phosphine-activated thiol-modified DNA reacts with maleimide-labeled lipids, resulting in lipid-labeled DNA.¹³⁴ This method has been used for self-assembly of size-controlled liposomes on DNA templates,¹³⁵ placing and shaping liposomes in reconfigurable DNA nanocages¹³⁶ and for studying lipid transfer between bilayers on a programmable DNA origami platform.¹³⁷ The most common substrate for phosphorothioated DNA are alkyl-iodides.¹³⁸ This reaction does not only increase hydrophobicity of the DNA – it also neutralizes the charge of the backbone. This is particularly important when it comes to embedding a DNA structure, such as nanopore, into the bilayer, because it provides higher hydrophobic coverage of the pore when compared to cholesteryl- and porphyrin- modified DNA nanopores.^{139,140}

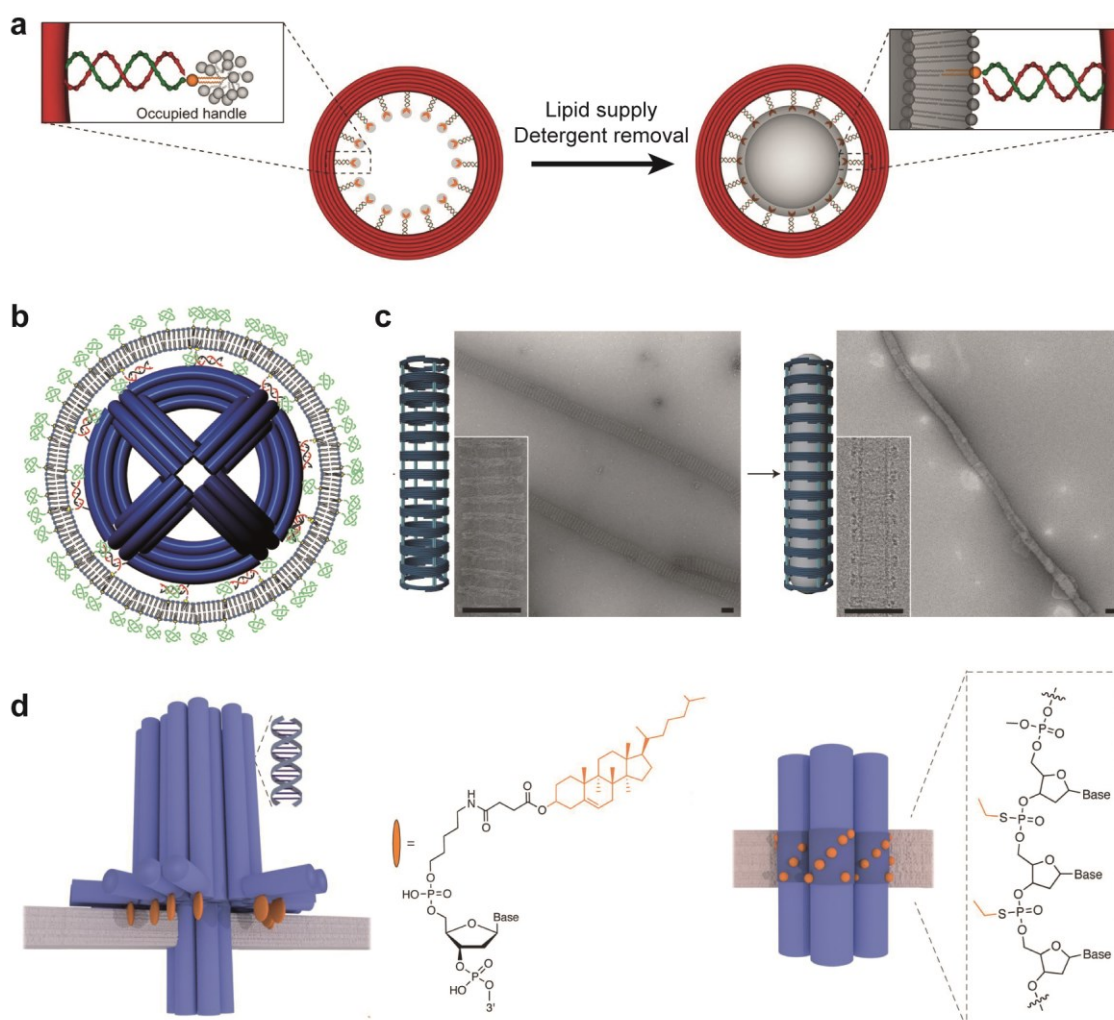


Figure 1-14. Interactions between hydrophobically functionalized DNA structures and lipids. **a)** DNA origami ring functionalized with 1,2-dioleoyl-sn-glycero-3-phosphoethanolamine (DOPE), which serve as seeds for vesicle formation (left). The functionalized rings were mixed with lipids in detergent and after the detergent removal, the liposomes with precise diameter were formed (right).¹³⁵ Adapted with permission from Springer Nature: Nature Chemistry [135], copyright (2016). **b)** DNA origami octahedron contains DNA-lipid conjugates that were the base for the assembly of fused lipid bilayer wrapped around the DNA structure¹⁰⁸. Adapted with permission from ref. [108], copyright (2014), American Chemical Society. **c)** DNA origami nanocages with lipid modifications pointing towards inside are used for templated assembly of width-defined membrane tubules.¹³⁶ Adapted with permission from Springer Nature: Nature Chemistry [135], copyright (2017). **d)** DNA origami nanopores that span lipid bilayers, featuring cholesterol-lipid anchors (left, center) and alkylated phosphorothioates.^{128,139,141} Panel c (left) is adapted with permission

1.3 DNA nanotechnology

from The American Association for the Advancement of Science: Science [128], copyright 2012. Panel c (right) is adapted with permission from ref. [139], copyright (2013), American Chemical Society.

Chapter 2 Motivation and objectives

Phospholipid bilayers and lipid-associated proteins perform a variety of functions vital to the survival of organisms. Since studies and manipulation *in vivo* are inherently challenging, several *in vitro* membrane-mimetic systems have been developed. Controlling the size and shape of introducing functional elements in a defined way is, however, difficult to achieve with common discoidal systems based on polymers, peptides or membrane scaffold proteins.

The aim of this dissertation was to employ the programmability of DNA nanotechnology to generate a novel membrane-mimetic system. Using DNA nanotechnology, arbitrarily shaped structures with precise dimensions can be created. Furthermore, the assembled DNA structures can be functionalized with Å precision with a large variety of artificial elements in a modular and programmable fashion. In Chapter 3, a strategy to prepare discoidal phospholipid bilayer structures encapsulated by an alkylated ds DNA minicircle is discussed, with the aim of assembling DNA-encircled lipid bilayers (DEBs) that provide control of size, shape and stability of engineered membrane mimetics.

In DEB technology, the lipid bilayer is stabilized by a 2 nm thick dsDNA minicircle, which stabilizes bilayers consisting of short-chain lipids. While this system provides a reliable way of reconstituting bilayers of programmable diameter, we wanted to expand its utility further, as reducing the design constraints of the DEBs will allow to tailor them to a wider variety of proteins. We have identified two ways to further improve the system: first by enabling lipid bilayer reconstitution in smaller-diameter minicircles and, in second place, by enabling the reconstitution of bilayers with longer-chain lipids. A solution that could help on both sides is to double the thickness of the DNA scaffold; the additional thickness would help with longer-chain lipids, while the additional alkylation points would provide more stable anchoring of the bilayer rim, leading to a smaller minimum diameter. This strategy, called “double-decker scaffold”, is discussed in Chapter 4.

As mentioned above, introducing functional elements in common membrane mimetic systems remains challenging; one of the keys to overcoming these issues is to ensure

the correct orientation of the protein within the lipid membrane. By exploiting the versatility of DNA, an approach to modify both the CCR5 and the DEBs with complementary DNA strands was taken. These additional anchor points would lock the protein in place, while keeping the desired orientation. This approach is discussed in Chapter 5.

Chapter 3 DNA-encircled lipid bilayers (DEBs)

The work presented in this chapter is published and sections 3.2, 3.3 and 3.44 were adapted with permission from Royal Society of Chemistry: Nanoscale ref [A], Copyright (2018). The coarse-grained molecular dynamics simulations were performed by Prof. Thomas Huber (The Rockefeller University, Prof. Sakmar Lab) and Dr. Xavier Periole (Aarhus University, then Prof. Schiøtt Lab). Protein expression and lipid phase transition studies were done by Madhumalar Subramanian (Helmholtz Zentrum Dresden – Rossendorf, Prof. Fahmy Lab). AFM imaging and tSEM imaging were done by Dr. Michael Matthies and Dr. Nayan Agarwal, respectively (former Ph.D. students at the Center of Advancing Electronics Dresden, TU Dresden, then Dr. Schmidt Lab).

3.1 Introduction

Cell compartmentalization by membranes is crucial in biology and membrane-associated proteins contribute to fundamental cellular processes in energy conversion, cell communication and signal transduction. Membrane protein function is often linked to conformational transitions which may be critically affected by lipid protein interactions.^{142–146} As *in vivo* investigations are often very challenging, such functional implications of lipid protein interactions¹⁴⁷ can be more easily studied *in vitro* with artificial membrane-mimetic systems which provide a native-like lipid environment. For example, planar discoidal nanoscale lipid bilayers surrounded by amphipathic polymers¹⁴⁸ or surfactant-like helical peptides¹⁴⁹ have been described. Other than in spherical vesicles, these bilayers provide access to both sides of the bilayer, which may become important when studying transmembrane proteins and signal transduction. Most commonly, discoidal planar bilayers are assembled from dimeric apolipoprotein AI-derived proteins, which encircle a lipid bilayer, thereby sealing its hydrophobic rim to form nanodiscs (NDs). These membrane scaffold proteins (MSPs) typically support lipid bilayers of 10–16 nm in diameter.^{65,150,151}

The demand for controlling the size and shape of discoidal membrane mimetics has been met by expression of MSP variants.⁶⁷

DNA nanotechnology provides an alternative approach to create membrane nanoparticles with defined and programmable parameters⁹⁸ since it has proven to enable the fast de novo design of arbitrarily shaped structures.¹⁰² For large, mega-Dalton-sized structures, typically measuring tens to hundreds of nanometers, the DNA origami approach became particularly popular due to its robustness and versatility.^{152–154} For some applications, smaller structures such as tetrahedra,¹¹⁶ icosahedra,¹⁵⁵ or structures from DNA minicircles (MCs)^{90,91,107,119,156,157} consisting of fewer synthetic oligonucleotides can be better suited and are more economical. Due to the full addressability of DNA structures, they can be functionalized with Å precision with a large variety of artificial elements¹⁵⁴ including small molecules, fluorophores, functional groups, biomolecules or inorganic nanoparticles¹⁰⁷ in a modular and programmable fashion.

With the aim of leveraging these advantages of DNA nanotechnology for the design and synthesis of nanoscale discoidal lipid bilayers in the size range of NDs, we developed protein-independent DNA-encircled lipid bilayers (DEBs).

3.2 Results and discussions

3.2.1 DEB design

In our approach, we conceptually replaced the MSP of nanodiscs by a circular double-stranded DNA minicircle (dsMC). For this, alkylated oligonucleotides were hybridized to a single-stranded minicircle (ssMC) such that all alkyl chains point to the inside and thus stabilize the lipid bilayer. An overview of the strategy can be observed in Figure 3-1.

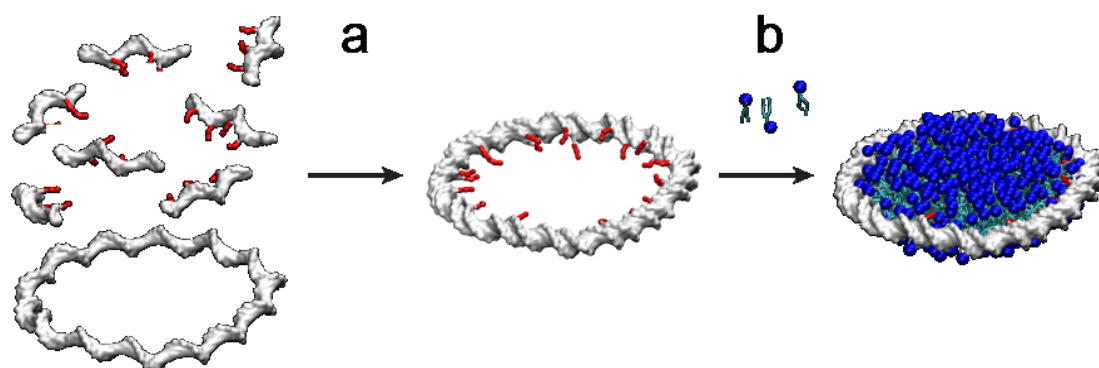


Figure 3-1. Assembly of the DEBs. a) ssDNA MCs (bottom) react with 7 complementary strands, each carrying 4 alkyl groups in red (top) forming a double-stranded DNA MC b) in the presence of lipids, bilayer is formed inside the ds DNA MC, resulting in DEB formation.

3.2.2 DEB formation strategy

Assembly of DEBs can be broken down into four steps: alkylation of the complementary oligonucleotides, ssMC assembly, dsMC assembly and DEB assembly.

ssMC assembly

Single-stranded DNA minicircles were assembled by splint ligating a 147 bases long linear oligonucleotide consisting of 14 intrinsically curved A-tracts within the sequence to facilitate the formation of rings with a diameter on the nanometer scale (16 nm). After the ligation, the residual long oligonucleotides, splints and linear side products were enzymatically removed by a treatment with Exonuclease I/III (Figure 3-2 b). The synthesis of the ssMC was confirmed by a denaturing PAGE gel (Figure 3-2 c)

Alkylation of complementary strands

In order to enable lipid-DNA interaction, we needed to introduce hydrophobic groups to the DNA. Our approach was based on selective alkylation of phosphorothioates (PTOs), established by Gut and Beck in 1995.¹³⁸ In this reaction, alkyl iodide reacts with the thiol group on PTO-labeled DNA via nucleophilic substitution to yield alkyl-protected DNA. Our short 21-nt complementary strands were functionalized with two or four internal PTO groups. These strands reacted with an excess of ethyl iodide, butyl iodide or decyl iodide

3.2 Results and discussions

(Figure 3-2 a). As a result, the modified phosphorothioate is not charged anymore, which increases the affinity of the modified DNA segment to the lipid bilayer rim. The respective alkylated oligonucleotides were HPLC purified and alkylation was confirmed by ESI mass spectrometry.

dsMC assembly

The dsMCs were formed by hybridization of the ssMC with seven complementary alkylated oligonucleotides (Figure 3-2 d). The position of the alkylation (specific thymidines in A-tracts) was chosen in a way that forced the alkyl groups to be oriented towards the center of the ring. Excess oligonucleotides were removed by ultrafiltration and the double-stranded minicircles (dsMCs) were then analyzed by native agarose gel electrophoresis (Figure 3-2 e), atomic force microscopy (AFM) and transmission scanning electron microscopy (tSEM) (Figure 3-3).

DEB assembly

Three different types of lipids were selected for the DEB formation, unless otherwise stated. As the main component of the bilayer, saturated phospholipids with short chains were chosen. Secondly, lipids with positively charged heads were selected in order to interact with negatively charged phosphate groups of the dsDNA ring. The phosphate groups next to the alkylated PTO groups will be preferentially targeted due to the additional Van-der-Waals interactions between the lipid and alkyl chains. In order to visualize the presence of the lipid bilayer in the dsDNA-nanodisc complex, a fluorescently labelled lipid was incorporated.

After the selected lipids were dissolved in detergent, dsDNA rings were added in stoichiometric ratio (lipid : MC was 450:1) and the complex was formed by removing the detergent (Figure 3-2 f-g).

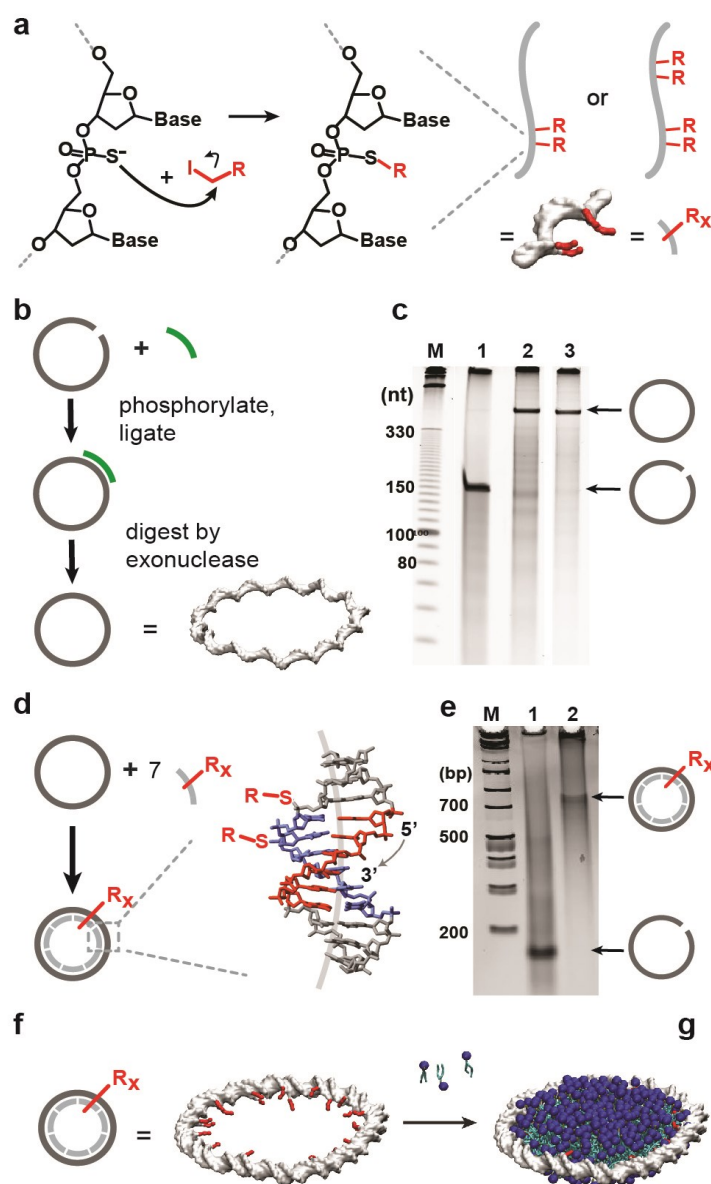


Figure 3-2. Synthesis of DEBs. a) Short oligonucleotides with two or four phosphorothioates are alkylated with alkyl iodides (red). b) A circular single-stranded template is synthesized by enzymatic splint ligation from a long, linear oligonucleotide (grey). Residual splints (green) and linear templates are digested by exonuclease treatment. c) A denaturing PAGE gel confirms the synthesis of the single-stranded minicircle (ssMC). M, molecular size marker (nt); lane 1, linear long oligonucleotide; lane 2, ligation reaction before exonuclease treatment; lane 3, exonuclease digest. d) The ssMC is hybridized with seven alkylated oligonucleotides into double-stranded MCs (dsMC). The position of alkylations, and the intrinsic curvature of the A-tracts (grey line in the center of the helix,

3.2 Results and discussions

exaggerated) in a model of an A-tract^{84,158} (adapted from PDB structure 1FZX). Adenosines are colored red, thymidines blue. e) Native PAGE gel. M, marker (base pairs); 1, linear long oligonucleotide; 2, the assembled dsMC complex. f) The dsMC is incubated with phospholipids (blue) to form a mature DEB (g).

3.2.3 DEB analysis

Assembled and purified DEBs were characterized by atomic force microscopy (AFM) and transition scanning electron microscopy (tSEM). AFM imaging of the dsMCs and DEBs revealed a doubling of the height of the empty DNA minicircles from ~1.3 nm to ~2.5 nm due to the addition of the lipid bilayer (Figure 3-3 a-c). Absolute diameters or heights of soft, compressible biomolecules can usually not be measured with standard AFM imaging due to the mechanical deformation during scanning caused by the AFM tips and additional deformations caused by interactions with highly charged surfaces. As a result, both the DNA (actual thickness = 2 nm) and the DMPC bilayer (thickness = 4-5 nm) appear thinner than in force-free environments. The tSEM images (Figure 3-3 d-f) also confirm the presence of a lipid bilayer in the DEBs with short (14 ethyl) and longer (28 decyl) alkyl chains.

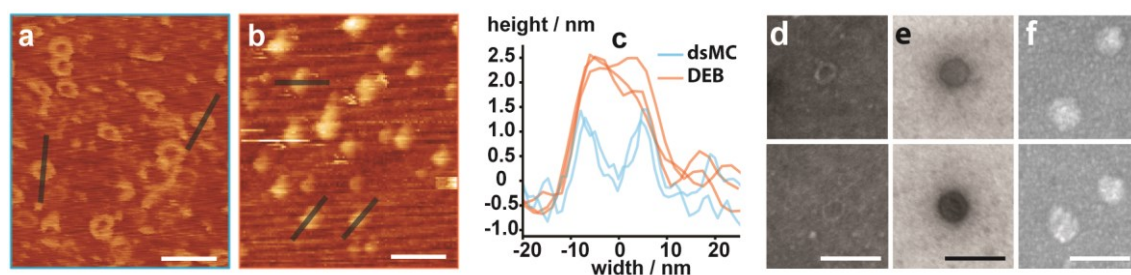


Figure 3-3. Analysis of dsMCs and DEBs. a) An AFM image of empty dsMCs ($R = 4$ butyl) and corresponding DEBs (b). c) Height profiles. d) tSEM images of empty dsMCs. e) tSEM image of a DEB with 14 ethyl modifications (positively stained). f) tSEM image of a DEB with 28 decyl modifications. Scale bars, 50 nm.

Assembled DEBs were purified either by size-exclusion chromatography (SEC) or by ultracentrifugation, where DEBs formed one sharp band, coming from the fluorescent lipid, that contained both lipids and DNA. The intensity of the band depends on dsMC hydrophobicity: namely, the intensity was higher for DEBs containing 28 decyl groups

3.2 Results and discussions

than DEBs containing 28 butyl groups. The decyl-alkylated DEBs show higher lipid retention rate, leading to increased fluorescence of the ultracentrifuge layer due to the higher concentration of lipids, as can be seen in Figure 3-4 a-c.

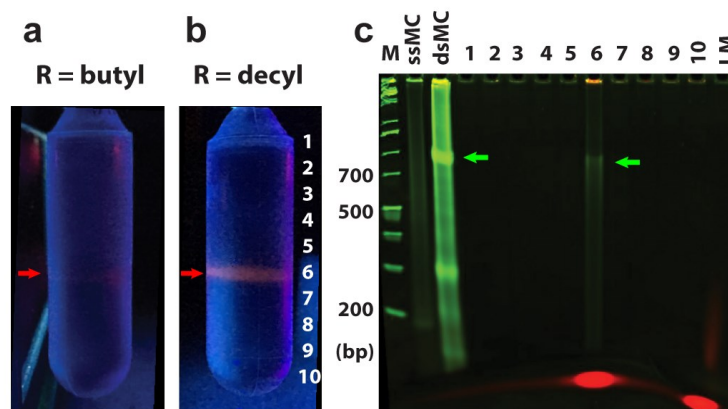


Figure 3-4. Analysis of DEBs. Gradient ultracentrifugation results of Rhodamine-PE- containing DEBs with 28 butyl groups (a), and 28 decyl groups (b). The latter was analyzed by native SDS PAGE (c). LM = control lipid mix

In syntheses of ssMCs at high concentrations, dimeric ligation products occurred as a side product (Figure 3-5). They were separated by SEC from the monomers and exhibited twice the circumference of monomers (Figure 3-5 d, e). This result demonstrates that the DEB approach can be extended to enable designs with custom sizes.

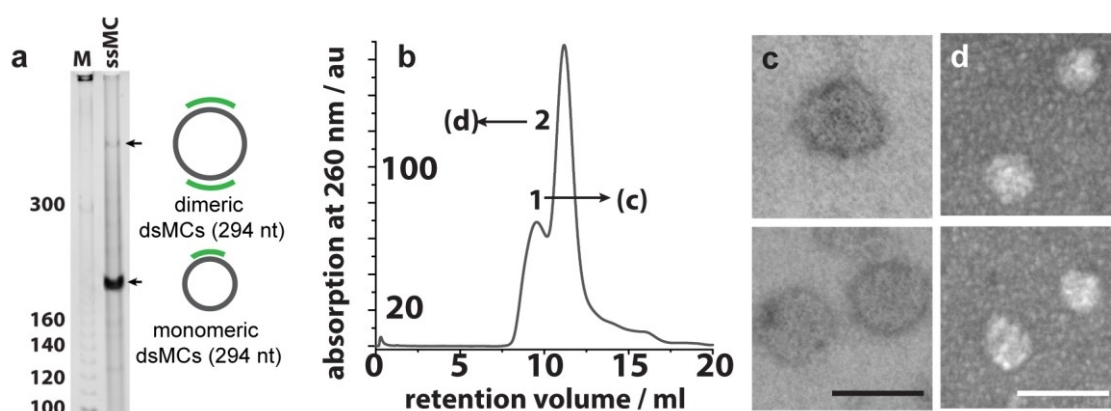


Figure 3-5. Analysis of dimeric ligation products. a) Denaturing PAGE gel (6 %) of a splint ligation experiment for the synthesis of ssMC after exonuclease treatment. For entropic reasons, circularizations are favored over polymerizations. In some experiments, dimeric

3.2 Results and discussions

single-stranded minicircles were observed as side products. Note that the electrophoretic mobility of the ssMC is different from the one in Figure 3-2 c. In general, circulated oligonucleotides have a lower mobility than their linear equivalents, but the extent of this difference is a function of the concentration of the PAGE gel. In Figure 3-2 c, a 15% gel was used, whereas a 6% gel is shown that was chosen to increase the resolution for the high molecular weight ssMC dimer. The splints (green) are only added to the scheme for clarity; they are digested during the exonuclease step. b) Elution profile of a size exclusion chromatography (SEC) run of a DEB preparation. Fraction 1 contains dimeric DEBs (c), fraction 2 monomers (d). Scale bars, 50 nm

3.2.4 Lipid phase transition in DEBs

We compared the thermotropic phase transition of DMPC in conventional MSP-based NDs with that of DEBs by using the emission of the lipophilic dye LAURDAN as a sensor of lipid order.¹⁵⁹ The dye binds at the sub-headgroup region of lipids. Its excited state energy depends on the dipolar relaxation processes in its environment leading to a red shift of LAURDAN fluorescence with increasing hydration that accompanies the gel to liquid phase transition of the lipid. Therefore, the phase transition can be monitored by the relative intensity difference measured at two LAURDAN emission wavelengths, i.e. the so-called general polarization (GP).¹⁶⁰ The midpoint temperature T_m for the gel to liquid transition of DMPC in DEBs was 25 °C and agrees with literature data on DMPC vesicles,¹⁶¹ whereas DMPC in NDs showed a slightly higher T_m (31 °C) as reported (Figure 3-6 a, b).¹⁶¹

However, the change of the GP value in DEBs was only ~50 % of that in NDs transition, which may indicate restricted lipid mobility at the alkylated DNA-lipid interface. Upon doping of the DMPC bilayer with the cationic lipid DMTAP, no phase transition was observed (Figure 3-6 c, d), which we attribute to the additional electrostatic interactions of the positively charged head groups with the dsMC, and to a preferential binding of LAURDAN at the DNA lipid interface.

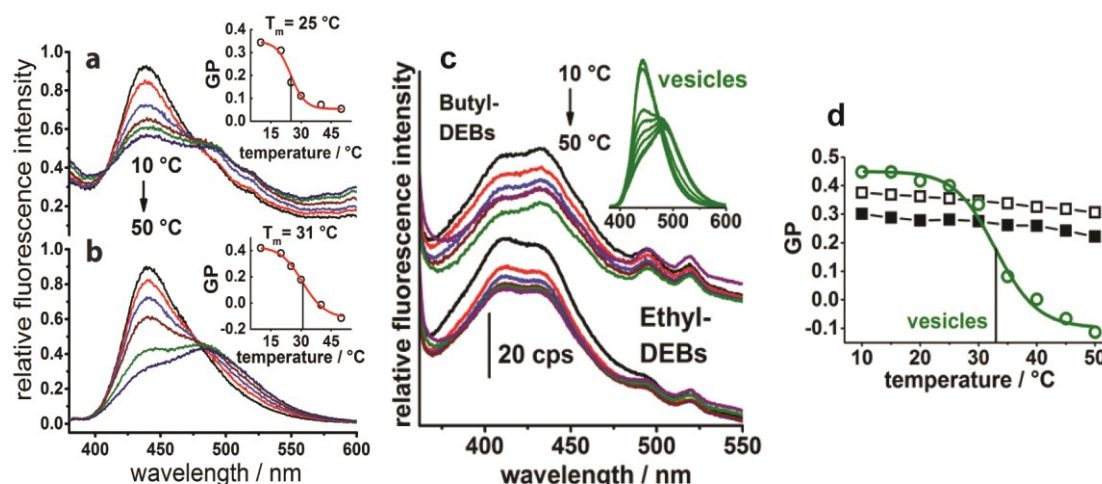


Figure 3-6. Lipid phase transition of DEBs. Emission spectra of LAURDAN ($\text{exc} = 340 \text{ nm}$) in DMPC-filled DEBs carrying two ethyl groups per hybridized 21-mer (a) and in MSP-based NDs (b) recorded at 10 °C, 20 °C, 25 °C, 30 °C, 40 °C and 50 °C. Inserts show the temperature dependence of the generalized polarization, $GP = (I_{440} - I_{490}) / (I_{440} + I_{490})$ which reveals the gel to liquid phase transition of the lipid bilayer (T_m : transition midpoint temperature).¹²⁹ c) Emission spectra of LAURDAN ($\lambda_{\text{exc}} = 340 \text{ nm}$) in DMTAP:DMPC (1:10) with DEBs carrying four ethyl or butyl chains per 21-mer (cps: counts per second). Insert: LAURDAN emission from the identical lipid mixture in vesicles. d) The generalized polarization (GP) calculated from the intensities at 435 nm and 495 nm indicates a marginal phase transition in both ethylated (open squares) and butylated (filled squares) DEBs. The GP value determined for vesicles comprised of the same DMTAP/DMPC mixture (circles) evidences a phase transition with $T_m = 33 \text{ °C}$.

3.2.5 Coarse-grained simulations of DEBs

In order to calculate stability of the complexes, we prepared coarse grain molecular dynamics (CGMD) simulations of a DEB using the MARTINI force field (Figure 3-7).^{162,163} The simulations show that both the position of alkyl chains on the dsDNA ring and their length play a crucial role in the stability of DEBs: specifically, they showed that the shorter alkyl chains (ethyl – octyl) do not anchor the lipid bilayer completely, leading to the reduced stability of the DEBs, whereas the longer alkyl chains (decyl, dodecyl) stabilize the complex during the entire simulation period (5 μs). These results are not completely in agreement with experimental results since the DEBs with lower alkylation points were

3.2 Results and discussions

assembled (14 ethyl groups, Figure 3-7 e). However, the yield of the DEBs with 28 decyl groups was higher than yield of DEBs with 28 butyl groups (as discussed in Section 3.2.3), which can be explained with lower stability of the DEBs with less alkyl groups. The DEB with 28 decyl groups was stable over a 5-microsecond duration with the 4 nm thick DMPC bilayer encircled by the 2 nm thick dsDNA rim. The interaction of the alkyl chains (Figure 3-7 a-b, red) with the lipid bilayer could also be clearly observed, demonstrating the effectiveness of our modification strategy.

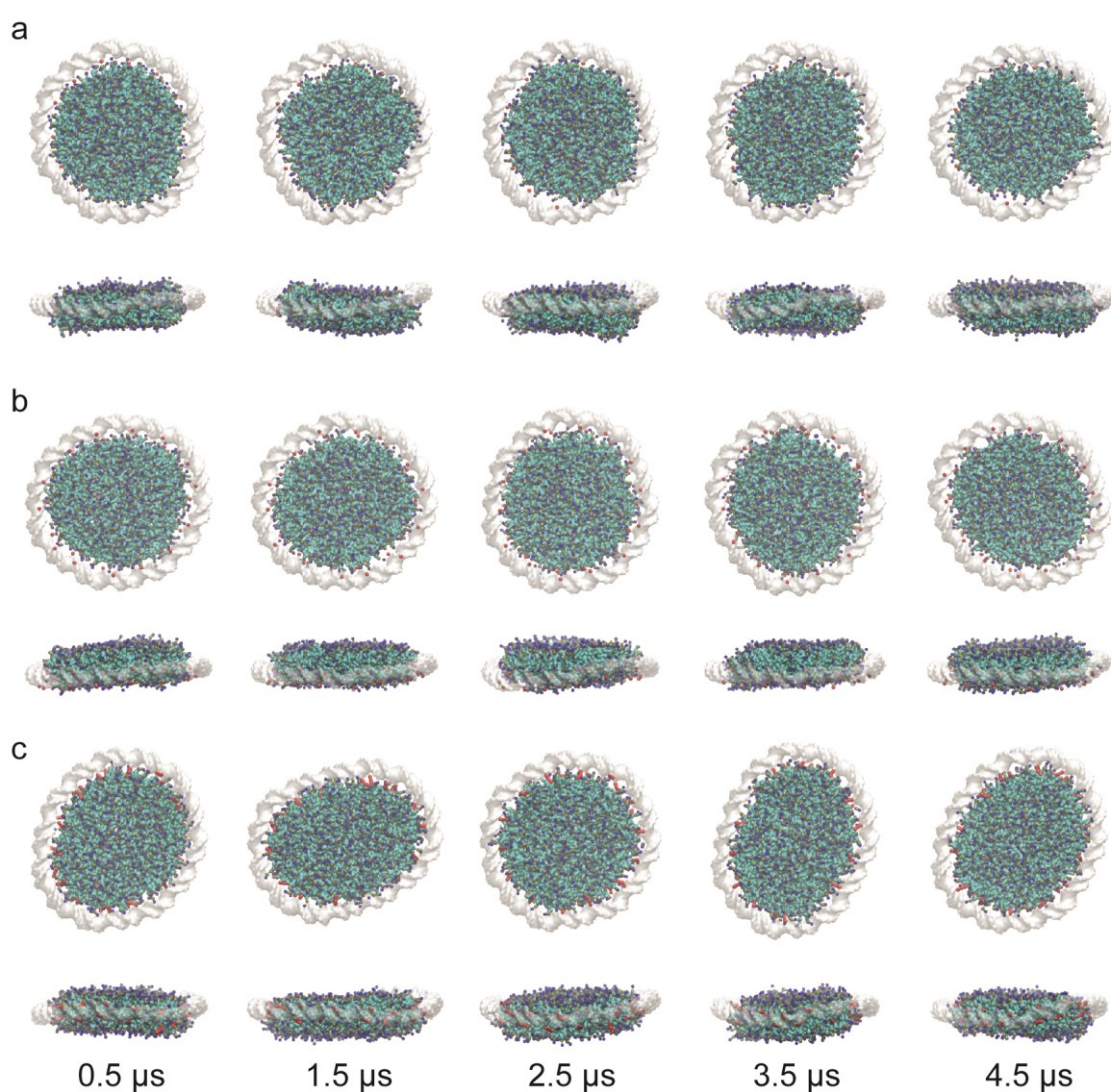


Figure 3-7. Coarse grain molecular dynamics model of a DEB composed of a 147 bp dsMC with 14 butyl (a), 28 butyl (b) and 28 dodecyl (c) groups and 434 DMPC lipids. DNA is white, alkyl chains red, DMPC head groups blue. Snapshots were taken after

1-microsecond intervals. Up: view down the membrane normal of a structure at the end of the 5 microseconds long trajectory. Down: View rotated 90 degrees.

3.3 Conclusions and outlook

In summary, we report the formation of DEBs as a novel strategy to prepare nanoscale discoidal bilayer structures encapsulated by an alkylated dsMC. The difficulty in preparing nanoscale membrane mimetics is to prevent formation of vesicles, which are the preferred state of lipid bilayers. Thus far, only the shaping of spherical vesicles with DNA structures has been reported. With the DEB technology we have realized for the first time the use of DNA to assemble planar lipid bilayers with dimensions that are comparable to protein-stabilized NDs. In contrast to the DNA origami approach, which requires hundreds of oligonucleotides and expensive single-stranded scaffold strands, the minimalistic DEB design can be accomplished with only two commercial synthetic oligonucleotides and facilitates upscaling. Only one oligonucleotide has to be chemically modified, and the chosen alkylation of phosphorothioate is among the most economical and scalable modification approaches. We have demonstrated a high alkylation density of up to two DNA backbone alkylations per helical turn without additional linkers, to stabilize the lipid bilayer. In addition to the demonstrated ease of DEB size variation, the core structure of DEBs is provided by a covalently circularized ssMC. The proposed DEB design is thus inherently independent of more sophisticated biochemistry required for improving stability and monodispersity of protein-based scaffolds via circularization.⁶⁸ We anticipate that further developments of the DEB technology will provide a nanoscale membrane mimetic that profits from the attractive links to DNA technology towards higher order assemblies and spatial arrangements of lipid bilayers for studying their interactions with membrane-associated proteins.

3.4 Methods

3.4.1 Materials

Enzymes and respective buffers were purchased from New England Biolabs. Oligonucleotides were synthesized by Integrated DNA Technologies and chemicals were purchased from Sigma- Aldrich unless stated otherwise. Lipids in chloroform solution were

purchased from Avanti Polar Lipids. Denaturing polyacrylamide gel electrophoresis (PAGE) gels (15% TBE urea gels), SYBR Gold gel stain and Pierce detergent removal columns were purchased from Thermo Fisher Scientific. Ladders for the PAGE were either 10 bp ladder (Invitrogen) or O'GeneRuler™ 1kb plus ladder (Thermo Fisher).

Oligonucleotide sequences

short oligonucleotide with 2 phosphorothioate (PTO) groups: 5'-TTT TTC ACA CTT T*TT* CAC ACT-3'

short oligonucleotide with 4 PTO groups: 5'-TT*T T*TC ACA CTT T*TT* CAC ACT-3'

(asterisks indicate the locations of backbone phosphorothioates)

long oligonucleotide: 5'-(TGT GAA AAA AGT GTG AAA AAG)₇-3'

splint: 5'-CTT TTT TCA CAC TTT TTC AC-3'

3.4.2 Alkylation of short oligonucleotides

The chemical modification of the phosphorothioated oligonucleotides was conducted by following a modified protocol of Gut and Beck.¹³⁸ Phosphorothioate-modified oligonucleotides (20 nmol, 21 nt) were reacted with 1 µmol alkyl-iodide in 90% DMF (Alfa Aesar) and 10% 30 mM Tris-HCl pH 7.5 (1000 µL). The mixture was incubated at 65 °C for 4 h. The excess of the organic solvent was removed by gel permeation using NAP-25 columns (GE Healthcare). The collected water fraction was purified by reversed phase HPLC (loaded volume: 125 µL per run) using a Dionex (ICS-5000+ TC) system with a MultoKrom 100-5 C18 column (flow rate 1 mL/min) using the following gradient starting points (difference to 100%: triethyl ammonium acetate (TEAA; 20 mM; pH 8 with 3% acetonitrile (ACN))):

0 min, 3% ACN

10 min, 10 % ACN

25 min, 21% ACN

30 min, 100% ACN

35 min, 100% ACN

40 min, 3% ACN

The retention time for the starting compound (phosphorothioated oligonucleotide) was 8.1 min, whereas the retention time for the alkylated oligonucleotides was 15.2 min (2 ethyl groups per short oligonucleotide), 19.0 min (4 butyl groups per short oligonucleotide) and 26.1 min (4 decyl groups per short oligonucleotide). The eluted samples were collected for further experiments and characterization.

Mass spectrometry

The mass of the alkylated oligonucleotides was determined from the collected HPLC fractions with a combined HPLC-MS system (Waters ACQUITY UPLC S4 with a Ultra Performance/Waters ACQUITY TQ Detector). The masses of the functionalized oligonucleotides were determined by deconvolution of the peaks with multiple charges.

3.4.3 ss DNA MC design and preparation

The long oligonucleotide (147 nt, IDT Ultramer) and the splint (19 nt) were designed with the OligoAnalyzer Tool (idtdna.com) disregarding potential sequences with strong secondary structures. The long oligonucleotide (3.33 μ M, 100 pmol) was hybridized to the splint (66.67 μ M, 2 nmol) in 1X ligase buffer (50 mM Tris-HCl, 10 mM MgCl₂, 1 mM ATP, 10 mM DTT, pH 7.5; total volume: 30 μ L) using a 12 min thermal annealing program (80 °C, 1 min, 80 °C – 25 °C -5 °C/min, 25 °C hold). The annealed mixture was diluted twofold in 1X ligase buffer and treated with 1 μ L polynucleotide kinase (10 000 units/mL) and 1 μ L T4 ligase (400 000 units/mL) for 1 h at room temperature, after which another 0.5 μ L of each enzyme were added and the reaction mixture was incubated for one more hour at 30 °C. The mixture was purified with Zymo Oligo Clean & Concentrator columns (Zymo research) according to the manufacturer's protocol and the DNA was recovered in 40 μ L of water. The non-circular byproducts or linear oligonucleotides were digested in 1X exonuclease I buffer (67 mM Glycine-KOH, 6.7 mM MgCl₂, 10 mM β -ME, pH 9.5) supplemented with 1X exonuclease III buffer (10 mM Bis-Tris-Propane-HCl, 10 mM MgCl₂, 1 mM DTT, pH 7), and 1.5 μ L of exonuclease I (20 000 units/mL) and 1.5 μ L exonuclease III (20 000 units/mL; total volume: 55 μ L) for 3 h at 37 °C. The removal of the enzymes and buffer exchange were performed with Zymo Oligo Clean & Concentrator. ssMCs were recovered in 20 μ L of water and analyzed by denaturing PAGE.

Denaturing PAGE

For the denaturing PAGE analysis, 15% gels were cast with 1X TBE buffer (100 mM Tris base, 100 mM boric acid, 2 mM EDTA) containing 6 M urea and run in 1x TBE buffer. 9 μ L of sample solution were mixed with 9 μ L of 2X gel loading dye (7 M urea, 89 mM Tris, 89 mM boric acid, 2 mM EDTA, pH 8.0, 12% Ficoll, 0.01% bromophenol blue, 0.02% xylene cyanole). As a reference, 2 μ L of 10 bp DNA ladder (Thermo Scientific) were added. The gels were run at 200 V, 55 °C for 45 min inside an isolating Styrofoam box filled with ~2 L of hot tap water, after which they were stained and imaged the same way as described native PAGE (see below).

3.4.4 dsDNA MC formation

The ds DNA MCs were formed by hybridization of the ssDNA ring (7 μ M) with complementary alkylated oligonucleotides (70 μ M) using a 12 min thermal annealing program (80 °C, 1 min, 80 °C – 25 °C -5 °C/min, 25 °C hold) in 12 mM MgCl₂ and 5 mM TE buffer (50 μ L). The excess of the complementary oligonucleotides was removed by ultrafiltration as described below. The purified ds MCs were analyzed by native PAGE.

Purification of ds MCs with ultrafiltration columns

Passivation of the ultrafiltration filter (10 kDa MWCO, Amicon Ultra, AMD Millipore) membranes was carried out by incubating them in 400 μ L of 1X buffer H (50 mM HEPES pH 7.4, 200 mM Na₂SO₄ and 5 mM MgSO₄) for 30 min, after which the buffer was passed through the filters at 14,000 rfc for 2 min. The assembled ds DNA MC solution was added to the passivated filters and washed two times with 400 μ L of 1X buffer H at 14,000 rfc for 13 min. After the final wash, the filter was reversed, placed in a fresh tube, and centrifuged at 1,000 rfc for 2 min. The collected purified dsMC solution was used for further characterization and reactions.

Native PAGE

For the native PAGE analysis, 10% gels were cast with 1X TBE buffer containing 12 mM MgCl₂. Running buffer contained 1X TBE buffer and 12 mM MgCl₂. 15 μ L of sample solution were mixed with 3 μ L of 6X gel loading dye (50% glycerol, 5 mM Tris-HCl, 1 mM EDTA, 12 mM MgCl₂, 0.25% bromophenol blue and 0.25% of xylene cyanol). Electrophoresis was performed at 65 V for 12 h at room temperature. As a reference, 2 μ L of

1 kb plus DNA ladder (Thermo Scientific) were added. After the electrophoresis, the gel was removed from the gel cassette and stained for 10 min with 1X SYBR Gold in 50 mL 1X TBE supplemented with 5% ethanol and imaged with a Typhoon FLA 9500 gel scanner (GE Healthcare) using the excitation wavelength of 488 nm suitable for SYBR Gold stained gels.

3.4.5 DEB formation and purification

14:0 DMTAP (1,2-dimyristoyl-3-trimethylammonium-propane), 14:0 Rhodamine-PE (1,2-dimyristoyl-sn-glycero-3-phosphoethanolamine-N-(lissamine rhodamine B sulfonyl)) and DMPC (1,2-dimyristoyl-sn-glycero-3-phosphocholine) were mixed in a 9.9:1.4:88.7 molar ratio to reach 112.3 μ L total volume. The chloroform was evaporated using an argon line for 2 h, followed by drying under vacuum for the next 2 h. The lipid film was dissolved in 90 μ L of 60 mM sodium cholate in buffer H (final concentration: 1.5 mM) and sonicated five times for 1 min. Next, 30 μ L of the ds DNA MCs were added (2.4 μ M) to obtain a ratio of 450 lipids per dsMC and the mixture was incubated for 1 h at room temperature. The detergent was removed with Pierce detergent removal columns according to manufacturer's protocol and eluted in 120 μ L buffer H. DEBs were further purified in 50mM HEPES (containing 100 mM Na_2SO_4 and 8 mM MgSO_4) on a Superdex 200 Increase column (GE Healthcare) at a flow rate of 0.75 ml/min using an Akta Avant system (GE Healthcare).

Ultracentrifugation

Unpurified DEB solution (120 μ L) was mixed with 630 μ L of 45% iodixanol in 1X buffer H and placed at the bottom of a centrifuge tube (6.0 mL, 13 x 64 mm, Beckman Coulter). Six additional layers of iodixanol solution (26%, 22%, 18%, 14%, 10%, 6%, and 2%) in 1X buffer H (750 μ L) were added to the centrifuge tube. The tube was spun in a SW-41-Ti rotor (Beckman Coulter) at 41,000 rpm = 288,000 rfc and 4 °C for 6 h, after which the contents were fractionated (500 μ L per fraction) and analyzed by MgCl_2 -supplemented SDS PAGE (see below).

MgCl_2 -supplemented SDS PAGE

MgCl_2 -supplemented SDS PAGE gels (10%) were cast with 0.13 M Tris-HCl buffer pH 8.8, 12 mM MgCl_2 and 0.05% SDS. 6.25 mM Tris-HCl buffer with 12 mM MgCl_2 and

0.05% SDS was used as a running buffer. 10 μ L of sample solution (DEBs carrying 2 ethyl chains per 21-mer) were mixed with 10 μ L of SDS gel loading dye (0.2 M Tris HCl, 0.1% SDS, 20% Glycerol and 0.25% of bromophenol blue). Electrophoresis was performed at 65 V for 12 h. As a reference, 3 μ L of 1 kb plus DNA ladder (Thermo Scientific) were added. The gel was imaged with a Typhoon FLA 9500 gel scanner using the excitation wavelength of 575 nm suitable for 14:0 Rhodamine PE signal. After the first imaging, the gel was post-stained with SYBR Gold and imaged the same way as native PAGE.

tSEM characterization

Carbon-coated TEM grids (400 mesh copper, carbon on Formvar, Science Services Munich) were plasma-treated for 15 s. 4 μ L of the sample solution were applied on the TEM grid and incubated for 5 min. The excess solution was removed from the grid with a filter paper wick. Next, 5 μ L of a 1% uranyl formate solution was applied for 90 s to stain the DEBs, and the solution was removed with a filter paper. The samples were scanned on a Gemini SEM500 (Zeiss) SEM/STEM system operated at 10 kV.

AFM imaging

70 μ L of a 0.01% poly-L-ornithine solution was applied on a freshly cleaved mica plate. After 1 min the plate was washed with water and blown dry using compressed air. A small circle (diameter ca. 3 mm) was drawn using a permanent marker. 3 μ L of sample were applied into the center of the circle and incubated for 1 min. Next, the mica plate was covered with 70 μ L of imaging buffer (5 mM Tris-HCl pH 8.0 supplemented with 120 mM NiCl_2). The scans are performed using a Cypher ES AFM (Asylum research) using BL-AC40TS tips (BioLever Mini, Olympus). The AFM was operated in AC mode, at a scanning frequency of 0.5 Hz and a set point of 300 mV. Height profiles were obtained with Gwyddion software.

3.4.6 Expression and purification of MSP1D1

The standard expression of MSP1D12 was adapted from literature.¹⁶⁴ Briefly, the MSP1D1- pET28a plasmids were grown overnight in BL21Gold (DE3) cells (Agilent Technologies) at 37 °C in double strength YT medium containing 50 μ g/mL kanamycin. After induction with 0.3 mM isopropyl- β -D-thiogalactopyranoside, the temperature was decreased to 28 °C. The cells were harvested 4 h later, frozen in liquid nitrogen, and

stored at -80°C until further use. For purification, cells were resuspended in buffer A (50 mM Tris-HCl, 200 mM NaCl, pH 7.4) containing protease inhibitors (Roche Applied Science) and lysed twice by sonicating at 30% amplitude for two minutes with repeated 30 s pulse and 30 s pause. Cell debris was removed by centrifugation (15,000 g, 70 min, 4°C). Imidazole was added to the supernatant to a final concentration of 25 mM. The sample was loaded onto a Ni-NTA column (GE-Healthcare), equilibrated with buffer B (buffer A containing 25 mM imidazole). The column was washed with buffer B. Finally, the protein was eluted by gradient elution using increasing concentrations of imidazole (280 mM, 500 mM and 1 M; one CV each). Fractions containing MSP1D1 were identified by SDS-PAGE. A desalting step with PD10 columns (GE Healthcare) equilibrated with buffer A was performed to remove imidazole. The desalted MSP1D1 sample was concentrated using Vivaspin4 columns (Sartorius) and the final protein concentration measured by absorbance at 280 nm using a calculated extinction coefficient of $21,430\text{ M}^{-1}\text{ cm}^{-1}$ and a molecular weight of 24,793 kDa (ProtParam, ExPASy). Purified MSP1D1 was frozen in liquid nitrogen and stored at -80°C until further use.

3.4.7 Assembly of MSP-based lipid nanodiscs

The protocol of phospholipid nanodisc assembly was adapted from the original publication. A completely dried DMPC (1,2-dimyristoyl-sn-glycero-3-phosphocholine, Avanti Lipids) lipid film was solubilized in buffer A, containing cholate as detergent twice the concentration of the lipid, and sonicated until a clear solution was obtained. The respective lipid/sodium cholate solution and MSP1D1 were mixed to yield a final concentration of 12 mM lipid and 0.2 mM MSP1D1 (DMPC:MSP1D1 = ratio 60:1). For fluorescence measurements, LAURDAN was added in a ration 1:200 to DMPC, respectively. The mixture was incubated for 1 h at 25°C . The detergent was removed with Detergent Removal spin columns (Pierce). The approximate size and the homogeneity of the DMPC-filled nanodiscs were verified by size exclusion chromatography.

3.4.8 Fluorescence measurements of LAURDAN-labeled DEBs and vesicles

Fluorescent measurements were performed a Fluorolog 3 FL3-11 (HORIBA Europe GmbH, Oberursel). Samples containing 1-(6-(dimethylamino)-2-naphthalyl)-1-dodecanon (LAURDAN) in 100 μL cuvettes were excited at 340 nm (10 nm bandwidth) and the general polarization (GP) calculated⁵ from emissions at 440 and 490 nm as $\text{GP} = (I_{440} -$

I490) / (I440 + I490) if not stated otherwise. Scan speed was 100 nm min⁻¹ and 900 V photomultiplier voltage was chosen. The emission spectrum was averaged from 4 scans. A thermostatted cuvette holder connected to a circulating water bath was used to record temperature-dependent spectra after three minutes of thermal equilibration.

3.4.9 Coarse-grain molecular dynamics calculations

Models

A circular DNA model in a standard internal coordinate representation (with tilt, roll, twist, shift, slide, and rise inter base pair step parameters) was generated with a modified version of the vdna-plugin-2.27 using vmd-1.9.3.8. The plugin was modified to include the repeating 21-mer sequence motif. The internal coordinates were converted into an atomistic model using the rebuild module of the x3dna-2.39 package with non-standard residues encoding the chain breaks between the 21mers and the alkylated phosphorothioates. For the coarse-grained models, a separate model was built with unmodified bases to facilitate the conversion to the Martini model, which then was modified to include chain breaks and alkylations. This atomistic model of the ring/DNA complex was converted into a MARTINI-v2.2 coarse grained model using the martinize script. The MARTINI force field for lipids and its extension to DNA were used in combination with the EIneDyn approach to maintain the structure of the DNA backbone. A tight elastic network was applied as suggested by Uusitalo et al.¹⁶³ This CGMD approach is well suited to study complex biological membranes. Inspired by a recent study by Maingi et al,¹⁴⁰ conventional MARTINI beads and parameters were used to describe the S-alkyl chains modifications to the DNA rings. The S atom was mapped to the phosphate group to which it was chemically linked in the atomistic model. This new backbone bead was assigned a P5 type and the charge was set to zero. The beads of the alkyl chain were modeled by a C2 bead. All additional bonds were given a 4.5 nm reference value and a 5000 kJ/mol·nm⁻². Bond angles of the first bead of the chain relative to the backbone beads (previous and following bead, at 105 and 145 degrees, respectively, and with a force constant of 50 kJ/mol·rad⁻²) were used to restrict the orientation of the chain. The remaining bond angles were set to 180 degrees with a 25 kJ/mol·rad⁻² force constant. Improper dihedrals were used to force planarity of the backbone bead anchor of the alkyl chain, its neighbors

in the chain and the first bead of the chain. This precaution prevents back flips of the chain.

Simulations

All molecular dynamics simulations were performed using the GROMACS simulation package version 5.1.19. Conventional simulation setups associated with the MARTINI were used. These include a 20 fs time step for production run, a 0.9 nm cutoff and 500 kJ/mol·nm⁻² force constant for Elnedyn, and non-bonded interactions (van der Waals and electrostatic) cutoff at 1.1 nm and shifted to zero using the potential-modifier implementation in GROMACS. A relative dielectric screening constant of 15 and the Verlet neighbor search were used. The DNA, the membrane bilayer (DMPC), and the aqueous phase (water plus ions when present) were coupled independently to an external temperature bath at 300 K using Berendsen and Bussi thermostats ($\tau_T=0.5$ ps) for equilibration and for production, respectively. The pressure was weakly coupled to an external bath at 1 bar using a relaxation time of 2 ps following a semi-isotropic pressure scheme. Each system was run for 5 microseconds.

Chapter 4 Further improvements of DEBs

Madhumalar Subramanian (Helmholtz-Zentrum Dresden-Rossendorf, Prof. Fahmy Lab) contributed to this work by doing SEC of double-deckers. Artistic representation of double-deckers was done by Dr. Michael Matthies, former member at the Center of Advancing Electronics Dresden, TU Dresden, Schmidt Lab.

4.1 Introduction

Membrane proteins (MPs) perform a variety of functions vital to the survival of organisms, thus understanding their behavior is of utmost importance for unraveling physiological processes.¹ Due to their hydrophobic regions, MPs are prone to aggregation and precipitation in solution.⁵⁰ Consequently, biophysical studies including crystallization and structure determination of MPs are challenging.^{55,71,73} This can be overcome by inserting MPs into artificial cell membranes (see section 1.2.4 for more details), such as conventional nanodiscs (NDs), which consist of a phospholipid bilayer stabilized by a membrane scaffold protein (MSP).^{66,67} These proteins play an important role in nanodisc stabilization, but do not provide control over size and shape of the nanodisc.⁶⁸

To overcome these issues, we recently engineered DNA-encircled lipid bilayers (DEBs), where we leveraged the programmability of DNA nanotechnology to create phospholipid bilayers stabilized by a double-stranded DNA minicircle.¹⁶⁵ DNA nanotechnology provides an alternative approach to create membrane nanoparticles with defined and programmable parameters¹⁶⁶ since it has proven to enable the fast de novo design of arbitrarily shaped structures.⁹⁸ DEBs are made of multiple copies of an alkylated oligonucleotide hybridized to a single-stranded minicircle, in which up to two alkyl chains per helical turn point to the inside of the toroidal DNA ring. When phospholipids are added, a bilayer is observed to self-assemble within the ring such that the alkyl chains of the oligonucleotides stabilize the hydrophobic rim of the bilayer. This prevents the formation of vesicles and supports thermotropic lipid phase transitions. DEBs are completely free of protein

and can be synthesized from commercially available components using routine equipment. The diameter of DEBs can be varied in a predictable manner. The well-established toolbox from structural DNA nanotechnology will ultimately enable the rational design of DEBs so that their size, shape or functionalization can be adapted to the specific needs of biophysical investigations of lipidic phases and the properties of membrane proteins embedded into DEB nanoparticle bilayers (Chapter 3).

Although this system has been proven to reproducibly reconstitute the bilayers with programmable diameter, it has potential for further improvements. First of all, one dsDNA helix is only 2 nm thick. This is not enough to accommodate long-chain lipids. Secondly, since current alkylation patterns are not sufficient to stabilize the lipid bilayer inside smaller DEBs, it is necessary to modify the DEB scaffold in order to assemble DEBs with smaller diameter.

In this chapter, we explore the option of using a larger and improved DNA-based scaffold for lipid bilayer assembly in order to ensure proper anchoring of a large variety of lipids. To achieve this, we created a scaffold that consists of two interconnected DNA helices, called DNA double-decker. This structure has a thickness of ~4 nm and contains two times more hydrophobic strands in comparison to the previous system, which should be sufficient in protecting the lipid bilayer rim and providing more stable anchoring of the bilayer.

4.2 Results and discussions

4.2.1 Strategy to design DNA double-deckers

Our approach proposes the assembly of the lipid bilayer stabilized with DNA instead of MSP. In comparison to our previous approach where we used one DNA minicircle for stabilization of the lipid bilayer (Section 3.2.1), here we use two interconnected DNA minicircles, called double-deckers. DNA double-deckers consist of one long circular DNA scaffold that is held together by alkylated staples, resembling the shape of two dsDNA rings stacked on top of each other. An overview of the strategy can be observed in Figure 4-1.



Figure 4-1. Artistic representation of double-decker showing the scaffold (grey) folded into two stacked rings with staples.

4.2.2 Assembly strategy of functionalized DNA double-deckers

Assembly of double-decker scaffold

To assemble the circular double-decker scaffold, three linear oligonucleotides (101 bp, 100 bp and 93 bp) were ligated with three splints (Figure 4-2 a). In order to support the circularization of the DNA in the double-decker assembly, the oligonucleotides consist of several A-tracts, which provide the curvature for the double-decker assembly, which makes circularization easier. After the ligation, the residual linear products were removed with Exonuclease I/III (Figure 4-2 a). The assembly products were analyzed by denaturing PAGE gel, confirming that the final product contains only 294 nt long circularized ssDNA (Figure 4-2 b).

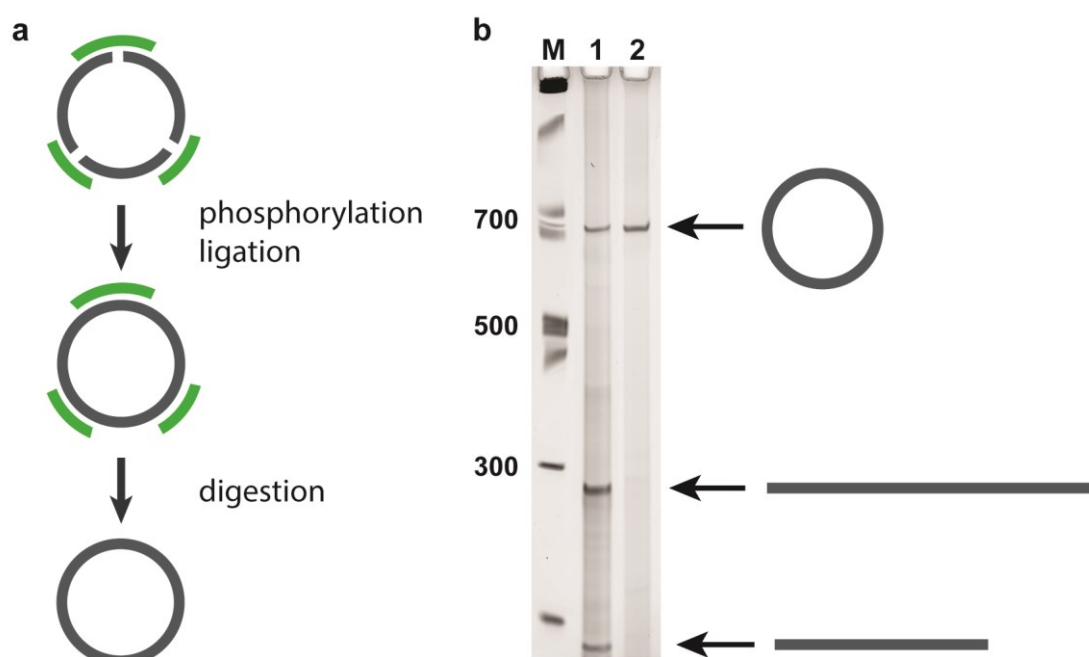


Figure 4-2. Double-decker scaffold assembly and analysis. a) double-decker scaffold was assembled by splint ligation of three linear oligonucleotides, followed by Exonuclease digestion b) 6% denaturing PAGE of assembled double-decker scaffold: M, molecular size marker (nt); lane 1, ligation reaction before exonuclease treatment; lane 2, exonuclease digest

Staple alkylation

Similar to our previous approach (Section 3.2.2), we introduced hydrophobic groups to our system by alkylating DNA staples such that two alkyl groups per helical turn were present. In order to connect part of the scaffold in the upper ring with part of the scaffold in the lower ring, the staples are 42 nt long, which is twice as long as the complementary strands for DEBs (Figure 4-3). This means that the alkylated staples carry two times more alkyl groups than the complementary strands for single minicircle design. This is of particular importance when it comes to purification of the alkylated staples: namely, due to their increased hydrophobicity, they could not be purified by techniques used for the purification of the short strands (e.g. HPLC, C18 column). The hydrophobic interactions between the alkylated staples and the column material stopped DNA from being eluted from the column. Therefore, it was necessary to purify the alkylated staples with a less hydrophobic HPLC column, which was C4.

4.2 Results and discussions

The increased number of hydrophobic groups in the staples also affected the sample preparation for HPLC: namely, the alkylation yield was increased tenfold (calculated from peak area on chromatogram) when chloroform extraction of the sample was conducted prior to HPLC purification. This way, the alkylated staples were purified from the excess of alkyl-iodide, which resulted in better solubility of the staples in water. The optimizations of staple alkylation are discussed in detail in the following section.

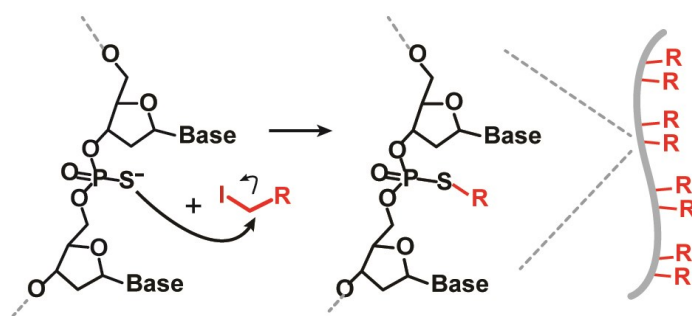


Figure 4-3. Alkylation of double-decker staples. Alkyl iodides (butyl-iodide, decyl-iodide) react with phosphorothioates (8 per staple), resulting in alkylated DNA strand.

Double-decker assembly

The double-deckers were assembled by hybridization of the double-decker scaffold with 7 staples. As shown on Figure 4-4, two staples participate in the scaffold crossover, whereas the remaining five staples connect the upper part of the scaffold to the lower part of the scaffold via single crossovers. For this design, single crossovers were chosen over double crossovers because they induce minimal twist on the DNA.^{167,168} This provides more control over the alkyl group positioning, which is crucial for lipid bilayer reconstitution. However, one double crossover is present, as the scaffold crossover must still be present as shown in the figure. To drive folding of the scaffold uniformly and ensure precise orientation of the hydrophobic functionalizations, the scaffold had several A-tracts next to its crossover. The crossovers of the staples 1 and 5 (Figure 4-4) were positioned half a helical turn from the center of A-tracts on upper minicircle and one helical turn from the center of A-tracts in lower minicircle. This way, A-tracts are present in each helical turn (either in the upper or the lower ring), which provides orientation control of the alkyl groups without long repetitive sequences. As with the design described in Section 3.2.2, the position of alkylation (specific thymidines in A-tracts) was chosen to orient the alkyl groups towards the center of the double-decker. This was

4.2 Results and discussions

achieved by positioning phosphorothioates at the end of the A-tracts for the upper ring, whereas the lower ring had phosphorothioate modifications at the beginning of A-tracts. Recently, Dr. Yusuke Sato (Kent State University, Dr Schmidt Lab) designed a double decker with A-tracts in the lower ring shifted by 5 nucleotides. This way, the curvature of the A-tracts follows the orientation of each staple in the bottom ring, which enables more precise control of the orientation of the phosphorothioates. On the other hand, that design has exclusively double crossovers, which might induce twist in the structure.

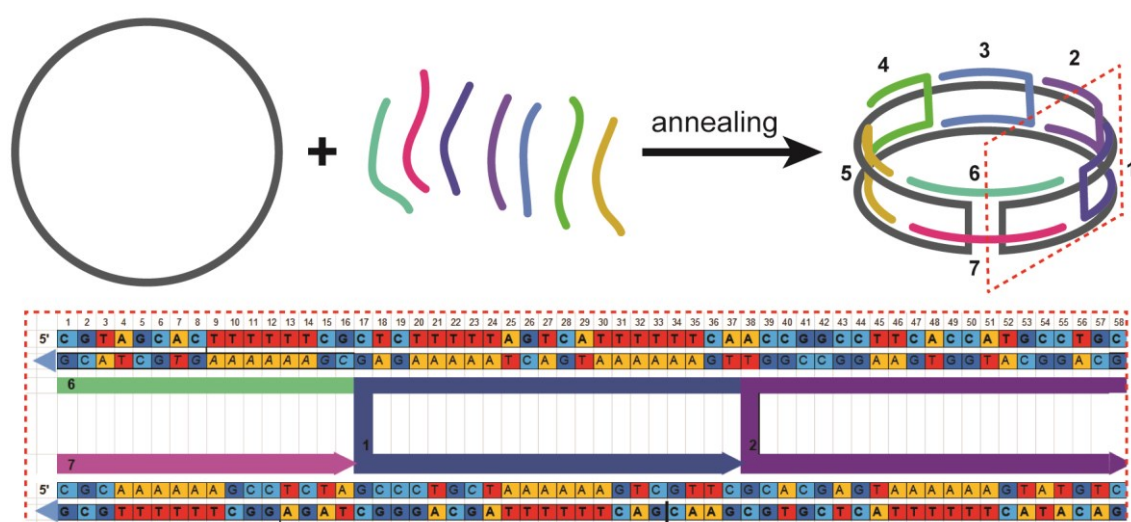


Figure 4-4. Assembly of double-deckers. The double-decker scaffold (left) is hybridized with seven alkylated oligonucleotides into the double-decker ring (right). Bottom: sequence design of the scaffold crossover and staples 1 and 2.

4.2.3 Optimization of double-decker staple alkylation

As described in the previous chapter, the procedure used to prepare the alkylated short strands in DEBs (21 nt, 2-4 PTO groups; Section 3.2.2) could not be applied for double-decker staple (42 nt, 8 PTO groups) preparation. Therefore, in order to achieve the highest possible yield, it was necessary to optimize the conditions of both the reaction and purification steps.

Optimization of reaction conditions

In order to determine the time needed for alkylation to occur, the reaction mixture was sampled at several time points (0 h, 0.5 h, 1 h, 2 h and 4 h) during the reaction. Initially,

4.2 Results and discussions

the reaction was performed following the protocol by Gut and Beck,¹³⁸ where DNA was alkylated at pH 8.0 and later on analyzed by denaturing PAGE gel. Since the alkylation introduces hydrophobic groups to the strands while removing the negative charge from the phosphorothioates, alkylated DNA staples will migrate slower than the unmodified ones. However, the PAGE gel analysis showed that the amount of oligonucleotides gets drastically reduced during the reaction (Figure 4-5), which can be attributed to aggregation of alkylated staples during the reaction. The results were independent of alkylation agent (butyl-iodide, decyl-iodide), as well as the material and grade of the reaction vessels used. Solubilization of the reaction products in different organic solvents also did not increase the amount of DNA, leading us to believe that the reaction conditions should be modified as the initial DNA material might behave differently.

It has been reported that alkyl-phosphorothioates are sensitive towards hydrolysis in basic conditions ($\text{pH} > 8$).^{169,170} In order to prevent hydrolysis during the reaction and potentially increase the amount of DNA, the pH of the reaction was changed from 8.0 to 7.5. The PAGE analysis of the reaction mixture after the same time points (0 h, 0.5 h, 2 h and 4 h) showed that the amount of DNA increased. Furthermore, it showed that highest possible alkylation occurs after 2 h of incubation at 65 °C. The same test was performed at pH 7.0 and 8.5, but the concentration of recovered DNA after the reaction was too low to be detected photometrically.

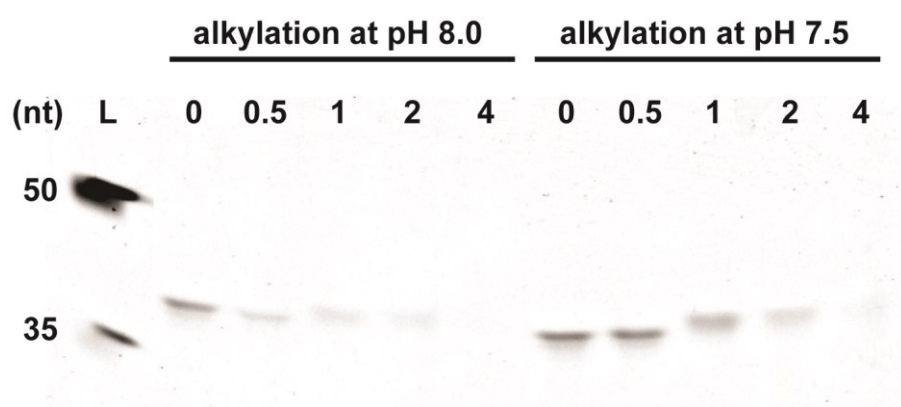


Figure 4-5. Denaturing PAGE of alkylation products. Alkylation of double-decker staples with decyl iodide at pH 8.0 (left) leads to DNA loss 30 minutes after the reaction. On the other hand, alkylation at pH 7.5 (right) results in higher yield of alkylated DNA, showing that the optimal time for reaction is 2 h. L, ladder (nt)

Optimization of purification conditions

The alkylation of the staples was followed by the removal of excess alkyl-iodides and organic solvents. This step is particularly important because it enables better resolution on reversed-phase (RP)-HPLC. For the alkylation of DEB complementary strands, the excess of alkyl-iodide was removed by gel permeation using resin-based columns prior to RP-HPLC purification. However, this approach was not successful for the purification of the double-decker staples as no DNA could be detected in the flowthrough. One of the possible reasons might be the increased hydrophobicity of alkylated staples, which increases binding to the column and subsequently reduces the elution of the alkylated staples. In order to overcome this, the column-free method for alkyl-iodide removal was developed, where the excess of alkyl-iodide was removed by chloroform extraction. For this, the solvent was evaporated after the reaction and the pellet was dissolved in a water: acetonitrile solution 50:50. Upon addition of chloroform and vortexing, the mixture separated into water and organic phases. The amount of DNA in both phases was determined photometrically, showing that the DNA was present exclusively in the aqueous phase, while the alkyl-iodides remained in the organic phase. The implementation of this purification step resulted in a 30-fold yield increase (calculated from the peak area on the HPLC chromatogram) when compared to the sample without extraction (Figure 4-6).

Finally, the sample was purified with RP-HPLC. As discussed in Section 3.2.2, DEB complementary strands were purified by RP-HPLC by using C18 column. However, the alkylated double-decker staples could not be eluted from the column due to strong interactions with carbon chains in the column. Elution of the staples did not occur even when solvents with low relative polarity (e.g. tetrahydrofuran - THF) were used as a mobile phase. Therefore, it was necessary to use a column with less hydrophobic functionalization. A C4 column was selected for this; the butyl-modified staples were eluted between 8 min and 10 min, whereas the decyl-modified staples were eluted between 12 min and 18 min (Figure 4-6). The broad peak for decyl-staples is probably the consequence of incomplete alkylation, where staples with less alkyl groups are at the beginning of the peak and the ones with more at the end.

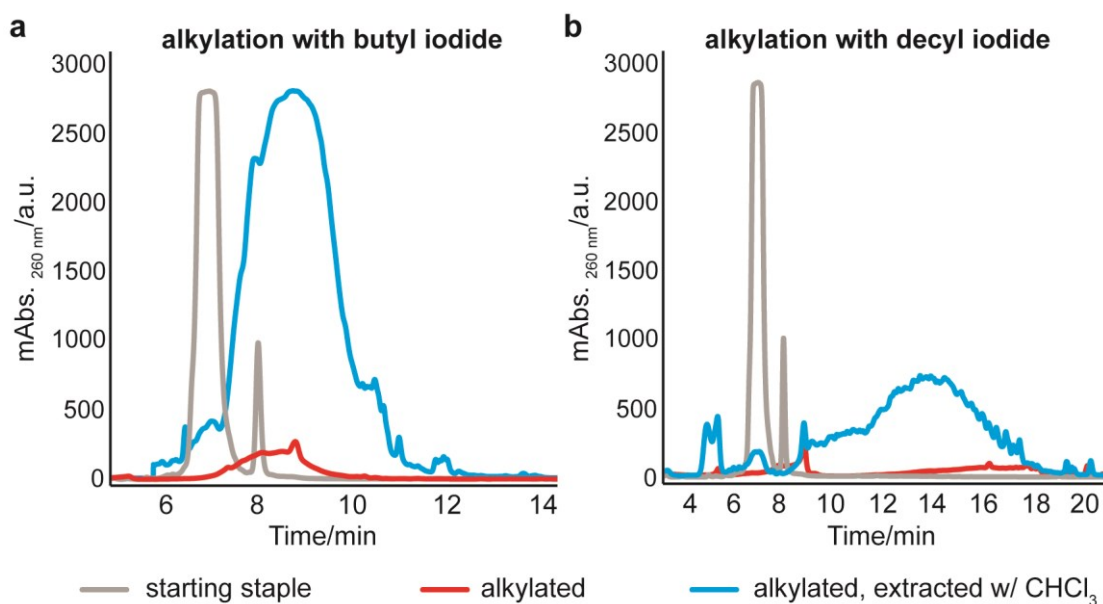


Figure 4-6. HPLC chromatograms of alkylated staples. Alkylation products with and without chloroform extraction are in blue and red, respectively, while the starting staple is in gray. a) butyl-alkylated staples are eluted between 8 min and 10 min b) decyl-alkylated staples are eluted between 12 min and 18 min. Both chromatograms show the increase in yield for samples purified by chloroform extraction

4.2.4 Double-decker characterization

Double-deckers were folded by slow annealing in the presence of MgCl_2 and purified by agarose gel electrophoresis (Figure 4-7). The double-deckers without alkyl groups form one clear band on the gel, whereas the alkylated double-deckers show aggregation (Figure 4-7 a). Although Mg^{2+} is often used for DNA nanotechnology assemblies, it can induce lipid aggregation.^{171,172} Since the double-deckers have twice as many hydrophobic groups as DEBs, the aggregation effect from Mg^{2+} is stronger. In order to prevent that, the structures were assembled in NaCl, which showed aggregations only with decyl-labeled double-deckers. However, when assembled with NaCl and detergent, the aggregates in alkylated double-deckers were not observed (Figure 4-8 a).

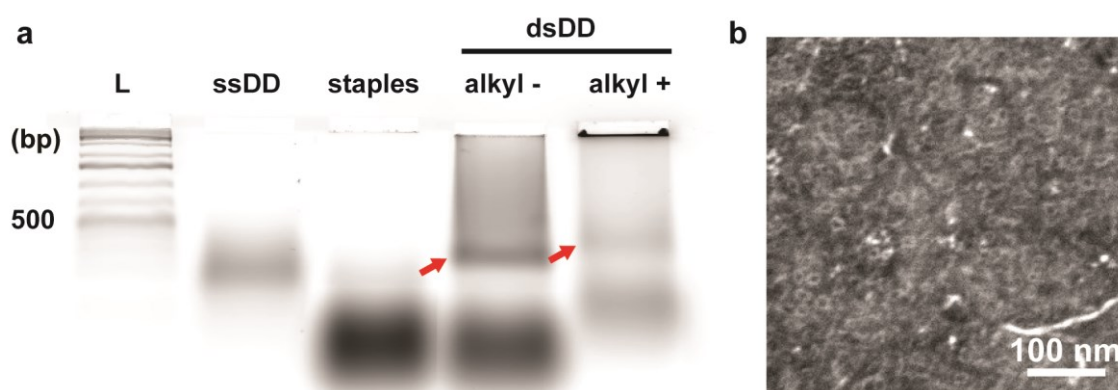


Figure 4-7. Analysis of non-functionalized double-deckers (dsDDs) assembled in MgCl_2 buffer. a) AGE of reaction products, showing correctly folded structures (red arrows) and aggregates for alkylated dsDDs. L, ladder (bp); ssDD, double-decker scaffold b) tSEM image of gel-purified non-functionalized double-deckers

The product bands were excised and analyzed by atomic force microscopy (AFM) and transmission scanning electron microscopy (tSEM). The results are shown in Figure 4-7 b and Figure 4-8 b-d, demonstrating that the double-deckers assembled successfully. The tSEM analysis showed that both alkylated and non-alkylated double-deckers tend to accumulate on certain areas on the grid, resulting in densely packed electron micrographs. This effect was independent of the concentration of double-deckers, leading us to believe it was due to electrostatic interactions between double-deckers and areas on the grid created during the plasma discharge step. AFM analysis of double-deckers showed that the average height of double-deckers is 2.5 nm, which is double the height of dsMCs (Section 3.2.3). As with DEBs (1.3 nm instead of 2 nm), height of the double-deckers measured by AFM was lower than calculated (2.5 nm instead of 4 nm) due to the strong electrostatic interactions between the DNA and the surface.

4.2 Results and discussions

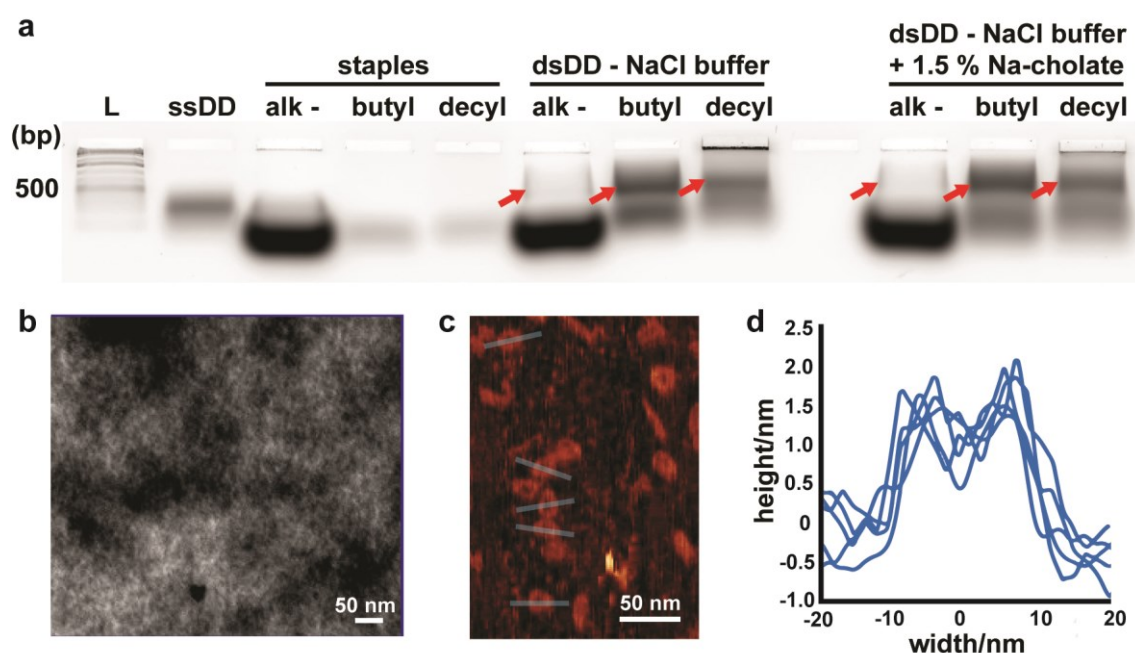


Figure 4-8. Analysis of alkylated double-deckers (dsDDs) assembled in NaCl buffer. a) AGE of the reaction products shows the correctly folded structures (red arrows) for assemblies with and without sodium-cholate (Na-cholate). When assembled with Na-cholate, dsDDs with decyl groups form less aggregates. L, ladder (base pairs), ssDD, double-decker scaffold b) tSEM image of butyl-alkylated dsDDs c) AFM image of decyl-alkylated dsDDs with height profile (d)

4.2.5 Approaches for lipid bilayer assembly in double-deckers

As was the case with DEBs (Section 3.2.3), the characterization of functionalized double-deckers was followed by the lipid bilayer reconstitution. Initially, the conditions for the lipid bilayer reconstitution were based on the ones for DEBs, where lipids solubilized in sodium-cholate were mixed with DNA. The lipid bilayer formation occurred when the detergent was removed with detergent-removal columns. However, this method did not result in a lipid bilayer inside the double-deckers (Figure 4-9). Assuming the detergent removal step was the critical parameter, other detergent removal methods were applied, including dialysis and size-exclusion chromatography of diluted detergent mix; these were also unsuccessful. Similarly, changing the detergent or lipids did not lead to positive results. There are several reasons for this: first of all, there is still room for improvement of the incubation and detergent removal steps, such as changing the detergent or buffer

4.3 Conclusion and outlook

composition and applying reduced force during the detergent removal (gravity flow instead of centrifugation of the samples). Secondly, the double-decker design shows chirality: namely, during the assembly, the scaffold crossover can be oriented in two ways, generating two structures. One of them has alkyl groups oriented towards the inside of the torus, whereas the other one has the alkyl groups oriented towards the outside: in the latter the bilayer cannot be formed. Finally, since A-tracts in the lower ring are not completely synced with crossovers, it is possible that the design of the lower ring need to be changed.

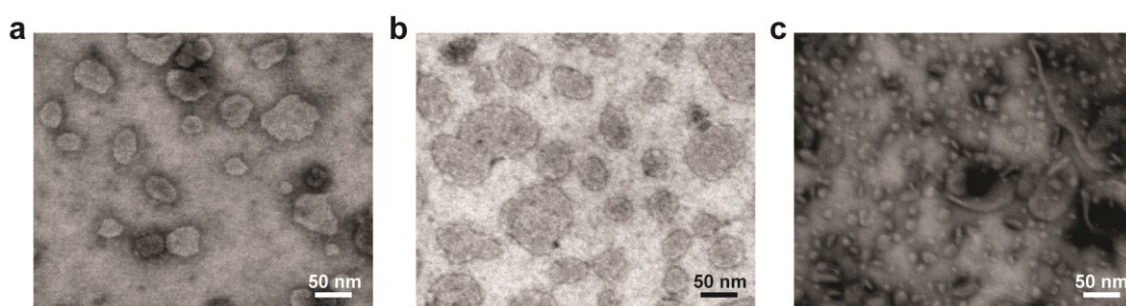


Figure 4-9. tSEM micrographs of attempts to synthesize lipid- double-deckers. a) Butyl-functionalized double-deckers with DMPC dissolved in sodium-cholate, which was removed by detergent columns. b) Decyl- functionalized double-deckers with DMPC dissolved in sodium cholate and β -octyl glucoside; the detergents were removed by detergent columns. c) Decyl-functionalized double-deckers with DMPC dissolved in sodium cholate and β -octyl glucoside; the detergents were removed by dialysis.

4.3 Conclusion and outlook

In this work, we showed that alkylated double-deckers can be robustly assembled. Alkylated DNA structures can be used for membrane mimetic system assemblies (DEB technology), which has been discussed in Chapter 3. In comparison to DEBs, the assembled double-deckers are thicker and carry two times more alkyl groups, which can potentially provide stronger anchoring of the bilayer. Furthermore, the lipid composition of the bilayer can be finely tuned since the increased thickness of the scaffold provided by double-deckers enables the reconstitution of lipids with longer chains.

In future experiments, we aim to prove the hypothesis that the double-deckers can be used as a scaffold for the lipid bilayer reconstitution. This can be done by controlling the

chirality of the structures and by adjusting the lipid bilayer assembly conditions, such as lipid and detergent composition and detergent removal protocol. Later, the lipid-filled double-deckers can be used for membrane protein (MP) reconstitution and studying MP interaction with ligands. In order to lock the orientation of the MP, it can be labeled with DNA strands and attached to the complementary strands on double-decker.

The ultimate goal of the project is to establish a new method for the structure determination of MPs by X-ray free electron laser (XFEL). In order to do that, MPs will be reconstituted in lipid-filled double-deckers and aligned on a tubular 6-helix bundle or a flat DNA origami structure. Furthermore, the interaction of two or more different MPs could also be analyzed by dimerized or trimerized DEBs. These interactions could be better observable by attaching quantum dots, fluorophores or gold nanoparticles to double-deckers.

4.4 Methods

The methods listed in this section are unique to this chapter, while the ones that were common with the previous chapters were not mentioned again (3.4.1, 0 and 0).

4.4.1 Materials

Oligonucleotide sequences

Staples with 8 PTO groups:

5'- CGAAAA*AG*TGCTACGTC*CA*GAGAAAA*AC*GAAGAAAA*GT*G -3'

5'- CTTACACT*AA*AAAATCTGT*CG*CTGACCGC*AA*AAAAGCCT*CT*A -3'

5'- TGAAAA*AT*GACTAAAA*GA*GGCCCTGCT*AA*AAAAGTCG*TT*C -3'

5'- GCAGGCA*TG*GTGAAGGCC*GG*TGCACGAGT*AA*AAAAGTAT*GT*C -3'

5'- GTGTGAG*AG*TAAGTCAAT*AA*CGATACTAT*AA*AAATCGTA*GA*A -3'

5'- CTATGG A*AG*CTAACAGCA*CG*AACTAAGTG*AA*AAAATCAT*GT*A -3'

5'- GCAAAAA*AG*GATGAAAA*GC*TGTGAGAGG*AA*AAAGGTCG*TG*A -3'

(asterisks indicate the locations of backbone phosphorothioates)

long oligonucleotides:

5'- TTACTCTCACACTCGTGCTGTTAGCTTCCATAGAGCTTTTTTCATCCTTTTTTGC
CACTTTTTCTTCGTTTTTTCTCTGGAGTCAGCGACAGATTTTTTAGT -3'

5'- GTAAGTCACGACCTTTTTCTCTCACTACATGATTTTTTCACTTAGTTTCTACGA
TTT TTATAGTATCGACATACTTTTTTACTCGTGCGAAC -3'

5'- GACTTTTTTAGCAGGGCTAGAGGCTTTTTTGCGCGTAGCATTTTTTCGCTCTTTT
TATCATTTTTTCAACCGGCCTTCACCATGCCTGCGTTATTGAC -3'

splints:

5'- GGAAAAAGGTCGTGACTTACACTAAAAATCTGTCGCTG -3'

5'- GCCCTGCTAAAAAGTCGTTGCGACGAGTAAAAAG -3'

5'- ACAGCACGAGTGTGAGAGTAAGTCAATAACGCAG -3'

4.4.2 Staple alkylation

The chemical modification of the phosphorothioated staples was conducted by following a modified protocol of Gut and Beck.¹³⁸ Phosphorothioate-modified oligonucleotides (20 nmol, 21 nt) were reacted with 1 μ mol alkyl-iodide in 90% DMF (Alfa Aesar) and 10% 30 mM Tris-HCl pH 7.5 (1000 μ L). The mixture was incubated at 65 °C for 4 h. The excess of the organic solvent was removed under reduced pressure and 200 μ L of 50% acetonitrile (ACN) and 150 μ L of chloroform were added to the resulting dry solid and mixed thoroughly. The above mixture was centrifuged at 2500 rcf for 30 s to separate the phases. The collected water phase was purified by reversed phase HPLC using a Dionex (ICS-5000+ TC) system with a MultoKrom 100-5 C4 column (flow rate 0.7 mL/min) using the following gradient starting points (difference to 100%: triethyl ammonium acetate (TEAA; 20 mM; pH 8 with 3% acetonitrile (ACN))):

0 min – 0% B

40 min – 100% B

45 min – 100% B

50 min – 0% B

The retention time for the starting compound (phosphorothioated oligonucleotide) was 7.0 min, whereas the retention time for the alkylated oligonucleotides was 9 min (8 butyl groups per staple) and between 13 min and 18 min (8 decyl groups per staple). The eluted samples were collected for further experiments and characterization.

4.4.3 Double-decker scaffold preparation

The long oligonucleotides (101 nt, 100 nt and 93 nt, Eurofins) and the splints (39 nt, 36 nt and 34 nt) were designed with the OligoAnalyzer Tool (idtdna.com) disregarding potential sequences with strong secondary structures. The long oligonucleotides (3.33 μ M each, 100 pmol) were hybridized to the splints (5 μ M each, 150 pmol) in 1X ligase buffer (total volume: 30 μ L) using a 12 min thermal annealing program (80 °C, 1 min, 80 °C – 25 °C - 5 °C/min, 25 °C hold). The annealed mixture was diluted twofold in 1X ligase buffer and treated with 1.5 μ L polynucleotide kinase and 1.5 μ L T4 ligase for 1.5 h at 30 °C. The mixture was purified with Zymo Oligo Clean & Concentrator columns (Zymo research) according to the manufacturer's protocol and the DNA was recovered in 30 μ L of water. The non-circular byproducts or linear oligonucleotides were digested in 1X exonuclease I buffer supplemented with 1X exonuclease III buffer, and 1.5 μ L of exonuclease I and 1.5 μ L exonuclease III (total volume: 55 μ L) for 3 h at 37 °C. The removal of the enzymes and buffer exchange were performed with Zymo Oligo Clean & Concentrator. ssDDs were recovered in 20 μ L of water and analyzed by denaturing PAGE (described in Section 3.4.3).

4.4.4 Double-decker preparation

The double-deckers were formed by hybridization of the double-decker scaffold (7 μ M) with alkylated staples (10.5 μ M) using a 20 min thermal annealing program (80 °C, 1 min, 80 °C – 60 °C - 5 °C/min, 57 °C, 1 min, 55 °C – 25 °C - 5 °C/min, 25 °C hold) in 150 mM NaCl, 5 mM TE buffer and 1.5 % sodium-cholate (50 μ L). The purified double-deckers were analyzed by agarose gel electrophoresis.

Agarose gel electrophoresis

For the AGE analysis, 1% agarose gels (Roche) were casted with 0.5X TBE buffer containing 12 mM MgCl₂ and stained with 1X Sybr safe DNA gel stain (Life technologies).

0.5X TBE buffer with 12 mM MgCl₂ was used as a running buffer. 15 µL of sample solution were mixed with 3 µL of 6X gel loading dye (50% glycerol, 5 mM Tris, 1 mM EDTA, 12 mM MgCl₂, 0.25% bromophenol blue and 0.25% of xylene cyanol). Electrophoresis was performed at 70 V for 2 h at 4 °C. As a reference, 3 µL of 1 kb plus DNA ladder (Thermo Scientific) were added. The gel was imaged with a Typhoon FLA 9500 gel scanner (GE Healthcare) using the excitation wavelength of 473 nm suitable for SYBR safe stained gels. For purification of the double-deckers and for experiments involving quantum dot functionalized 6-HBs, 0.75% agarose gels were casted and the electrophoresis was performed at 70 V for 2 h at 4 °C. The running buffer was cooled to 4 °C before usage. The samples were extracted from the gel with DNA gel extraction columns (Bio-Rad, Freeze 'N Squeeze) by centrifuging the excised bands at 5,000 rcf for 10 min.

Chapter 5 Applications of DNA-encircled lipid bilayers to study GPCRs

The work described in this chapter was done at The Rockefeller University, Prof. Sakmar Lab and it has several contributors. Mizuho Horioka (Prof. Sakmar Lab) contributed equally to this work; her contribution included isolation, purification and characterization of DNA-labeled CCR5. Prof. Thomas Huber (Prof. Sakmar Lab) and Dr. Xavier Periole (Aarhus University, Prof. Schiøtt Lab) performed the coarse-grained molecular dynamics simulations. Prof. Thomas Huber designed the CCR5 construct and performed the SMD-TIRF experiments. Prof. Thomas Huber, Prof. Thomas Sakmar, Prof. Karim Fahmy and Dr. Thorsten-Lars Schmidt provided useful suggestions and numerous discussions. This work will be submitted for publication soon after submission of the dissertation.

5.1 Introduction

Lipid bilayers and lipid-associated proteins play a crucial role in biology.^{1,142,173} Since studies and manipulation *in vivo* are inherently challenging, several *in vitro* membrane-mimetic systems have been developed. Common systems are based on polymers,¹⁴⁸ peptides¹⁷⁴ or proteins.^{65,66} With these methods, however, it is difficult to control the size and shape or to introduce functional elements in a defined way. Therefore, we created DNA-encircled bilayers (DEBs), consisting of a phospholipid bilayer stabilized by an alkylated dsDNA minicircle (Chapter 3). For this, alkylated oligonucleotides are hybridized to a single-stranded DNA minicircle (ssMC) such that all alkyl chains point to the inside stabilizing the lipid bilayer.

Having established a technique to assemble lipid bilayers stabilized by dsDNA ring, we continued to examine whether this platform can be used for membrane protein reconstitution and locking the membrane protein orientation. For that, we decided to use C-C chemokine receptor type 5 (CCR5) as a model receptor. CCR5 is a chemokine receptor

(Section 1.2.2) expressed on macrophages, monocytes, dendritic cells, T-cells, fibroblasts and neuronal cells.¹⁷⁵ It participates in the inflammatory response by directing cells to sites of inflammation.¹⁷⁶ Furthermore, it is required for the cellular entry of HIV-1 and represents one of the main therapeutic targets for HIV-1 treatment.¹⁷⁷ The only FDA-approved drug that targets CCR5 is maraviroc, which is an allosteric inhibitor.¹⁷⁸ CCR5 ligands include CCL3, CCL4 (MIP 1 α and 1 β , respectively), CCL3L1 and CCL5 (RANTES). As the crystallographic structures of CCR5-maraviroc complex¹⁷⁹ and CCR5-CCL5 binding site¹⁸⁰ have already been determined, CCR5 has a potential to be a good model receptor.

In this chapter, we explore the option of using DEBs as a reconstitution system for CCR5 which will control the orientation of the protein. To achieve this, we designed the receptor construct with multiple protein tags. DNA-labeling of the receptor occurs through reaction of SNAP- and CLIP- tag with benzylguanine (BG) and benzylcytosine (BC)-labeled fluorescent oligonucleotides, respectively. The DNA-labeled receptor is purified using tandem affinity purification, where epitope tags on N and C termini are used to purify the full length receptor. Finally, the stability of the DEBs chosen for CCR5 reconstitution was calculated using coarse grained molecular dynamics simulations.

5.2 Results and discussions

5.2.1 Strategy for DEB-CCR5 complex assembly

To generate a CCR5-DEB complex in which the orientation of CCR5 is locked, we decided to reconstitute the ssDNA-labeled CCR5 in DEBs labeled with complementary ssDNA. Hybridization of the strands from CCR5 with the ones on DEBs would aid with the insertion of the CCR5 into the bilayer, while allowing the control of its orientation.

CCR5 design

The CCR5 construct was designed to provide the binding sites for the ssDNA while keeping the protein functional and providing features for the protein analysis. This was achieved by designing a construct with multiple protein tags (Figure 5-1). The FLAG and 1D4 tags are located at the N-terminal and C-terminal of the protein, respectively. They are responsible for protein purification, ensuring that only the full protein construct is used

5.2 Results and discussions

in the later experiments. In order to provide a reaction site for ssDNA attachment, the construct contained SNAP and CLIP tags which were oriented on the opposite sides of the CCR5. Additionally, to immobilize the protein on the surface and allow fluorescence studies, the protein had two OLLAS tags.

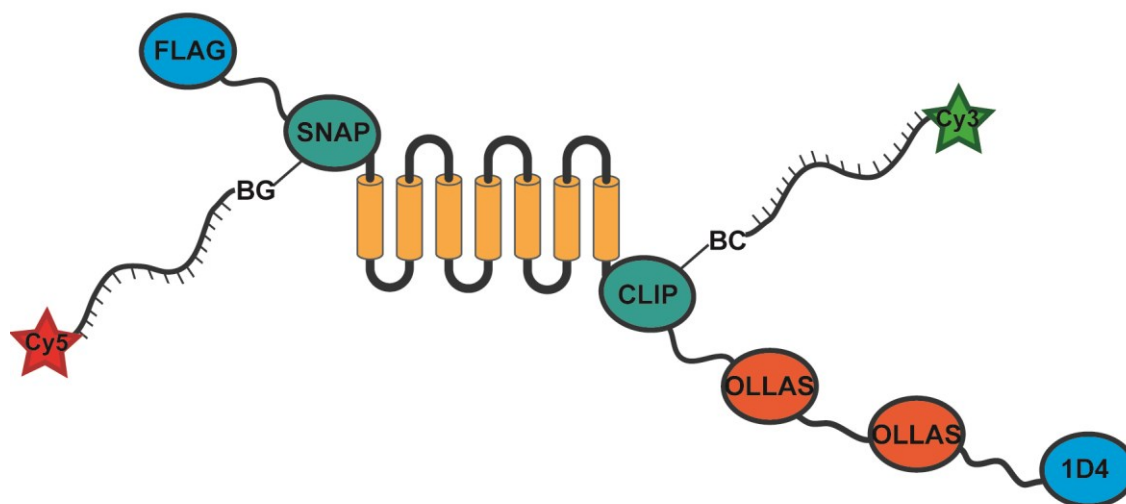


Figure 5-1. CCR5 construct. On the top and bottom side of the transmembrane domains of the protein (yellow) are located SNAP and CLIP tags (green), respectively. These tags serve as a reaction site for fluorescently-labeled DNA strands. FLAG and 1D4 tags are used for tandem affinity purification, whereas the two OLLAS tags were used for protein immobilization on the surface.

DEB design

To determine the ideal size of the DEB for the protein reconstitution, molecular models of ds DNA minicircles with various sizes (84 bp, 105 bp, 126 bp and 147 bp) were generated. As shown in Figure 5-2, the 84 bp and 105 bp minicircles would be the proper size for the receptor. However, the edge of the bilayer reconstituted in small minicircles would have a large positive curvature, which will decrease the stability of the bilayer. Furthermore, the characterization of small minicircles (84 bp) can be challenging. Therefore, we decided to reconstitute the protein in 105 bp minicircles and 126 bp minicircles. In contrast to the original DEB design where repetitive sequence was used (Chapter 3), the 105 bp and 126 bp minicircles were designed with five and six different addresses for the alkylated oligonucleotides, respectively. These alkylated oligonucleotides provide additional functions. Two oligonucleotides have protruding strands that interact with the

5.2 Results and discussions

oligonucleotide-labeled CCR5. One has a protruding sequence to hybridize with the oligonucleotide that is attached to the SNAP-tag, while the second one has a protruding sequence to hybridize with the oligonucleotide on the CLIP-tag. Both of these protruding strands point in the opposite direction, roughly perpendicular to the plane of the minicircle. This way, the strands on the opposite sides of the protein will hybridize to the strands on the dsDNA minicircle, leaving the protein in the bilayer with the desired orientation. A third oligonucleotide carries a protruding strand for optional surface immobilization with a biotinylated oligo, while the remaining oligonucleotides either have no additional function or they carry a Cy3 or Cy5 dye.

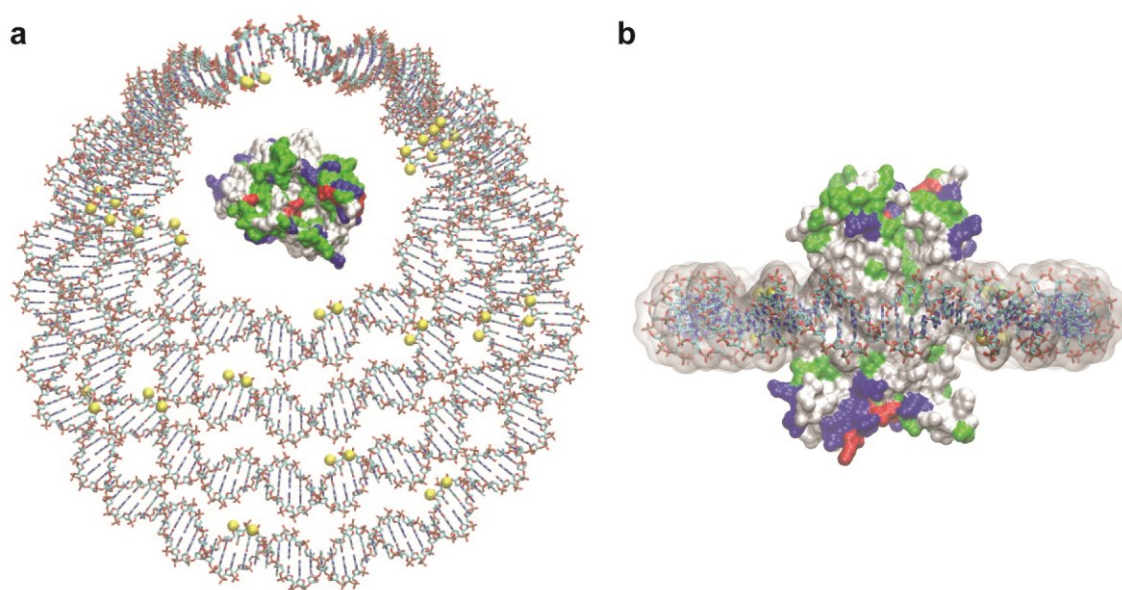


Figure 5-2. Molecular models of CCR5 in DNA minicircles. The GPCR is shown as a solvent-accessible surface colored by residue type (white, hydrophobic; green, polar; blue, basic; red, acidic). The positions of the alkyl groups are indicated by yellow spheres. a) CCR5 in 84 bp, 105 bp, 126 bp and 147 bp rings (top view) b) side view of CCR5 in 84 bp minicircle.

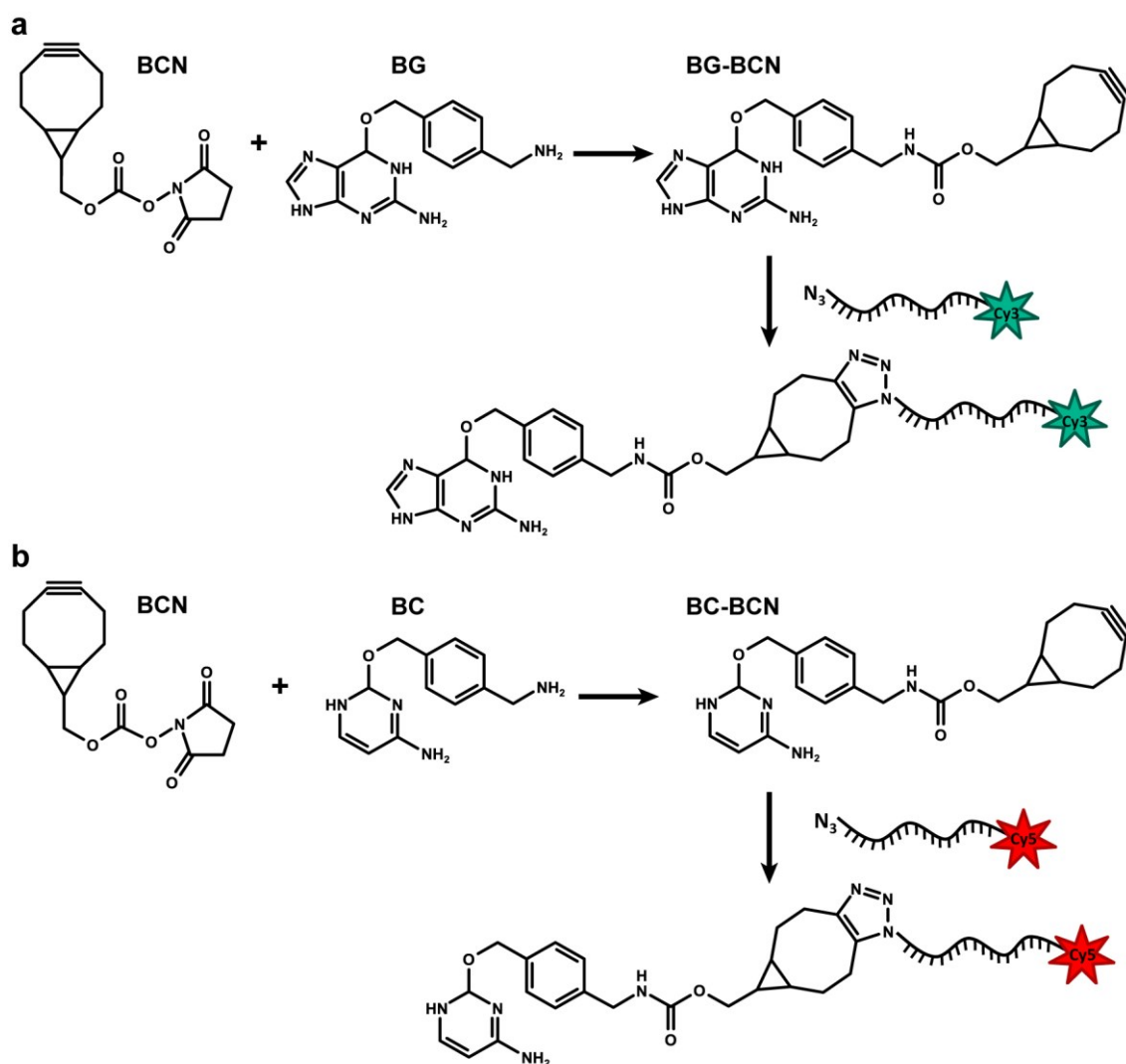
5.2.2 DNA labeling

To label the oligonucleotides that will react with the SNAP- and CLIP- tags and hybridize with the protruding strands from DEBs, we used strain-promoted azide-alkyne cycloaddition. These oligonucleotides had azido group on one end and a fluorophore on the other end (Cy5 and Cy3 for SNAP- and CLIP- tag, respectively). The azido group for the

5.2 Results and discussions

SNAP- binding oligonucleotide reacted with BG-BCN whereas the azido group for the CLIP-binding oligonucleotide reacted with BC-BCN. BG-BCN and BC-BCN were synthesized by reacting BCN (N-(((1R,8S,9s)-Bicyclo[6.1.0]non-4-yn-9-yl)methoxy)carbonyloxy)succinimide) with BG and BC, respectively. Synthesized molecules were purified by HPLC and their structures were confirmed by LC-MS.

The 2-step labeling of oligonucleotides enables the fine tuning of reactants and reaction conditions, providing custom SNAP- and CLIP- tag substrates. This way, we assembled substrates of higher polarity by introducing BCN with PEG spacer, thus generating BG-PEG-BCN and BC-PEG-BCN. Oligonucleotides labeled with these compounds have higher solubility in water, which leads to their higher accessibility during the reaction with protein and, therefore, potentially increase the yield of the labeled protein.



5.2 Results and discussions

Figure 5-3. Synthesis of substrates for the CCR5 tags. a) Synthesis of the SNAP substrate. In first reaction BCN reacts with BG, forming BG-BCN, which in second reaction conjugates with azido group on the Cy3-labeled oligonucleotide. b) Synthesis of the CLIP- substrate, where BCN reacts with BC, forming BC-BCN. BC-BCN reacts with azido group on the Cy5-labeled oligonucleotide, forming the BC-BCN oligonucleotide.

5.2.3 CCR5 labeling and purification

In order to isolate full-length receptor from receptor truncation products, we employed a tandem affinity purification strategy, described by Rico et. al.¹⁸¹ The transfected HEK293T cells expressing SNAP-CCR5-CLIP were lysed with a buffer containing DDM, CHAPS, and CHS. To immobilize the solubilized receptor, the 1D4-Sepharose immunoaffinity matrix was used. The receptor was fluorescently labeled on-resin, washed several times and eluted using 1D4 peptide. Since the 1D4 tag is located on the C-terminal of the receptor, this purification step removes the cellular components and C-terminal receptor truncations. Since this step does not remove N-terminal truncations, the second immunoaffinity purification was performed using anti-FLAG M2 agarose, which resulted in full-length receptor without truncations. The purification products were analyzed by dual-color near-infrared (NIR) immunoblotting. To assess labeling efficiency, the receptors were immobilized on the surface and single-molecule detection total internal reflection fluorescence (SMD-TIRF) was used.

To test the CCR5 labeling and purification conditions, the SNAP- and CLIP- tag were initially labeled with ATTO 549 and ATTO 647, respectively. The NIR immunoblot analysis showed that the protein is present after the 1D4 elution. However, a large fraction of protein is lost during the FLAG purification step, yielding in poor recovery of the full construct (Figure 5-4 a, left). Consequently, the amount of purified protein did not increase when it was labeled with fluorescently-labeled oligonucleotides (Figure 5-4 a, middle), suggesting that the FLAG purification conditions need to be improved. Furthermore, the SMD-TIRF analysis showed that labeling with oligonucleotides was not effective due to presence of many single-labeled receptors. Therefore, it was needed to change both labeling and FLAG-purification conditions.

Since the initial labeling and FLAG elution were done in a buffer containing detergents, HEPES and glycerol, we hypothesized that the lack of salts might be responsible for the

5.2 Results and discussions

low yield because of several reasons. First of all, the presence of salts will reduce the electrostatic interaction between the protein and anti-FLAG M2 agarose end therefore increase the amount of eluted protein. Secondly, it should reduce the electrostatic repulsion between labeling oligonucleotides and negatively charged surface of the protein and micelles. Therefore, we performed labeling and FLAG-elution experiments in a buffer containing 150 mM NaCl. To increase the stability of the receptor, DOPC and DOPS were added in trace amounts. This contributed to a significant increase of the yield, which is represented by increased fluorescence of the protein band on NIR immunoblot gels (Figure 5-4 a, right). However, the SMD-TIRF analysis showed low labeling efficiency of the receptors labeled with oligonucleotides with many signals from SNAP-tag and low signals from CLIP-tag. In contrast, the receptors labeled with fluorophores showed high labeling efficiency, showing that labeling with DNA needs to be optimized.

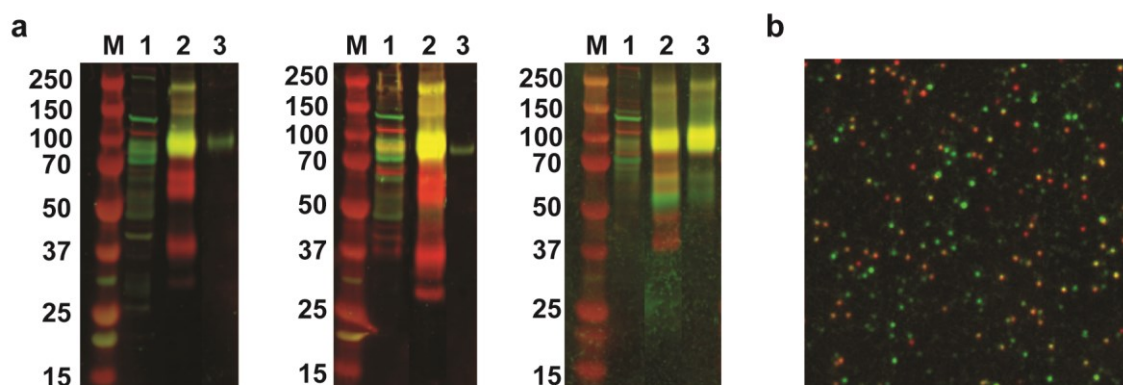


Figure 5-4. Analysis of labeled CCR5. a) Reducing SDS-PAGE and NIR-immunoblot of CCR5-labeled with fluorophores (left), oligonucleotides (center) and oligonucleotides in NaCl-supplemented buffer (right) after 1D4/FLAG tandem affinity purification. M, marker; 1, cell lysate; 2, 1D4 elution; 3, FLAG elution. Full-length SNAP-CCR5-CLIP (~75 kDa, yellow band) was detected using antibodies against the 1D4 (red) and FLAG (green) epitopes. b) SMD-TIRF of oligonucleotide-labeled CCR5 in presence of NaCl, followed by the sequential purification with complementary oligonucleotides. Green, signal from Cy3-labeled oligonucleotide on the SNAP tag; red, signal from Cy-5 labeled oligonucleotide on the CLIP tag.

To maximize the labeling efficiency of the receptor with oligonucleotides, several labeling methods were employed. At first, we hypothesized that the presence of ssDNA might be

5.2 Results and discussions

responsible for reduced labeling efficiency. Therefore, we tried labeling in the presence of short strands (hexamers) complementary to SNAP- and CLIP- tag oligonucleotides, but it did not increase the labeling efficiency. In order to check whether labeling kinetics is sequence-dependent, we swapped the CLIP- and SNAP- oligonucleotides. The SMD-TIRF showed that the SNAP- tag labeling was effective, which was not that case with CLIP-tag; this proved that labeling does not depend on the DNA sequence. Then, we hypothesized that high hydrophobicity of BG- and BC- BCN attached on charged DNA can behave as a detergent, forming micelles and making them inaccessible to SNAP and CLIP tags, resulting in lower labeling efficiency. Therefore, we decided to label the oligonucleotides with BG- and BC- BCN having 3 PEG residues, resulting in reduced hydrophobicity and detergent-like behavior. This approach, however, did not result in increased double-labeled receptors. Finally, the double-purification was employed, where the tandem affinity purification was followed by the sequential purification with oligonucleotides. In the latter step, the oligonucleotide-labeled CCR5 was attached to the beads functionalized with complementary to the CLIP oligonucleotide, washed and released from the beads by strand displacement. Later on, the same procedure was employed for the SNAP oligonucleotides. This step dramatically improved the fraction of double-labeled receptors from 9% to 41% (Figure 5-4 b).

5.2.4 Coarse-grained simulations of DEBs for CCR5 reconstitution

The stability of the DEBs chosen for CCR5 reconstitution was calculated by coarse grained molecular dynamics simulations using the Martini force field. The simulations show that the lipid bilayer cannot be stabilized in DEBs containing short alkyl chains (ethyl-octyl), leading to the complete disassembly of the system (Figure 5-5 a, b). On the other hand, the dodecyl alkyl groups (Figure 5-5 c) stabilize the bilayer during the entire simulation period (5 μ S). Lipid bilayer assembly in butyl and decyl-modified MCs was experimentally tested, revealing that these modifications are not sufficient in anchoring the lipid bilayer.

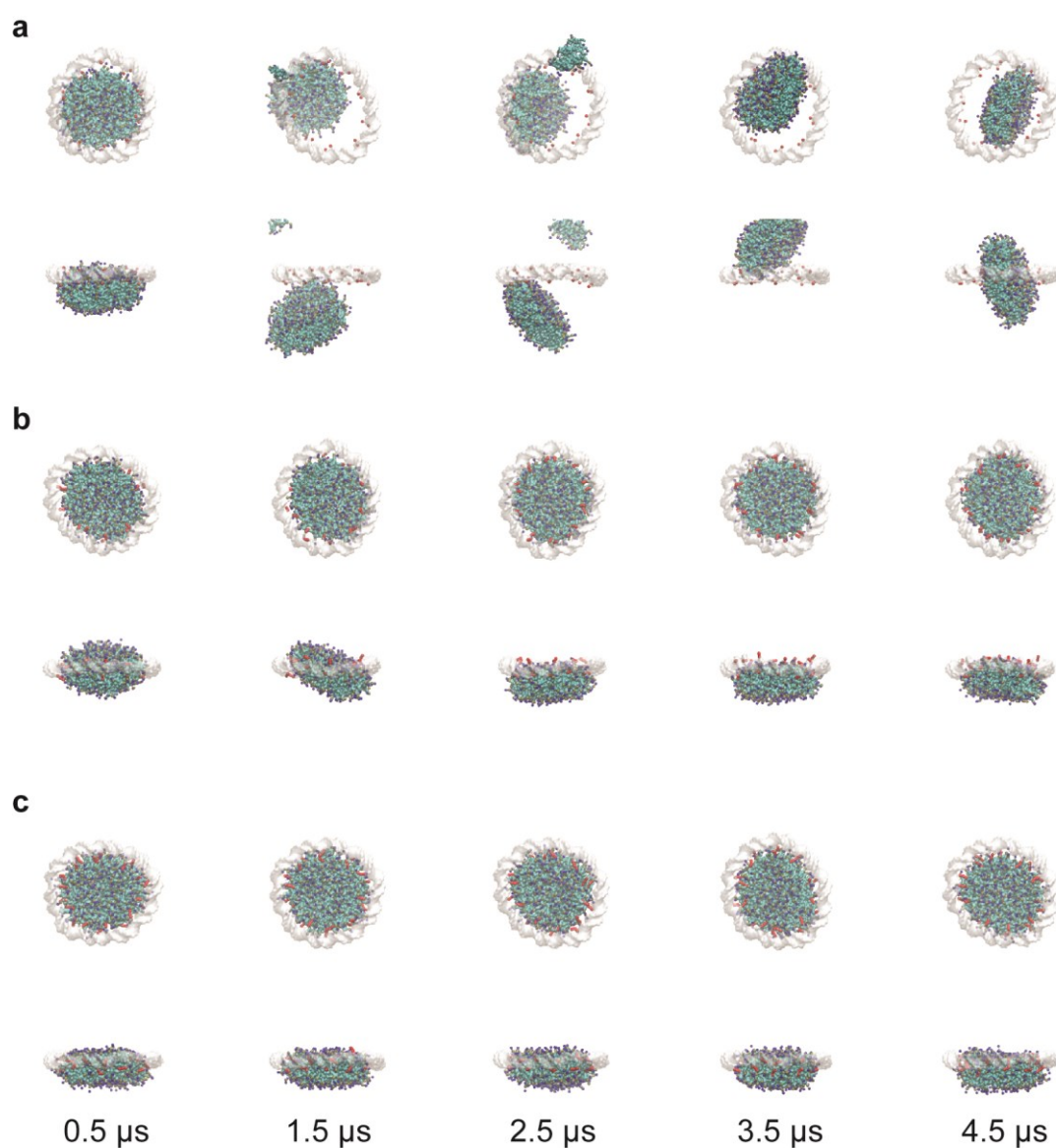


Figure 5-5. Coarse grained molecular dynamics model of a DEB composed of a 105 bp dsMC with 20 butyl (a), 20 octyl (b) and 20 dodecyl (c) groups and lipids. DNA is white, alkyl chains red, DMPC head groups blue. Snapshots were taken after 1-microsecond intervals. Up: view down the membrane normal of a structure at the end of the 5 micro-seconds long trajectory. Down: View rotated 90 degrees.

5.3 Conclusions and outlook

In conclusion, we have established a method to produce, purify and characterize receptors conjugated with oligonucleotides. The labeling oligonucleotides are formed in a 2-step reaction that can be modified to provide a variety of products. The preparation of double-labeled CCR5 with oligonucleotides is the first step in the DEB-CCR5 complex assembly, where CCR5 will be reconstituted in DEBs with protruding strands. The protruding strands on DEBs will hybridize to oligonucleotides on the protein which will provide control of its orientation. Furthermore, DNA-labeled receptors have a great potential for numerous studies, including their arrangement on DNA origami structures. This way, the programmable, self-assembled receptor arrays with sub-nanometer precision can be formed.

5.4 Methods

The methods listed in this section are unique to this chapter, while the ones that were common with the previous chapters were not mentioned again (3.4.1, 453.4.9). Methods described in Sections 5.4.3, 5.4.4 and 5.4.5 are based on the protocols¹⁸¹ developed by Dr Carlos Rico and Prof. Thomas Huber (The Rockefeller University, Sakmar Lab).

5.4.1 Materials

Oligonucleotide sequences

SNAP- tag oligonucleotide: 5' – /5AzideN/CCTCCTCTCTTCCTTCACC/3Cy3Sp/ – 3'

CLIP- tag oligonucleotide: 5' – /5Cy5/CCACCACCATCAACCAAC/3AzideN/ – 3'

DNA minicircle (MC) sequence (105 bp): 5' – GCTAAAAACGCGCAAAAATGTCTAAA
AAAGTGTGAAAAAGTGTGAAAAAGTGTGAAAAAGTGTGAAAAAGGCTGAAAAAT
GCAGAAAAACGTGCAAAAAGT – 3'

DNA MC splint: 5' – GCGCGTTTTTTAGCACTTTTTGC – 3'

DNA MC complementary strand hybridizing to the SNAP-tag oligonucleotide: 5' – GTT
GGTTGATGGTGGTGGCGCGTTT*TT*TAGCACTTT*TT*G – 3' (asterisks indicate the
locations of backbone phosphorothioates)

DNA MC complementary strand hybridizing to the CLIP-tag oligonucleotide: 5' – CAC GTTT*TT*TCTGCATTT*TT*CAGCCTGGTGAAGGAAGAGAGGAGG – 3'

DNA MC biotin strand: 5' – TT*TT*TAGACATTT*TT*CGATGTCTTCGACATAAACAT CCCTT/3Biotin/ – 3'

DNA MC Cy3 strand: 5' – TT*T T*TC ACA CTT T*TT* ACG CAT/3Cy3Sp/ – 3'

DNA MC Cy5 strand: 5' – /5Cy5/TT*TT*TGTCGATGT*GT*G – 3'

5.4.2 Labeling oligonucleotides for SNAp tag and CLIP tag

BG-BCN and BC-BCN synthesis

In order to generate BG-BCN and BC-BCN, two reactions were set with 11 μ M of BG-NH₂ and BC-NH₂ in dried DMSO, respectively. Each of them was made to react with 1.5 molar equivalents of BCN-NHS ester and 1.5 molar equivalents of trimethylamine. Total volume of each reaction was 390 μ L. The samples were incubated for 90 min with constant nutation, after which the reaction volume was separated in 4 tubes, mixed with 1 mL diethyl ether and centrifuged for 7 min at 20.000 rcf and 4 °C. The supernatant was discarded and the precipitate was purified by reversed phase HPLC using a X system with Protein and peptide C18 250x10 mm column, GraceVydac (flow rate 4.5 mL/min, monitor absorbance 250 nm) using the following gradient starting points (difference to 100%: trifluoroacetic acid (TFA; 0.1%)):

0 min, 5% B (70% acetonitrile (ACN) and 0.1% TFA in H₂O)

5 min, 10% B

25 min, 70% B

28 min, 100% B

30 min, 100% B

32 min, 10% B

Both BG-BCN and BC-BCN were eluted at 24.4 min and collected for further characterization.

Oligonucleotide labeling with BG-BCN and BC-BCN

To conduct the conjugation reaction, 50 μ M of Cy5-azido and Cy3-azido labeled oligonucleotides reacted with 1mM BG-BCN and BC-BCN in 100 μ L, respectively. After overnight incubation, the samples were mixed with 50 μ L 5 mM TE buffer and 50 μ L DMSO and purified by reversed phase HPLC using a X system with Protein and peptide C18 250x4.6 mm column, GraceVydac (flow rate 1.5 mL/min) using the following gradient starting points (difference to 100%: triethyl ammonium acetate (TEAA; 20 mM; pH 8)):

0 min, 0% B (acetonitrile)

5 min, 7% B

35 min, 100% B

37 min, 100% B

39 min, 7% B

The conjugated Cy5-BG and Cy3-BC oligonucleotide were eluted at 19.1 min and 16.8 min, respectively and collected for further characterization.

5.4.3 CCR5 preparation and labeling

Ten 100-mm x 20-mm polystyrene dishes were plated with HEK293T cells at 4.0×10^6 cells/dish in DMEM + 10% FBS. 24 hours post-plating, 100 μ L of Plus Reagent was mixed with 80 μ g of CCR5-SNAP in 7.5 mL of DMEM. In a separate vessel, 170 μ L of lipofectamine reagent was mixed with 5 mL of DMEM. After 15 minutes, the transfection solutions were mixed and incubated for an additional 15 minutes. Media was removed from HEK293T cells and supplemented with 2.8 mL of DMEM. 1.2 mL of the transfection solution was added to each plate and the cells were incubated for 4 hours before supplementing the media with 4 mL of DMEM + 20% FBS. 24 hours post-transfection, media was removed from the cells and cells were harvested in 2 mL/dish of PBS and 1 mM phenylmethylsulfonyl fluoride (PMSF). Cells were pelleted in a 50 mL vessel at 1,500 rpm using a Beckman GS-6R centrifuge at 4 °C for 5 minutes. The harvesting solution was removed and the cell pellet was solubilized in 5 mL of Navratilova Lysis buffer (20 mM HEPES pH 7.4, 0.1 M $(\text{NH}_4)_2\text{SO}_4$, 1 mM CaCl_2 , 5 mM MgCl_2 , 10% Glycerol, 0.1%

CHS, 1.0% DDM, 1.0% CHAPS) supplemented with a protease inhibitor cocktail (complete, mini, EDTA-free, Roche, Product No. 11836170001) for 2 hours at 4 °C. Cell lysates were then centrifuged at 55,000 rpm for 30 minutes, 4 °C, using a TLA 100.3 rotor. The supernatant was added to 600 µL of 50% slurry 1D4 mAb Sepharose 2B resin and incubated overnight at 4 °C. Resin was pelleted in a GS-6R for 5 minutes, 2,000 rpm, 4 °C and then transferred to a Ultrafree-MC-HV Durapore PVDF 0.45 µm centrifugal unit. SNAP-CCR5-CLIP was labeled in 400 µL of Buffer T (150 mM NaCl, 2.75*10⁻⁶ % DOPC, 1.18*10⁻⁶ % DOPS, 0.02% CHS, 0.1% CHAPS, 0.1% DM, 50 mM HEPES pH 7.4, 10% glycerol) with 3 µL of 2 µM SNAP-oligo and CLIP-oligo and 1 mM DTT for 2 h at 4°C. Resin was then washed 3 x 0.5 mL in Buffer T for 30 minutes each at 4 °C. CCR5-DNA complex was eluted from the 1D4 resin by incubating the sample with 1D5 peptide in Buffer T (0.33 mg/mL) twice for 30 minutes on ice and eluting by centrifugation. 1D4 purified CCR5-SNAP was added to 100 µL of FLAG M2 resin and incubated overnight at 4 °C. FLAG resin was transferred to a separate Durapore spin filter and washed 3 times with 0.5 mL of Buffer N for 30 minutes each at 4 °C. CCR5-DNA was eluted by incubating the resin twice with 100 µL of buffer T and FLAG peptide (200 µg/mL) for 30 minutes on ice. The FLAG purified CCR5-DNA was further analyzed by NIR-immunoblotting and fluorescence correlation spectroscopy.

5.4.4 NIR-immunoblotting

Samples were mixed with DTT at 150 mM final concentration and NuPAGE loading buffer. Samples were loaded into a NuPAGE 4-12% Bis-Tris gel in MES-SDS buffer. Electrophoresis was conducted at a constant voltage of 115V. The gel was removed from the cassette and rinsed in water before equilibrating in Western Transfer buffer (48 mM Tris, 39 mM glycine, 1.3 mM SDS, 20% MeOH, pH 9.2). 1 piece of Immobilon PVDF membrane-FI was incubated for 1 minute at room temperature in 100% MeOH. The PVDF membrane and 2 pieces of extra thick blot papers (Bio-Rad) were rinsed in Western transfer buffer. Western transfer was performed in a semi-dry apparatus for 45 minutes with a constant voltage of 18V. After electrophoresis, the membrane was placed in 10 mL of Odyssey blocking buffer (PBS) and incubated for 1 hour at room temperature. The membrane was then placed in 10 mL of blocking buffer with anti-1D4 mouse monoclonal (1:1,000), anti-FLAG rabbit polyclonal (1:1,000) antibodies, and 0.2% Tween-20. The membrane was incubated overnight at 4 °C. Membrane was then washed 5x5

minutes in 1x PBS-T (0.1% Tween-20). Membrane was incubated for 1 hour at room temperature in 10 mL blocking buffer supplemented with 0.2% Tween-20, 0.01% SDS, goat anti-mouse IR 680 RD (1:10,000), and goat anti-rabbit IR 800 CW (1:10,000). Membrane was washed again 5×5 minutes in 1× PBS-T and then 2×5 minutes in 1× PBS buffer. Membranes were visualized using a LICOR Odyssey SA using 100 μ m resolution, and intensity level 7 for both 700 and 800 nm excitations. Images were processed using Image Studio Lite Version 4.0 and ImageJ. For the line scan analysis, a rectangle of 45 × 120 pixels was drawn around the desired gel lane and set as First Lane under Analyze, Gels, in ImageJ. The command 'Plot Lanes' was then selected with vertical and horizontal scale factors set to 1.0 with uncalibrated optical density. Using the magic wand, an area under the curve was selected and saved as x and y coordinates for replotting in GraphPad Prism 7.

5.4.5 SMD-TIRF

The protocol for SMD-TIRF characterization was adopted from Naganathan *et al.*¹⁸² To silanize a microplate, freshly cleaned 384-well-glass-bottom microplate was loaded with 20 μ L 3-glycidyloxypropyl trimethoxysilane (GOPS, Aldrich) per well. After 60 min incubation at RT, the GOPS was removed by shaking off the plate over a sink. The plate was rinsed three times by evenly spraying 70% ethanol, which was removed by shaking off. The plate was covered in Whatman filter paper and centrifuged upside-down for 5 min at 500 rcf. The plate was covered with its lid and dried under reduced pressure overnight (less than 0.05 Torr/6.7 Pa pressure).

After drying, 10 μ L of coating solution (250 μ L of 20 mg/mL biotinyl-bovine serum albumin (biotinyl-BSA) (final concentration 1 mg/mL), 10 μ L 5% bovine serum albumin BSA (final concentration 0.1 mg/mL), 2.24 mL H₂O, 2.5 mL 0.2 M borate, 1.85 μ L 10% n-dodecyl- β -D-maltoside (DM), filtered with Steriflip) were loaded to each well of the silanized microplate. The plate was centrifuged for 5 min at 500 rcf and incubated in a sealed plastic bag with a wet filter paper. For the first 90 min the plate was incubated at RT, followed by overnight incubation at 4 °C. Next day, the wells were aspirated manually using a fine tip placed in a corner of the well bottom. This was followed by loading 10 μ L of blocking solution (300 μ L 1 M Tris base, 2.7 mL H₂O, 3 mL 0.2 M borate, filtered with Steriflip) per well and centrifuging the plate for 5 min at 500 rcf. After the centrifugation, the plate was

incubated for 30 min at RT, after which the wells were aspirated and loaded with 20 μ L purified water per well. The water was aspirated and the plate was dried under laminar flow for 2 h at RT.

To immobilize NeutrAvidin on the BSA-coated surface, 10 μ L of priming solution (10 μ L 0.37% DM, 990 μ L PBS) were loaded to each well and aspirated. Later on, 10 μ L of NeutrAvidin solution (6 μ L 10 mg/mL NeutrAvidin, 40 μ L 5% BSA, 10 μ L 0.37% DM, 944 μ L PBS, centrifuged for 10 min at 12,000 rcf) was loaded to each well, incubated for 15 min at RT and aspirated. 10 μ L of blocking solution (40 μ L 5% BSA, 10 μ L 0.37% DM, 944 μ L PBS) were loaded to each well and incubated for 10 min at RT.

To immobilize biotinylated antibody, 10 μ L of biotinylated antibody solution (10 μ g biotinylated 1D4 (e.g., 1.84 μ L 5.42 mg/mL 1D4-ss-biotin), 40 μ L 5% BSA, 10 μ L 0.37% DM, 950 μ L PBS) were loaded to each well and incubated for 15 min at RT. After the wells were aspirated, 10 μ L of biotin solution (3 μ L 1 mM biotin (3 μ M final concentration), 40 μ L 5% BSA, 10 μ L 0.37% DM, 947 μ L PBS) were loaded to each well and incubated for 10 min at RT. After the aspiration of the wells, 10 μ L of blocking solution (40 μ L 5% BSA, 10 μ L 0.37% DM and 950 μ L PBS) were loaded to each well and incubated for 10 min at RT. The wells were aspirated and loaded with 20 μ L of CCR5 sample in serial dilutions (1:10, 1:100, 1:1000, 1:10000), to which 80 μ L of imaging buffer (1.6 μ L 10.9 U/ μ L GOD (27.8 mg 195.7 U/mg glucose oxidase (final concentration 10.9 U/ μ L), 150 μ L purified water 322 μ L 78% glycerol (final concentration 50%), filtered with Ultrafree-MC spin filter), 8.5 μ L 272 U/ μ L CAT, 5 μ L 200 mM Trolox in DMSO, 5 μ L 200 mM MV (methyl viologen dichloride hydrate) and 40 μ L 10% glucose). The sample was imaged using a customized SMD-TIRF microscopy workstation based on a Zeiss AxioVert 200M inverted microscope (laser power for the three lasers (488, 561, 642 nm) was 50 mW, exposure time 500 ms, electron-multiplying (EM) gain 200, analog-to digital converter (ADC) range 12e⁶/unit).

Bibliography

- (1) Alberts, B.; Johnson, A.; Lewis, J.; Raff, M.; Roberts, K.; Walter, P. *Molecular Biology of the Cell*, 4th ed.; Garland Science, 2002.
- (2) Mouritsen, O. G.; Bagatolli, L. A. *LIFE - AS A MATTER OF FAT: Lipids in a Membrane Biophysics Perspective*; Springer, 2015.
- (3) Gennis, R. B. *Biomembranes: Molecular Structure and Function*; Springer Science & Business Media, 2013.
- (4) Singer, S. J.; Nicolson, G. L. The Fluid Mosaic Model of the Structure of Cell Membranes. *Science* **1972**, 175 (4023), 720–731.
- (5) Lingwood, D.; Simons, K. Lipid Rafts As a Membrane-Organizing Principle. *Science* **2010**, 327 (5961), 46–50.
- (6) Kusumi, A.; Fujiwara, T. K.; Chadda, R.; Xie, M.; Tsunoyama, T. A.; Kalay, Z.; Kasai, R. S.; Suzuki, K. G. N. Dynamic Organizing Principles of the Plasma Membrane That Regulate Signal Transduction: Commemorating the Fortieth Anniversary of Singer and Nicolson's Fluid-Mosaic Model. *Annu. Rev. Cell Dev. Biol.* **2012**, 28 (1), 215–250.
- (7) Nicolson, G. L. The Fluid—Mosaic Model of Membrane Structure: Still Relevant to Understanding the Structure, Function and Dynamics of Biological Membranes after More than 40years. *Biochim. Biophys. Acta BBA - Biomembr.* **2014**, 1838 (6), 1451–1466.
- (8) Israelachvili, J. N. Refinement of the Fluid-Mosaic Model of Membrane Structure. *Biochim. Biophys. Acta BBA - Biomembr.* **1977**, 469 (2), 221–225.
- (9) Karp G.; Iwasaj.; Marshall W. *Karp's Cell and Molecular Biology: Concepts and Experiments*, 8th ed.; Willey, 2010.
- (10) Abrahamsson, S. *Structure of Biological Membranes*; Springer Science & Business Media, 2013.
- (11) Cullis, P. R.; Kruijff, B. de. Lipid polymorphism and the functional roles of lipids in biological membranes *Biochim. Biophys. Acta BBA - Biomembr.* **1979**, 559 (4), 399–420.
- (12) Daleke, D. L. Regulation of Transbilayer Plasma Membrane Phospholipid Asymmetry. *J. Lipid Res.* **2003**, 44 (2), 233–242.
- (13) Ingólfsson, H. I.; Melo, M. N.; van Eerden, F. J.; Amarez, C.; Lopez, C. A.; Wassenaar, T. A.; Periole, X.; de Vries, A. H.; Tieleman, D. P.; Marrink, S. J. Lipid Organization of the Plasma Membrane. *J. Am. Chem. Soc.* **2014**, 136 (41), 14554–14559.
- (14) Elam, W. A. Physical Biology of the Cell. *Yale J. Biol. Med.* **2014**, 87 (1), 96.
- (15) Strandberg, E.; Tiltak, D.; Ehni, S.; Wadhwani, P.; Ulrich, A. S. Lipid Shape Is a Key Factor for Membrane Interactions of Amphipathic Helical Peptides. *Biochim. Biophys. Acta BBA - Biomembr.* **2012**, 1818 (7), 1764–1776.
- (16) Bassereau, P.; Sens, P. *Physics of Biological Membranes*; Springer, 2018.
- (17) Hjort Ipsen, J.; Karlström, G.; Mouritsen, O. G.; Wennerström, H.; Zuckermann, M. J. Phase Equilibria in the Phosphatidylcholine-Cholesterol System. *Biochim. Biophys. Acta BBA - Biomembr.* **1987**, 905 (1), 162–172.
- (18) Hoekstra, D.; Maier, O.; Wouden, J. M. van der; Slimane, T. A.; IJzendoorn, S. C. D. van. Membrane Dynamics and Cell Polarity the Role of Sphingolipids. *J. Lipid Res.* **2003**, 44 (5), 869–877.
- (19) Macháň, R.; Hof, M. Lipid Diffusion in Planar Membranes Investigated by Fluorescence Correlation Spectroscopy. *Biochim. Biophys. Acta BBA - Biomembr.* **2010**, 1798 (7), 1377–1391.
- (20) Vermeer, L. S.; de Groot, B. L.; Réat, V.; Milon, A.; Czaplicki, J. Acyl Chain Order Parameter Profiles in Phospholipid Bilayers: Computation from Molecular Dynamics Simulations and Comparison with ²H NMR Experiments. *Eur. Biophys. J.* **2007**, 36 (8), 919–931.

- (21) Bassolino-Klimas, D.; Alper, H. E.; Stouch, T. R. Mechanism of Solute Diffusion through Lipid Bilayer Membranes by Molecular Dynamics Simulation. *J. Am. Chem. Soc.* **1995**, *117* (14), 4118–
- (22) Stevens, M. J.; Hoh, J. H.; Woolf, T. B. Insights into the Molecular Mechanism of Membrane Fusion from Simulation: Evidence for the Association of Splayed Tails. *Phys. Rev. Lett.* **2003**, *91* (18), 188102.
- (23) Simons, K.; Ikonen, E. Functional Rafts in Cell Membranes. *Nature* **1997**, *387* (6633), 569–572.
- (24) Simons, K.; Toomre, D. Lipid Rafts and Signal Transduction. *Nat. Rev. Mol. Cell Biol.* **2000**, *1* (1), 31–39.
- (25) Varshney, P.; Yadav, V.; Saini, N. Lipid Rafts in Immune Signalling: Current Progress and Future Perspective. *Immunology* **2016**, *149* (1), 13–24.
- (26) Helenius, A.; Simons, K. Solubilization of Membranes by Detergents. *Biochim. Biophys. Acta BBA - Rev. Biomembr.* **1975**, *415* (1), 29–79.
- (27) Lichtenberg, D.; Robson, R. J.; Dennis, E. A. Solubilization of Phospholipids by Detergents Structural and Kinetic Aspects. *Biochim. Biophys. Acta BBA - Rev. Biomembr.* **1983**, *737* (2), 285–304.
- (28) Seddon, A. M.; Curnow, P.; Booth, P. J. Membrane Proteins, Lipids and Detergents: Not Just a Soap Opera. *Biochim. Biophys. Acta BBA - Biomembr.* **2004**, *1666* (1), 105–117.
- (29) Dominguez, A.; Fernandez, A.; Gonzalez, N.; Iglesias, E.; Montenegro, L. Determination of Critical Micelle Concentration of Some Surfactants by Three Techniques. *J. Chem. Educ.* **1997**, *74* (10), 1227.
- (30) Hansson, P.; Jönsson, B.; Ström, C.; Söderman, O. Determination of Micellar Aggregation Numbers in Dilute Surfactant Systems with the Fluorescence Quenching Method. *J. Phys. Chem. B* **2000**, *104* (15), 3496–3506.
- (31) Thévenot, C.; Grassl, B.; Bastiat, G.; Binana, W. Aggregation Number and Critical Micellar Concentration of Surfactant Determined by Time-Dependent Static Light Scattering (TDSLS) and Conductivity. *Colloids Surf. Physicochem. Eng. Asp.* **2005**, *252* (2), 105–111.
- (32) Helenius, A.; McCaslin, D. R.; Fries, E.; Tanford, C. [63] Properties of Detergents. In *Methods in Enzymology*; Elsevier, 1979; Vol. 56, pp 734–749.
- (33) Uhlén, M.; Fagerberg, L.; Hallström, B. M.; Lindskog, C.; Oksvold, P.; Mardinoglu, A.; Sivertsson, Å.; Kampf, C.; Sjöstedt, E.; Asplund, A.; et al. Tissue-Based Map of the Human Proteome. *Science* **2015**, *347* (6220), 1260419.
- (34) Yildirim, M. A.; Goh, K.-I.; Cusick, M. E.; Barabási, A.-L.; Vidal, M. Drug—Target Network. *Nat. Biotechnol.* **2007**, *25* (10), 1119–1126.
- (35) Jastrzebska, B. GPCR – G Protein Complexes – the Fundamental Signaling Assembly. *Amino Acids* **2013**, *45* (6).
- (36) Pautsch, A.; Schulz, G. E. High-Resolution Structure of the OmpA Membrane Domain¹¹Edited by D. C. Rees. *J. Mol. Biol.* **2000**, *298* (2), 273–282.
- (37) Gallego, O.; Betts, M. J.; Gvozdenovic-Jeremic, J.; Maeda, K.; Matetzki, C.; Aguilar-Gurrieri, C.; Beltran-Alvarez, P.; Bonn, S.; Fernández-Tornero, C.; Jensen, L. J.; et al. A Systematic Screen for Protein–Lipid Interactions in *Saccharomyces Cerevisiae*. *Mol. Syst. Biol.* **2010**, *6* (1), 430.
- (38) Nogi, T.; Fathir, I.; Kobayashi, M.; Nozawa, T.; Miki, K. Crystal Structures of Photosynthetic Reaction Center and High-Potential Iron-Sulfur Protein from *Thermochromatium Tepidum*: Thermostability and Electron Transfer. *Proc. Natl. Acad. Sci. U. S. A.* **2000**, *97* (25), 13561–13566.
- (39) Hanlon, C. D.; Andrew, D. J. Outside-in Signaling – a Brief Review of GPCR Signaling with a Focus on the *Drosophila* GPCR Family. *J. Cell Sci.* **2015**, *128* (19), 3533–3542.
- (40) Hauser, A. S.; Attwood, M. M.; Rask-Andersen, M.; Schiöth, H. B.; Gloriam, D. E. Trends in GPCR Drug Discovery: New Agents, Targets and Indications. *Nat. Rev. Drug Discov.* **2017**, *16* (12), 829–

- (41) Hilger, D.; Masureel, M.; Kobilka, B. K. Structure and Dynamics of GPCR Signaling Complexes. *Nat. Struct. Mol. Biol.* **2018**, 25 (1), 4–12.
- (42) Park, S. H.; Das, B. B.; Casagrande, F.; Tian, Y.; Nothnagel, H. J.; Chu, M.; Kiefer, H.; Maier, K.; Angelis, A. A. D.; Marassi, F. M.; et al. Structure of the Chemokine Receptor CXCR1 in Phospholipid Bilayers. *Nature* **2012**, 491 (7426), 779–783.
- (43) Hauser, A. S.; Attwood, M. M.; Rask-Andersen, M.; Schiöth, H. B.; Gloriam, D. E. Trends in GPCR Drug Discovery: New Agents, Targets and Indications. *Nat. Rev. Drug Discov.* **2017**, 16 (12), 829–842.
- (44) Lorenzen E.; Ceraudo E.; Berchiche Y. A.; Rico C. A.; Fürstenberg A.; Sakmar T. P.; Huber T. G protein subtype-specific signaling bias in a series of CCR5 chemokine analogs. *Sci. Signal.* **2018**, 11 (552), 1-11
- (45) Hughes, C. E.; Nibbs, R. J. B. A Guide to Chemokines and Their Receptors. *FEBS J.* **2018**, 285 (16), 2944–2971.
- (46) Allen, S. J.; Crown, S. E.; Handel, T. M. Chemokine:Receptor Structure, Interactions, and Antagonism. *Annu. Rev. Immunol.* **2007**, 25 (1), 787–820.
- (47) Bennett, L. D.; Fox, J. M.; Signoret, N. Mechanisms Regulating Chemokine Receptor Activity. *Immunology* **2011**, 134 (3), 246–256.
- (48) Murphy, P. M.; Baggiolini, M.; Charo, I. F.; Hébert, C. A.; Horuk, R.; Matsushima, K.; Miller, L. H.; Oppenheim, J. J.; Power, C. A. International Union of Pharmacology. XXII. Nomenclature for Chemokine Receptors. *Pharmacol. Rev.* **2000**, 52 (1), 145–176.
- (49) Rossi, D.; Zlotnik, A. The Biology of Chemokines and Their Receptors. *Annu. Rev. Immunol.* **2000**, 18 (1), 217–242. <https://doi.org/10.1146/annurev.immunol.18.1.217>.
- (50) Smith, S. M. Strategies for the Purification of Membrane Proteins. In *Protein Chromatography: Methods and Protocols*; Walls, D., Loughran, S. T., Eds.; Methods in Molecular Biology; Humana Press: Totowa, NJ, 2011; pp 485–496.
- (51) Baron, C.; Thompson, T. E. Solubilization of Bacterial Membrane Proteins Using Alkyl Glucosides and Dioctanoyl Phosphatidylcholine. *Biochim. Biophys. Acta BBA - Biomembr.* **1975**, 382 (3), 276–285.
- (52) Tribet, C.; Audebert, R.; Popot, J.-L. Amphipols: Polymers That Keep Membrane Proteins Soluble in Aqueous Solutions. *Proc. Natl. Acad. Sci.* **1996**, 93 (26), 15047–15050.
- (53) Phillips, R.; Ursell, T.; Wiggins, P.; Sens, P. Emerging Roles for Lipids in Shaping Membrane-Protein Function. *Nature* **2009**, 459 (7245), 379–385.
- (54) Dürr, U. H. N.; Soong, R.; Ramamoorthy, A. When Detergent Meets Bilayer: Birth and Coming of Age of Lipid Bicelles. *Prog. Nucl. Magn. Reson. Spectrosc.* **2013**, 69, 1.
- (55) Prosser, R. S.; Evanics, F.; Kitevski, J. L.; Al-Abdul-Wahid, M. S. Current Applications of Bicelles in NMR Studies of Membrane-Associated Amphiphiles and Proteins. *Biochemistry* **2006**, 45 (28),
- (56) Vold, R. R.; Prosser, R. S.; Deese, A. J. Isotropic Solutions of Phospholipid Bicelles: A New Membrane Mimetic for High-Resolution NMR Studies of Polypeptides. *J. Biomol. NMR* **1997**, 9 (3), 329–335.
- (57) Kang, C.; Vanoye, C. G.; Welch, R. C.; Van Horn, W. D.; Sanders, C. R. Functional Delivery of a Membrane Protein into Oocyte Membranes Using Bicelles. *Biochemistry* **2010**, 49 (4), 653–655.
- (58) Dürr, U. H. N.; Gildenberg, M.; Ramamoorthy, A. The Magic of Bicelles Lights Up Membrane Protein Structure. *Chem. Rev.* **2012**, 112 (11), 6054.
- (59) Akbarzadeh, A.; Rezaei-Sadabady, R.; Davaran, S.; Joo, S. W.; Zarghami, N.; Hanifehpour, Y.; Samiei, M.; Kouhi, M.; Nejati-Koshki, K. Liposome: Classification, Preparation, and Applications. *Nanoscale Res. Lett.* **2013**, 8 (1), 102.

- (60) Eytan, G. D. Use of Liposomes for Reconstitution of Biological Functions. *Biochim. Biophys. Acta BBA - Rev. Biomembr.* **1982**, 694 (2), 185–202.
- (61) Simeonov, P.; Werner, S.; Haupt, C.; Tanabe, M.; Bacia, K. Membrane Protein Reconstitution into Liposomes Guided by Dual-Color Fluorescence Cross-Correlation Spectroscopy. *Biophys. Chem.* **2013**, 184, 37–43.
- (62) Kamiya, K.; Takeuchi, S. Giant Liposome Formation toward the Synthesis of Well-Defined Artificial Cells. *J. Mater. Chem. B* **2017**, 5 (30), 5911–5923.
- (63) Smirnova, I. A.; Ädelroth, P.; Brzezinski, P. Extraction and Liposome Reconstitution of Membrane Proteins with Their Native Lipids without the Use of Detergents. *Sci. Rep.* **2018**, 8 (1), 1–6.
- (64) Sudbrack, T. P.; Archilha, N. L.; Itri, R.; Riske, K. A. Observing the Solubilization of Lipid Bilayers by Detergents with Optical Microscopy of GUVs. *J. Phys. Chem. B* **2011**, 115 (2), 269–277.
- (65) Banerjee, S.; Huber, T.; Sakmar, T. P. Rapid Incorporation of Functional Rhodopsin into Nanoscale Apolipoprotein Bound Bilayer (NABB) Particles. *J. Mol. Biol.* **2008**, 377 (4), 1067–1081.
- (66) Bayburt, T. H.; Sligar, S. G. Membrane Protein Assembly into Nanodiscs. *FEBS Lett.* **2010**, 584 (9), 1721–1727.
- (67) Denisov, I. G.; Sligar, S. G. Nanodiscs in Membrane Biochemistry and Biophysics. *Chem. Rev.* **2017**, 117 (6), 4669–4713.
- (68) Nasr, M. L.; Baptista, D.; Strauss, M.; Sun, Z.-Y. J.; Grigoriu, S.; Huser, S.; Plückthun, A.; Hagn, F.; Walz, T.; Hogle, J. M.; et al. Covalently Circularized Nanodiscs for Studying Membrane Proteins and Viral Entry. *Nat. Methods* **2017**, 14 (1), 49–52.
- (69) Mörs, K.; Roos, C.; Scholz, F.; Wachtveitl, J.; Dötsch, V.; Bernhard, F.; Glaubitz, C. Modified Lipid and Protein Dynamics in Nanodiscs. *Biochim. Biophys. Acta BBA - Biomembr.* **2013**, 1828 (4), 1222–1229.
- (70) Nath A.; Koo P.K.; Rhoades E.; Atkins W.M. Allosteric Effects on Substrate Dissociation from Cytochrome P450 3A4 in Nanodiscs Observed by Ensemble and Single-Molecule Fluorescence Spectroscopy. *J. Am. Chem. Soc.* **2008**, 130 (47) 15746–15747
- (71) Rosenbaum, D. M.; Zhang, C.; Lyons, J. A.; Holl, R.; Aragao, D.; Arlow, D. H.; Rasmussen, S. G. F.; Choi, H.-J.; DeVree, B. T.; Sunahara, R. K.; et al. Structure and Function of an Irreversible Agonist- β 2 Adrenoceptor Complex. *Nature* **2011**, 469 (7329), 236–240.
- (72) Efremov, R. G.; Leitner, A.; Aebersold, R.; Raunser, S. Architecture and Conformational Switch Mechanism of the Ryanodine Receptor. *Nature* **2015**, 517 (7532), 39–43.
- (73) Inagaki, S.; Ghirlando, R.; White, J. F.; Gvozdenovic-Jeremic, J.; Northup, J. K.; Grisshammer, R. Modulation of the Interaction between Neurotensin Receptor NTS1 and Gq Protein by Lipid. *J. Mol. Biol.* **2012**, 417 (1), 95–111.
- (74) Milić, D.; Veprintsev, D. B. Large-Scale Production and Protein Engineering of G Protein-Coupled Receptors for Structural Studies. *Front. Pharmacol.* **2015**, 6.
- (75) Watson, J. D.; Crick, F. H. C. Molecular Structure of Nucleic Acids: A Structure for Deoxyribose Nucleic Acid. *Nature* **1953**, 171 (4356), 737–738.
- (76) Yakovchuk, P.; Protozanova, E.; Frank-Kamenetskii, M. D. Base-Stacking and Base-Pairing Contributions into Thermal Stability of the DNA Double Helix. *Nucleic Acids Res.* **2006**, 34 (2), 564–574.
- (77) Pohl, F. M. Polymorphism of a Synthetic DNA in Solution. *Nature* **1976**, 260 (5549), 365–366.
- (78) Dickerson, R. E.; Klug, A. Base Sequence and Helix Structure Variation in B and A DNA. *J. Mol. Biol.* **1983**, 166 (3), 419–441.
- (79) Liu, R.; Liu, H.; Chen, X.; Kirby, M.; Brown, P. O.; Zhao, K. Regulation of CSF1 Promoter by the SWI/SNF-like BAF Complex. *Cell* **2001**, 106 (3), 309–318.

- (80) Gagna, C. E.; Kuo, H.; Lambert, W. C. TERMINAL DIFFERENTIATION AND LEFT-HANDED Z-DNA: A REVIEW. *Cell Biol. Int.* **1999**, 23 (1), 1–5. <https://doi.org/10.1006/cbir.1998.0327>.
- (81) Herbert, A.; Rich, A. Left-Handed Z-DNA: Structure and Function. *Genetica* **1999**, 106 (1–2), 37–47.
- (82) Haran, T. E.; Mohanty, U. The Unique Structure of A-Tracts and Intrinsic DNA Bending. *Q. Rev. Biophys.* **2009**, 42 (1), 41–81.
- (83) MacDonald, D.; Herbert, K.; Zhang, X.; Polgruto, T.; Lu, P. Solution Structure of an A-Tract DNA Bend1 1 Edited by I. Tinoco. *J. Mol. Biol.* **2001**, 306 (5), 1081–1098.
- (84) Koo, H.-S.; Wu, H.-M.; Crothers, D. M. DNA Bending at Adenine · Thymine Tracts. *Nature* **1986**, 320 (6062), 501–506.
- (85) Ulanovsky, L. E.; Trifonov, E. N. Estimation of Wedge Components in Curved DNA. *Nature* **1987**, 326 (6114), 720–722.
- (86) Calladine, C. R.; Drew, H. R.; McCall, M. J. The Intrinsic Curvature of DNA in Solution. *J. Mol. Biol.* **1988**, 201 (1), 127–137.
- (87) Arnott, S.; Selsing, E. Structures for the Polynucleotide Complexes Poly(DA) · Poly(DT) and Poly(DT) · Poly(DA) · Poly(DT). *J. Mol. Biol.* **1974**, 88 (2), 509–521.
- (88) Nadeau, J. G.; Crothers, D. M. Structural Basis for DNA Bending. *Proc. Natl. Acad. Sci.* **1989**, 86 (8), 2622–2626.
- (89) Ulanovsky, L.; Bodner, M.; Trifonov, E. N.; Choder, M. Curved DNA: Design, Synthesis, and Circularization. *Proc. Natl. Acad. Sci.* **1986**, 83 (4), 862–866.
- (90) Ackermann, D.; Schmidt, T. L.; Hannam, J. S.; Purohit, C. S.; Heckel, A.; Famulok, M. A Double-Stranded DNA Rotaxane. *Nat. Nanotechnol.* **2010**, 5 (6), 436–442.
- (91) Schmidt, T. L.; Heckel, A. Construction of a Structurally Defined Double-Stranded DNA Catenane. *Nano Lett.* **2011**, 11 (4), 1739–1742.
- (92) Rasched, G.; Ackermann, D.; Schmidt, T. L.; Broekmann, P.; Heckel, A.; Famulok, M. DNA Mini-circles with Gaps for Versatile Functionalization. *Angew. Chem. Int. Ed.* **2008**, 47 (5), 967–970.
- (93) Ackermann, D.; Rasched, G.; Verma, S.; Schmidt, T. L.; Heckel, A.; Famulok, M. Assembly of DsDNA Nanocircles into Dimeric and Oligomeric Aggregates. *Chem. Commun.* **2010**, 46 (23), 4154–4156.
- (94) Schmidt, T. L.; Nandi, C. K.; Rasched, G.; Parui, P. P.; Brutschy, B.; Famulok, M.; Heckel, A. Polyamide Struts for DNA Architectures. *Angew. Chem. Int. Ed.* **2007**, 46 (23), 4382–4384.
- (95) Hu, L.; Lu, C.-H.; Willner, I. Switchable Catalytic DNA Catenanes. *Nano Lett.* **2015**, 15 (3), 2099–2103.
- (96) Seeman, N. C. Nucleic Acid Junctions and Lattices. *J. Theor. Biol.* **1982**, 99 (2), 237–247.
- (97) Seeman, N. C. An Overview of Structural DNA Nanotechnology. *Mol. Biotechnol.* **2007**, 37 (3), 246–257.
- (98) Seeman, N. C.; Sleiman, H. F. DNA Nanotechnology. *Nat. Rev. Mater.* **2017**, 3 (1), 1–23.
- (99) Chen, J.; Seeman, N. C. Synthesis from DNA of a Molecule with the Connectivity of a Cube. *Nature* **1991**, 350 (6319), 631–633.
- (100) Zhang, Y.; Seeman, N. C. Construction of a DNA-Truncated Octahedron. *J. Am. Chem. Soc.* **1994**, 116 (5), 1661–1669.
- (101) Goodman, R. P.; Berry, R. M.; Turberfield, A. J. The Single-Step Synthesis of a DNA Tetrahedron. *Chem. Commun.* **2004**, No. 12, 1372–1373.
- (102) Rothmund, P. W. K. Folding DNA to Create Nanoscale Shapes and Patterns. *Nature* **2006**, 440 (7082), 297–302.

- (103) Andersen, E. S.; Dong, M.; Nielsen, M. M.; Jahn, K.; Subramani, R.; Mamdouh, W.; Golas, M. M.; Sander, B.; Stark, H.; Oliveira, C. L. P.; et al. Self-Assembly of a Nanoscale DNA Box with a Controllable Lid. *Nature* **2009**, 459 (7243), 73–76.
- (104) Matthies, M.; Agarwal, N. P.; Schmidt, T. L. Design and Synthesis of Triangulated DNA Origami Trusses. *Nano Lett.* **2016**, 16 (3), 2108–2113.
- (105) Hao, Y.; Kristiansen, M.; Sha, R.; Birktoft, J. J.; Hernandez, C.; Mao, C.; Seeman, N. C. A Device That Operates within a Self-Assembled 3D DNA Crystal. *Nat. Chem.* **2017**, 9 (8), 824–827.
- (106) Mao, C.; Sun, W.; Shen, Z.; Seeman, N. C. A Nanomechanical Device Based on the B–Z Transition of DNA. *Nature* **1999**, 397 (6715), 144–146.
- (107) Gür, F. N.; Schwarz, F. W.; Ye, J.; Diez, S.; Schmidt, T. L. Toward Self-Assembled Plasmonic Devices: High-Yield Arrangement of Gold Nanoparticles on DNA Origami Templates. *ACS Nano* **2016**, 10 (5), 5374–5382.
- (108) Perrault, S. D.; Shih, W. M. Virus-Inspired Membrane Encapsulation of DNA Nanostructures To Achieve In Vivo Stability. *ACS Nano* **2014**, 8 (5), 5132–5140.
- (109) Douglas, S. M.; Chou, J. J.; Shih, W. M. DNA-Nanotube-Induced Alignment of Membrane Proteins for NMR Structure Determination. *Proc. Natl. Acad. Sci. U. S. A.* **2007**, 104 (16), 6644–6648.
- (110) Bellot, G.; McClintock, M. A.; Chou, J. J.; Shih, W. M. DNA Nanotubes for NMR Structure Determination of Membrane Proteins. *Nat. Protoc.* **2013**, 8 (4).
- (111) Douglas S. M.; Bachelet I.; Church G. M. A Logic-Gated Nanorobot for Targeted Transport of Molecular Payloads. *Science* **2012**, 335 (6070), 831–834
- (112) Derr, N. D.; Goodman, B. S.; Jungmann, R.; Leschziner, A. E.; Shih, W. M.; Reck-Peterson, S. L. Tug-of-War in Motor Protein Ensembles Revealed with a Programmable DNA Origami Scaffold. *Science* **2012**, 338 (6107), 662–665.
- (113) Saha, S.; Prakash, V.; Halder, S.; Chakraborty, K.; Krishnan, Y. A PH-Independent DNA Nanodevice for Quantifying Chloride Transport in Organelles of Living Cells. *Nat. Nanotechnol.* **2015**, 10 (7), 645–651.
- (114) Chen, Y.-J.; Groves, B.; Muscat, R. A.; Seelig, G. DNA Nanotechnology from the Test Tube to the Cell. *Nat. Nanotechnol.* **2015**, 10 (9), 748–760.
- (115) Jiang, Q.; Song, C.; Nangreave, J.; Liu, X.; Lin, L.; Qiu, D.; Wang, Z.-G.; Zou, G.; Liang, X.; Yan, H.; et al. DNA Origami as a Carrier for Circumvention of Drug Resistance. *J. Am. Chem. Soc.* **2012**, 134 (32), 13396–13403.
- (116) Veetil, A. T.; Chakraborty, K.; Xiao, K.; Minter, M. R.; Sisodia, S. S.; Krishnan, Y. Cell-Targetable DNA Nanocapsules for Spatiotemporal Release of Caged Bioactive Small Molecules. *Nat. Nanotechnol.* **2017**, 12 (12), 1183–1189.
- (117) Burns, J. R.; Lamarre, B.; Pyne, A. L. B.; Noble, J. E.; Ryadnov, M. G. DNA Origami Inside-Out Viruses. *ACS Synth. Biol.* **2018**, 7 (3), 767–773.
- (118) Li, D.; Mo, F.; Wu, J.; Huang, Y.; Zhou, H.; Ding, S.; Chen, W. A Multifunctional DNA Nano-Scorpion for Highly Efficient Targeted Delivery of mRNA Therapeutics. *Sci. Rep.* **2018**, 8 (1), 1–9.
- (119) Langecker, M.; Arnaut, V.; List, J.; Simmel, F. C. DNA Nanostructures Interacting with Lipid Bilayer Membranes. *Acc. Chem. Res.* **2014**, 47 (6), 1807–1815.
- (120) Dabkowska, A. P.; Michanek, A.; Jaeger, L.; Rabe, M.; Chworos, A.; Höök, F.; Nylander, T.; Sparr, E. Assembly of RNA Nanostructures on Supported Lipid Bilayers. *Nanoscale* **2015**, 7 (2), 583–596.
- (121) Gromelski, S.; Brezesinski, G. DNA Condensation and Interaction with Zwitterionic Phospholipids Mediated by Divalent Cations. *Langmuir* **2006**, 22 (14), 6293–6301.

-
- (122) Suzuki, Y.; Endo, M.; Sugiyama, H. Lipid-Bilayer-Assisted Two-Dimensional Self-Assembly of DNA Origami Nanostructures. *Nat. Commun.* **2015**, *6* (1), 1–9.
- (123) Börjesson, K.; Wiberg, J.; El-Sagheer, A. H.; Ljungdahl, T.; Mårtensson, J.; Brown, T.; Nordén, B.; Albinsson, B. Functionalized Nanostructures: Redox-Active Porphyrin Anchors for Supramolecular DNA Assemblies. *ACS Nano* **2010**, *4* (9), 5037–5046.
- (124) Kurz, A.; Bunge, A.; Windeck, A.-K.; Rost, M.; Flasche, W.; Arbuzova, A.; Strohbach, D.; Müller, S.; Liebscher, J.; Huster, D.; et al. Lipid-Anchored Oligonucleotides for Stable Double-Helix Formation in Distinct Membrane Domains. *Angew. Chem. Int. Ed.* **2006**, *45* (27), 4440–4444.
- (125) Rodríguez-Pulido, A.; Kondrachuk, A. I.; Prusty, D. K.; Gao, J.; Loi, M. A.; Herrmann, A. Light-Triggered Sequence-Specific Cargo Release from DNA Block Copolymer–Lipid Vesicles. *Angew. Chem.* **2013**, *125* (3), 1042–1046.
- (126) List, J.; Weber, M.; Simmel, F. C. Hydrophobic Actuation of a DNA Origami Bilayer Structure. *Angew. Chem. Int. Ed.* **2014**, *53* (16), 4236–4239.
- (127) Choi, K.; Kwon, I. C.; Ahn, H. J. Self-Assembled Amphiphilic DNA-Cholesterol/DNA-Peptide Hybrid Duplexes with Liposome-like Structure for Doxorubicin Delivery. *Biomaterials* **2013**, *34* (16), 4183–4190.
- (128) Langecker, M.; Arnaut, V.; Martin, T. G.; List, J.; Renner, S.; Mayer, M.; Dietz, H.; Simmel, F. C. Synthetic Lipid Membrane Channels Formed by Designed DNA Nanostructures. *Science* **2012**, *338* (6109), 932–936.
- (129) Göpflich, K.; Li, C.-Y.; Ricci, M.; Bhamidimarri, S. P.; Yoo, J.; Gyenes, B.; Ohmann, A.; Winterhalter, M.; Aksimentiev, A.; Keyser, U. F. Large-Conductance Transmembrane Porin Made from DNA Origami. *ACS Nano* **2016**, *10* (9), 8207–8214.
- (130) Beales, P. A.; Vanderlick, T. K. Partitioning of Membrane-Anchored DNA between Coexisting Lipid Phases. *J. Phys. Chem. B* **2009**, *113* (42), 13678–13686.
- (131) Kocabey, S.; Kempter, S.; List, J.; Xing, Y.; Bae, W.; Schiffels, D.; Shih, W. M.; Simmel, F. C.; Liedl, T. Membrane-Assisted Growth of DNA Origami Nanostructure Arrays. *ACS Nano* **2015**, *9* (4), 3530–3539.
- (132) Burns, J. R.; Howorka, S. Structural and Functional Stability of DNA Nanopores in Biological Media. *Nanomaterials* **2019**, *9* (4), 490.
- (133) Burns, J. R.; Al-Juffali, N.; Janes, S. M.; Howorka, S. Membrane-Spanning DNA Nanopores with Cytotoxic Effect. *Angew. Chem.* **2014**, *126* (46), 12674–12678.
- (134) Lin, C.; Perrault, S. D.; Kwak, M.; Graf, F.; Shih, W. M. Purification of DNA-Origami Nanostructures by Rate-Zonal Centrifugation. *Nucleic Acids Res.* **2013**, *41* (2), e40–e40.
- (135) Yang, Y.; Wang, J.; Shigematsu, H.; Xu, W.; Shih, W. M.; Rothman, J. E.; Lin, C. Self-Assembly of Size-Controlled Liposomes on DNA Nanotemplates. *Nat. Chem.* **2016**, *8* (5), 476–483.
- (136) Zhang, Z.; Yang, Y.; Pincet, F.; Llaguno, M. C.; Lin, C. Placing and Shaping Liposomes with Reconfigurable DNA Nanocages. *Nat. Chem.* **2017**, *9* (7), 653–659.
- (137) Bian, X.; Zhang, Z.; Xiong, Q.; Camilli, P. D.; Lin, C. A Programmable DNA-Origami Platform for Studying Lipid Transfer between Bilayers. *Nat. Chem. Biol.* **2019**, *15* (8), 830–837.
- (138) Gut, I. G.; Beck, S. A Procedure for Selective DNA Alkylation and Detection by Mass Spectrometry. *Nucleic Acids Res.* **1995**, *23* (8), 1367–1373.
- (139) Burns, J. R.; Stulz, E.; Howorka, S. Self-Assembled DNA Nanopores That Span Lipid Bilayers. *Nano Lett.* **2013**, *13*, (6) 2351–2356.
- (140) Maingi, V.; Burns, J. R.; Uusitalo, J. J.; Howorka, S.; Marrink, S. J.; Sansom, M. S. P. Stability and Dynamics of Membrane-Spanning DNA Nanopores. *Nat. Commun.* **2017**, *8*, 14784.
- (141) Howorka, S. Building membrane nanopores. *Nature Nanotech.* **2017**, *12*, 619–630.

- (142) Cymer, F.; von Heijne, G.; White, S. H. Mechanisms of Integral Membrane Protein Insertion and Folding. *J. Mol. Biol.* **2015**, *427* (5), 999–1022.
- (143) Sandoval, A.; Eichler, S.; Madathil, S.; Reeves, P. J.; Fahmy, K.; Böckmann, R. A. The Molecular Switching Mechanism at the Conserved D(E)RY Motif in Class-A GPCRs. *Biophys. J.* **2016**, *111* (1), 79–89.
- (144) Fischermeier, E.; Pospíšil, P.; Sayed, A.; Hof, M.; Solioz, M.; Fahmy, K. Dipolar Relaxation Dynamics at the Active Site of an ATPase Regulated by Membrane Lateral Pressure. *Angew. Chem. Int. Ed.* **2017**, *56* (5), 1269–1272.
- (145) Frey, L.; Lakomek, N.-A.; Riek, R.; Bibow, S. Micelles, Bicelles, and Nanodiscs: Comparing the Impact of Membrane Mimetics on Membrane Protein Backbone Dynamics. *Angew. Chem. Int. Ed.* **2017**, *56* (1), 380–383.
- (146) Zeppelin, T.; Ladefoged, L. K.; Sinning, S.; Periole, X.; Schiøtt, B. A Direct Interaction of Cholesterol with the Dopamine Transporter Prevents Its Out-to-Inward Transition. *PLOS Comput. Biol.* **2018**, *14* (1), e1005907.
- (147) Nyholm, T. K. M.; Özdirekcan, S.; Killian, J. A. How Protein Transmembrane Segments Sense the Lipid Environment. *Biochemistry* **2007**, *46* (6), 1457–1465.
- (148) Vargas, C.; Cuevas Arenas, R.; Frotscher, E.; Keller, S. Nanoparticle Self-Assembly in Mixtures of Phospholipids with Styrene/Maleic Acid Copolymers or Fluorinated Surfactants. *Nanoscale* **2015**, *7* (48), 20685–20696.
- (149) Imura, T.; Tsukui, Y.; Taira, T.; Aburai, K.; Sakai, K.; Sakai, H.; Abe, M.; Kitamoto, D. Surfactant-like Properties of an Amphiphilic α -Helical Peptide Leading to Lipid Nanodisc Formation. *Langmuir* **2014**, *30* (16), 4752–4759.
- (150) Bayburt, T. H.; Leitz, A. J.; Xie, G.; Oprian, D. D.; Sligar, S. G. Transducin Activation by Nanoscale Lipid Bilayers Containing One and Two Rhodopsins. *J. Biol. Chem.* **2007**, *282* (20), 14875–14881.
- (151) Rico, C. A.; Sakmar, T. P.; Huber, T. Optimized Zebrafish Apolipoprotein A-I Expression and Purification for Nabbs Assembly. *Biophys. J.* **2014**, *106* (2), 104a–105a.
- (152) Douglas, S. M.; Dietz, H.; Liedl, T.; Högberg, B.; Graf, F.; Shih, W. M. Self-Assembly of DNA into Nanoscale Three-Dimensional Shapes. *Nature* **2009**, *459* (7245), 414–418.
- (153) Hong, F.; Zhang, F.; Liu, Y.; Yan, H. DNA Origami: Scaffolds for Creating Higher Order Structures. *Chem. Rev.* **2017**, *117* (20), 12584–12640.
- (154) Goodman, R. P.; Schaap, I. a. T.; Tardin, C. F.; Erben, C. M.; Berry, R. M.; Schmidt, C. F.; Turberfield, A. J. Rapid Chiral Assembly of Rigid DNA Building Blocks for Molecular Nanofabrication. *Science* **2005**, *310* (5754), 1661–1665.
- (155) Schmidt, T. L.; Heckel, A. Pyrrole/Imidazole–Polyamide Anchors for DNA Tertiary Interactions. *Small* **2009**, *5* (13), 1517–1520.
- (156) Lu, C.-H.; Cecconello, A.; Qi, X.-J.; Wu, N.; Jester, S.-S.; Famulok, M.; Matthies, M.; Schmidt, T.-L.; Willner, I. Switchable Reconfiguration of a Seven-Ring Interlocked DNA Catenane Nanostructure. *Nano Lett.* **2015**, *15* (10), 7133–7137.
- (157) Gonçalves, D. P. N.; Schmidt, T. L.; Koeppel, M. B.; Heckel, A. DNA Minicircles Connected via G-Quadruplex Interaction Modules. *Small Wein. Bergstr. Ger.* **2010**, *6* (12), 1347–1352.
- (158) Gish, G.; Eckstein, F. DNA and RNA Sequence Determination Based on Phosphorothioate Chemistry. *Science* **1988**, *240* (4858), 1520–1522.
- (159) Parasassi, T.; De Stasio, G.; Ravagnan, G.; Rusch, R. M.; Gratton, E. Quantitation of Lipid Phases in Phospholipid Vesicles by the Generalized Polarization of Laurdan Fluorescence. *Biophys. J.* **1991**, *60* (1), 179–189.
- (160) Koynova, R.; Caffrey, M. Phases and Phase Transitions of the Phosphatidylcholines. *Biochim. Biophys. Acta BBA - Rev. Biomembr.* **1998**, *1376* (1), 91–145.

-
- (161) Denisov, I. G.; McLean, M. A.; Shaw, A. W.; Grinkova, Y. V.; Sligar, S. G. Thermotropic Phase Transition in Soluble Nanoscale Lipid Bilayers. *J. Phys. Chem. B* **2005**, *109* (32), 15580–15588.
- (162) Marrink, S. J.; Risselada, H. J.; Yefimov, S.; Tieleman, D. P.; de Vries, A. H. The MARTINI Force Field: Coarse Grained Model for Biomolecular Simulations. *J. Phys. Chem. B* **2007**, *111* (27), 7812–7824.
- (163) Uusitalo, J. J.; Ingólfsson, H. I.; Akhshi, P.; Tieleman, D. P.; Marrink, S. J. Martini Coarse-Grained Force Field: Extension to DNA. *J. Chem. Theory Comput.* **2015**, *11* (8), 3932–3945.
- (164) Denisov, I. G.; Grinkova, Y. V.; Lazarides, A. A.; Sligar, S. G. Directed Self-Assembly of Monodisperse Phospholipid Bilayer Nanodiscs with Controlled Size. *J. Am. Chem. Soc.* **2004**, *126* (11), 3477–3487.
- (165) Iric, K.; Subramanian, M.; Oertel, J.; Agarwal, N. P.; Matthies, M.; Periole, X.; Sakmar, T. P.; Huber, T.; Fahmy, K.; Schmidt, T. L. DNA-Encircled Lipid Bilayers. *Nanoscale* **2018**, *10* (39), 18463–18467.
- (166) Zhao, Z.; Zhang, M.; Hogle, J. M.; Shih, W. M.; Wagner, G.; Nasr, M. L. DNA-Corralled Nanodiscs for the Structural and Functional Characterization of Membrane Proteins and Viral Entry. *J. Am. Chem. Soc.* **2018**, *140* (34), 10639–10643.
- (167) Watson, J.; Hays, F. A.; Ho, P. S. Definitions and Analysis of DNA Holliday Junction Geometry. *Nucleic Acids Res.* **2004**, *32* (10), 3017–3027.
- (168) Wheatley, E. G.; Pieniazek, S. N.; Mukerji, I.; Beveridge, D. L. Molecular Dynamics of a DNA Holliday Junction: The Inverted Repeat Sequence d(CCGGTACCGG)4. *Biophys. J.* **2012**, *102* (3), 552–560.
- (169) Chen, M.; Maetzke, A.; Jensen, S. J. K.; Gothelf, K. V. Rearrangement of S-(2-Aminoethyl) Thiophosphates to N-(2-Mercaptoethyl)Phosphoramidates. *Eur. J. Org. Chem.* **2007**, *2007* (35), 5826–5833.
- (170) Fidanza J.A.; Ozaki H.; McLaughlin L.W. Site-specific labeling of DNA sequences containing phosphorothioate diesters *J. Am. Chem. Soc.* **1992**, *114* (14), 5509-5517
- (171) Schultz, Z. D.; Pazos, I. M.; McNeil-Watson, F. K.; Lewis, E. N.; Levin, I. W. Magnesium-Induced Lipid Bilayer Microdomain Reorganizations: Implications for Membrane Fusion. *J. Phys. Chem. B* **2009**, *113* (29), 9932–9941.
- (172) Leventis, R.; Gagne, J.; Fuller, N.; Rand, R.; Silvius, J. Divalent Cation Induced Fusion and Lipid Lateral Segregation in Phosphatidylcholine-Phosphatidic Acid Vesicles. *Biochemistry* **1986**, *25* (22), 6978–6987.
- (173) Menon, S. T.; Han, M.; Sakmar, T. P. Rhodopsin: Structural Basis of Molecular Physiology. *Physiol. Rev.* **2001**, *81* (4), 1659–1688.
- (174) Midtgaard, S. R.; Pedersen, M. C.; Kirkensgaard, J. J. K.; Sørensen, K. K.; Mortensen, K.; Jensen, K. J.; Arleth, L. Self-Assembling Peptides Form Nanodiscs That Stabilize Membrane Proteins. *Soft Matter* **2014**, *10* (5), 738–752.
- (175) Oppermann, M. Chemokine Receptor CCR5: Insights into Structure, Function, and Regulation. *Cell. Signal.* **2004**, *16* (11), 1201–1210.
- (176) Barmania, F.; Pepper, M. S. C-C Chemokine Receptor Type Five (CCR5): An Emerging Target for the Control of HIV Infection. *Appl. Transl. Genomics* **2013**, *2*, 3–16.
- (177) Dragic, T.; Trkola, A.; Thompson, D. A.; Cormier, E. G.; Kajumo, F. A.; Maxwell, E.; Lin, S. W.; Ying, W.; Smith, S. O.; Sakmar, T. P.; et al. A Binding Pocket for a Small Molecule Inhibitor of HIV-1 Entry within the Transmembrane Helices of CCR5. *Proc. Natl. Acad. Sci. U. S. A.* **2000**, *97* (10), 5639–5644.

- (178) Dorr, P.; Westby, M.; Dobbs, S.; Griffin, P.; Irvine, B.; Macartney, M.; Mori, J.; Rickett, G.; Smith-Burchnell, C.; Napier, C.; et al. Maraviroc (UK-427,857), a Potent, Orally Bioavailable, and Selective Small-Molecule Inhibitor of Chemokine Receptor CCR5 with Broad-Spectrum Anti-Human Immunodeficiency Virus Type 1 Activity. *Antimicrob. Agents Chemother.* **2005**, *49* (11), 4721–4732.
- (179) Tan Q.; Zhu Y.; Li J.; Chen Z.; Han G.W.; Kufareva I.; Li T.; Ma L.; Fenalti G.; Li J.; Zhang W.; Xie X.; Yang H.; Jiang H.; Cherezov V.; Liu H.; Stevens R.C.; Zhao Q.; Wu B. Structure of the CCR5 Chemokine Receptor–HIV Entry Inhibitor Maraviroc Complex. *Science* **2013**, *341* (6152), 1387–1390.
- (180) Abayev, M.; Rodrigues, J. P. G. L. M.; Srivastava, G.; Arshava, B.; Jaremko, Ł.; Jaremko, M.; Naider, F.; Levitt, M.; Anglister, J. The Solution Structure of Monomeric CCL5 in Complex with a Doubly Sulfated N-Terminal Segment of CCR5. *FEBS J.* **2018**, *285* (11), 1988–2003.
- (181) Rico, C. A.; Berchiche, Y. A.; Horioka, M.; Peeler, J. C.; Lorenzen, E.; Tian, H.; Kazmi, M. A.; Fürstenberg, A.; Gaertner, H.; Hartley, O.; et al. High-Affinity Binding of Chemokine Analogs That Display Ligand Bias at the HIV-1 Coreceptor CCR5. *Biophys. J.* **2019**, *117* (5), 903–919.
- (182) Naganathan, S.; Grunbeck, A.; Tian, H.; Huber, T.; Sakmar, T. P. Genetically-Encoded Molecular Probes to Study G Protein-Coupled Receptors. *JoVE J. Vis. Exp.* **2013**, No. 79, e50588.

Statement of academic honesty

I herewith declare that I have produced this dissertation as the result of my own work, except where otherwise indicated. The work was carried out without the prohibited assistance of third parties and without making use of aids other than those specified; notions taken over directly or indirectly from other sources have been identified as such. This dissertation has not previously been presented in identical or similar form to any other German or foreign examination board.

This dissertation period was from January 2016 to January 2020 and was carried out under the supervision of Dr. Thorsten-Lars Schmidt at the cfaed - Center for Advancing Electronics Dresden, Dresden University of Technology and Prof. Karim Fahmy at Helmholtz Zentrum Dresden – Rossendorf.

Katarina Iric

Dresden, 19.02.2020